

Integrated Nano Liquid Chromatography System On-a-Chip

Thesis by

Qing He

In Partial Fulfillment of the Requirements
for the Degree of

Doctor of Philosophy



California Institute of Technology

Pasadena, California

2006

(Defended June 21, 2005)

© 2006

Qing He

All Rights Reserved

To my wife

Acknowledgements

First and foremost, I would like to thank my advisor, Professor Yu-Chong Tai, for giving me the opportunity to work under his guidance on the fascinating field of MEMS. His admirable expertise, endless supply of ideas, and passion for work made my Ph.D. study fruitful and enjoyable. I will not forget the talks beyond academia that we had, especially those during long carpooling hours. He certainly has taught me not only how to succeed in academia, but also how to succeed in life.

My experience would not have been as meaningful without the other members of the group. My gratitude goes to the previous group members who helped me to start this journey, including Dr. Xing Yang, Dr. Tze-Jung Yao, Dr. Yong Xu, Dr. Ellis Meng, and Dr. Jun Xie. I am grateful to Xing, not only for helping me academically, but also for being a great friend in life. He gives help whenever needed and always provides invaluable advice. I still remember clearly how Yao taught me to draw my first mask and gave me tips on how to survive the Ph.D. program. Ellis is very nice and interesting to talk to and gives me lots of help. Yong and Jun always made themselves available to help me with my design and process issues, which enabled me to succeed faster. I am very fortunate to have Yong, Jun, and their wives to be among my best friends, who greatly enriched my life at Caltech.

Thanks to all my colleagues in the group: Matthieu Liger, Justin Boland, Ted Harder, Victor Chi-Yuan Shih, Scott Miserendino, Changlin Pang, Angela Tooker, Siyang Zheng, Po-Jui Chen, Quoc Quach, Wen Li, Nick Lo, Damien Rodger, Jason Shih, Tanya Owen, and Trevor Roper. Your support over the years is greatly appreciated. I dare not

attempt a list of friends and associates outside my group, but their contributions are significant and also appreciated.

The interdisciplinary nature of my work has allowed me to have many great collaborators. I would like to thank Prof. Terry D. Lee, Dr. Yunan Miao, and Dr. Jun Liu at City of Hope. They have provided much guidance and assistance for my research. The same gratitude goes to Prof. Jerry Pine, and his students Christopher Rutherglen and Jon Erickson for their assistance on my first neuro-cage project. I want to acknowledge Prof. Ray Deshaies, Dr. Siddharth Dasgupta, and Johannes Graumann for their help in the tandem-LC project. It has been a great pleasure to interact with and learn from these great people from different disciplines.

I am deeply grateful to my parents and my wife's parents who are always there for us. Especially, I want to thank my mother for her unconditional love. She cared so deeply for my education at every stage of my life, for which I am deeply appreciative. My mother-in-law helped tremendously when my first baby was born, which gave me plenty of time for research. The time she stayed with us was one of the merriest during my Ph.D. study.

Finally, my deepest gratitude is to my wife, whose love, support, and company has been one of the greatest sources of strength for me. She has the magic to make my longest days feel like the blink of an eye, while turning my bits and pieces of free time into fascinating lifetime memories. We have two incredible daughters who deserve attention, Katherine and Vivien, their smiles and laughter always keep me optimistic, energized, and inspired.

Abstract

Integrated Nano Liquid Chromatography System On-a-Chip

Thesis by

Qing He

Doctor of Philosophy in Electrical Engineering

California Institute of Technology

Integrated liquid chromatography (LC) chips are valued because of their significant advantages over conventional systems. However, they are very challenging to build due to the high complexity of LC systems and the need for high-level integration of many discrete microfluidic devices.

The goal of this thesis is to develop technologies and devices towards a totally integrated LC system on-a-chip. Using parylene microfluidics technology, all of the devices are integrated on silicon wafers with CMOS-compatible batch processes. Due to the small size of the on-chip LC columns, the chips all perform nano LC, which means that the flow rates are on the scale of nano liters per minute.

The thesis starts with the solution of the problem of bead integration, since most

LC columns are packed with micro-beads. A wafer-scale batch process is developed to integrate beads into micromachined devices. The technology is applied to make an LC-ESI (Electro-Spray Ionization) chip with an integrated bead column packed with 5 μm diameter C18 silica beads. The integrated ESI nozzle allows direct coupling to a mass spectrometer (MS).

Due to the high-pressure nature of LC operations, a complete LC chip must be able to both withstand and generate high pressures on-chip. Therefore, an anchoring technique is developed to dramatically increase the pressure rating of parylene devices from about 30 psi to 1000 psi. In addition, on-chip high-pressure generation is achieved with electrolysis-based micro-actuators.

An integrated ion liquid chromatography chip is demonstrated, which has on-chip column, filters, injection structure, and conductivity detector. The column is packed with 7 μm anion-exchange beads with a slurry packing technique. On-chip sample injection, separation, and detection of seven common anions are successfully demonstrated with a sensitivity of 1 ppm.

Finally, a microchip that demonstrates high-pressure LC with integrated ESI coupling to MS is presented. The capacity of the column, which is 6.5 cm long and packed with 5 μm C18 silica beads, is the highest of all the devices in the thesis. Gradient separation at a pressure of 450 psi and on-line MS detection of digested cytochrome c protein is successfully performed.

Table of Contents

| | | |
|------------------|---|----|
| Chapter 1 | Introduction | 1 |
| 1.1 | From IC to MEMS | 1 |
| 1.2 | Micro-Electro-Mechanical Systems | 3 |
| 1.2.1 | Introduction | 3 |
| 1.2.2 | Advantages | 4 |
| 1.2.3 | Fabrication Technologies | 6 |
| 1.2.4 | From MEMS to μ TAS | 7 |
| 1.3 | Microfluidics, Lab-on-a-Chip, and μ TAS | 7 |
| 1.3.1 | Introduction | 7 |
| 1.3.2 | Future Challenges | 9 |
| 1.4 | Parylene Microfluidics Technology | 11 |
| 1.4.1 | Introduction to Parylene | 11 |
| 1.4.2 | Parylene Technology for Liquid Chromatography On-a-Chip | 15 |
| 1.5 | Bibliography | 17 |
| Chapter 2 | Nano HPLC | 21 |
| 2.1 | High-Performance Liquid Chromatography | 21 |
| 2.1.1 | Introduction | 21 |
| 2.1.2 | History | 23 |
| 2.1.3 | Theory | 25 |
| 2.1.3.1 | Chromatogram and Important Equations | 25 |
| 2.1.3.2 | Band Broadening and van Deemter Equation | 29 |
| 2.1.3.3 | Band Broadening vs. Separation | 31 |
| 2.1.3.4 | Height Equivalent to a Theoretical Plate | 33 |

| | | |
|---|--|-----------|
| 2.1.4 | Instrumentation..... | 34 |
| 2.1.4.1 | Solvents..... | 35 |
| 2.1.4.2 | Pumps..... | 35 |
| 2.1.4.3 | Sample Injectors..... | 35 |
| 2.1.4.4 | Chromatographic Columns..... | 36 |
| 2.1.4.4.1 | Column Dimension..... | 36 |
| 2.1.4.4.2 | Column Packing Physical Properties..... | 37 |
| 2.1.4.4.3 | Base Material and Bonded Phases..... | 38 |
| 2.1.4.4.4 | Separation Mechanisms..... | 41 |
| 2.1.4.5 | Detectors..... | 42 |
| 2.2 | Nano HPLC..... | 46 |
| 2.2.1 | Definition..... | 46 |
| 2.2.2 | Miniaturization Benefits..... | 47 |
| 2.3 | Review of Nano HPLC Chips..... | 50 |
| 2.4 | Bibliography..... | 54 |
| Chapter 3 Bead Integration Technology and an LC-ESI/MS Chip..... | | 57 |
| 3.1 | Introduction..... | 57 |
| 3.2 | Working with Beads..... | 58 |
| 3.2.1 | Various Terms and Properties..... | 58 |
| 3.2.2 | Aggregation..... | 59 |
| 3.2.3 | Packing and Porosity..... | 60 |
| 3.2.4 | Applications in MEMS..... | 62 |
| 3.3 | Integrating Beads into Micromachined Device..... | 63 |
| 3.3.1 | The Method..... | 63 |
| 3.3.2 | Mixing and Spin-Coating..... | 66 |
| 3.3.3 | Patterning..... | 67 |

| | | |
|------------------|---|-----------|
| 3.3.4 | Parylene Coating..... | 68 |
| 3.3.5 | Releasing..... | 71 |
| 3.4 | LC-ESI/MS Chip with Integrated Bead Column..... | 73 |
| 3.4.1 | Introduction..... | 73 |
| 3.4.2 | Design..... | 73 |
| 3.4.3 | Microchip Fabrication and Packaging..... | 74 |
| 3.4.3.1 | Fabrication Process..... | 74 |
| 3.4.3.2 | Photoresist Releasing Issue..... | 77 |
| 3.4.3.3 | Packaging..... | 81 |
| 3.4.4 | Testing Results and Discussion..... | 82 |
| 3.4.4.1 | Bead Releasing and Column Packing..... | 82 |
| 3.4.4.2 | Pressure Rating..... | 86 |
| 3.4.4.3 | Electrospray to a Mass Spectrometer..... | 87 |
| 3.4.4.4 | Method Validation..... | 89 |
| 3.5 | Summary..... | 90 |
| 3.6 | Bibliography..... | 92 |
| Chapter 4 | High-Pressure Parylene Microfluidics..... | 95 |
| 4.1 | Introduction..... | 95 |
| 4.2 | High-Pressure Rating through Anchoring..... | 96 |
| 4.2.1 | Background..... | 96 |
| 4.2.2 | Design..... | 97 |
| 4.2.3 | Fabrication..... | 97 |
| 4.2.4 | High-Pressure Packaging..... | 99 |
| 4.2.5 | Pressure Rating Testing Results and Discussion..... | 103 |
| 4.3 | High-Pressure Generation through Electrolysis..... | 106 |
| 4.3.1 | Introduction..... | 106 |

| | | |
|---|---|------------|
| 4.3.2 | A Parylene Micro Electrolysis Actuator | 108 |
| 4.3.2.1 | Design and Fabrication | 108 |
| 4.3.2.2 | Electrolysis Bubble Generation and Recombination | 110 |
| 4.3.3 | An Electrolysis Device for High-Pressure Generation | 113 |
| 4.3.3.1 | Design and Fabrication | 113 |
| 4.3.3.2 | Testing Method and Results | 115 |
| 4.4 | Summary | 117 |
| 4.5 | Bibliography | 118 |
| Chapter 5 Ion Chromatography On-a-Chip | | 119 |
| 5.1 | Introduction | 119 |
| 5.1.1 | Abstract | 119 |
| 5.1.2 | Ion Chromatography | 120 |
| 5.1.3 | Nitrate Sensing | 123 |
| 5.2 | Microchip Design | 124 |
| 5.2.1 | Chip Design and Operation | 124 |
| 5.2.2 | Conductivity Sensing | 128 |
| 5.2.2.1 | Conductivity Response Theory | 128 |
| 5.2.2.2 | Conductivity Detector Cell Analysis | 132 |
| 5.2.2.3 | The On-Chip Conductivity Detector | 134 |
| 5.2.3 | Downscaling | 135 |
| 5.3 | Microchip Fabrication | 138 |
| 5.3.1 | Fabrication Process Flow | 138 |
| 5.3.2 | Chip Packaging | 142 |
| 5.4 | Testing Results and Discussion | 143 |
| 5.4.1 | Separation Column Packing | 143 |
| 5.4.2 | Pressure–Flow Rate Relation | 145 |

| | | |
|---|--|------------|
| 5.4.3 | Impedance Frequency Response..... | 147 |
| 5.4.4 | Ion Chromatography Separation..... | 149 |
| 5.5 | Summary..... | 151 |
| 5.6 | Bibliography..... | 153 |
| Chapter 6 A Nano HPLC/MS Chip..... | | 157 |
| 6.1 | Introduction..... | 157 |
| 6.2 | Design and Fabrication..... | 158 |
| 6.2.1 | Microchip Design..... | 158 |
| 6.2.2 | Fabrication Process..... | 159 |
| 6.2.3 | Processing Challenges..... | 164 |
| 6.2.3.1 | Bubbling..... | 164 |
| 6.2.3.2 | Black Silicon..... | 168 |
| 6.2.4 | Packaging..... | 169 |
| 6.3 | Testing Results and Discussion..... | 170 |
| 6.3.1 | Column Pressure Rating..... | 170 |
| 6.3.2 | Pressure–Flow Rate Relation..... | 170 |
| 6.3.3 | LC Separation with On-Line MS Detection..... | 172 |
| 6.4 | Summary..... | 173 |
| 6.5 | Bibliography..... | 175 |
| Chapter 7 Conclusion..... | | 177 |

List of Figures

| | |
|--|----|
| Figure 1-1 (a) The first transistor (Bell Labs); (b) The first integrated circuit (Texas Instruments); (c) Moore's law (Intel); (d) State-of-the-art CPU chip Pentium 4 (Intel)..... | 2 |
| Figure 1-2 Dimensions of MEMS, nanotechnology, and lab-on-a-chip..... | 3 |
| Figure 1-3 Famous MEMS devices | 5 |
| Figure 1-4 Illustration of bulk micromachining and surface micromachining | 7 |
| Figure 1-5 Chemical structures of parylene N, C, and D..... | 11 |
| Figure 1-6 Parylene deposition system and the involved chemical processes..... | 14 |
| Figure 1-7 Parylene microfluidic devices..... | 16 |
| Figure 2-1 Illustration of the chromatographic separation process | 22 |
| Figure 2-2 The inventor of chromatography, Tswett, and his chromatographic device ... | 23 |
| Figure 2-3 Chromatogram and its characteristic features | 25 |
| Figure 2-4 Illustration of band broadening during chromatographic elution | 29 |
| Figure 2-5 Four mechanisms of band broadening | 30 |
| Figure 2-6 Van Deemter Curve | 31 |
| Figure 2-7 Band broadening effect vs. separation effect | 32 |
| Figure 2-8 Definition of HETP | 34 |
| Figure 2-9 Schematics for a typical HPLC system..... | 34 |
| Figure 2-10 Injection valve working mechanism | 36 |
| Figure 2-11 Physical properties of liquid chromatographic beads | 37 |
| Figure 2-12 Chemical modification of silica surface..... | 39 |
| Figure 2-13 Chemical structure and 3D illustration of C18 functional groups on silica surface..... | 40 |
| Figure 2-14 Peak width remains nearly unchanged with column ID reduction | 48 |

| | |
|--|----|
| Figure 2-15 Effects of column ID and bead diameter reduction on separation performance | 49 |
| Figure 3-1 Two common particle packing structures (a) BCC; (b) FCC | 61 |
| Figure 3-2 One-shot pump and valve using expandable microspheres | 62 |
| Figure 3-3 Multi-analyte sensor using specially-coated beads | 63 |
| Figure 3-4 Pictures illustrating the major steps for integrating beads into parylene channel | 64 |
| Figure 3-5 Process flow for the testing device for bead integration technology | 65 |
| Figure 3-6 Spin rate effect on the coated photoresist-bead film | 66 |
| Figure 3-7. Spin-coated photoresist-bead film and the mixing ratio effect | 67 |
| Figure 3-8 Patterned bead-photoresist mixture film | 68 |
| Figure 3-9 Scanning electron microscopic pictures of patterned bead-photoresist films. 69 | |
| Figure 3-10 Beads sticking to subsequent parylene cover or to the substrate | 70 |
| Figure 3-11 Parylene thickness effect | 70 |
| Figure 3-12 Photoresist releasing issue | 72 |
| Figure 3-13 Polymer-assisted particle aggregation | 72 |
| Figure 3-14 Fabricated device pictures of the LC-ESI chip | 74 |
| Figure 3-15 Fabrication process flow for the liquid chromatography – electrospray ionization (LC-ESI) chip with integrated bead-column | 76 |
| Figure 3-16 Fluorescent diagnostic technique | 79 |
| Figure 3-17 The photoresist releasing issue in various forms | 80 |
| Figure 3-18 Schematics of the packaging jig for the microchip | 82 |
| Figure 3-19 Snapshots of released beads moving with liquid in a micro-channel | 83 |
| Figure 3-20 Snapshots of packing a column and electrospray to a mass spectrometer | 83 |
| Figure 3-21 Picture of a conventional externally-packed capillary LC column and ESI nozzle | 86 |
| Figure 3-22 Pictures of the mass spectrometer used in the testing | 88 |

| | |
|--|-----|
| Figure 3-23 A typical electrospray spectrum and chromatogram from the on-chip LC column and ESI nozzle | 88 |
| Figure 3-24 MS spectrum for an LC separation of digested cytochrome c using a capillary column packed with photoresist-contaminated-then-cleaned C18 beads | 90 |
| Figure 4-1 Illustration of parylene trench-anchoring and roughening-anchoring | 97 |
| Figure 4-2 Cross-sectional pictures of a trench-anchored parylene channel | 98 |
| Figure 4-3 Top view picture of a roughened moat surrounding a photoresist channel..... | 99 |
| Figure 4-4 Some of the existing coupling techniques..... | 100 |
| Figure 4-5 Exploded view of the packaging scheme | 101 |
| Figure 4-6 Illustration and picture of the packaging after assembly..... | 102 |
| Figure 4-7 Chemical structure of PEEK (polyether-ether-ketone) | 102 |
| Figure 4-8 Jig holes configuration | 103 |
| Figure 4-9 Top view picture of the device used in the pressure rating testing | 104 |
| Figure 4-10 Roughening-anchored channel before and after failure at high pressure.... | 106 |
| Figure 4-11 Trench-anchored channel before and after failure at high pressure | 106 |
| Figure 4-12 Cross-section of a sealed micro electrolysis actuation chamber | 108 |
| Figure 4-13 Top view of a self-sealing electrolysis actuator | 109 |
| Figure 4-14 Pictures of the sealed micro electrolysis actuator | 110 |
| Figure 4-15 Snapshots of activation and deactivation of the actuator filled with DI water | 111 |
| Figure 4-16 Snapshots of activation and deactivation of the actuator filled with 10% of acetonitrile in DI water | 112 |
| Figure 4-17 Snapshots of activation and deactivation of the actuator filled with 10% of methanol in DI water | 113 |
| Figure 4-18 Top view picture and cross-sectional illustration of the high-pressure electrolysis device..... | 114 |
| Figure 4-19 Electrolysis generated pressures at fixed currents | 116 |

| | |
|---|-----|
| Figure 4-20 Voltage versus balance pressure at fixed currents..... | 116 |
| Figure 5-1 Brita ion-exchange filter | 121 |
| Figure 5-2 (a) Fluorescent overview picture of the integrated ion chromatography chip before column packing. (b) Optical picture of the device after bead packing..... | 126 |
| Figure 5-3 3D illustration of the device..... | 126 |
| Figure 5-4 Illustration of the ion chromatography chip..... | 127 |
| Figure 5-5 Illustrations of on-chip injection, separation, and detection of the ion chromatography chip | 127 |
| Figure 5-6 Configurations of the interdigitated electrodes in the conductivity detector cell | 132 |
| Figure 5-7 Common anions separation using a commercial HPLC system | 135 |
| Figure 5-8 Fabrication process flow | 141 |
| Figure 5-9 Illustration and pictures of the fabricated device after bead packing..... | 142 |
| Figure 5-10 Packaged chip after wire bonding..... | 143 |
| Figure 5-11 Anion exchange beads used in the column packing..... | 144 |
| Figure 5-12 Pressure–flow rate curve for an on-chip packed column..... | 146 |
| Figure 5-13 Conductivity detector cell equivalent circuit | 147 |
| Figure 5-14 Theoretical impedance frequency response | 148 |
| Figure 5-15 Impedance frequency spectrum of the mobile phase solution in contact with the on-chip interdigitated platinum electrodes..... | 149 |
| Figure 5-16 Chromatogram of an on-chip ion chromatographic separation of seven anions | 150 |
| Figure 6-1 Overview of the HPLC-ESI/MS microchip before and after bead packing.. | 158 |
| Figure 6-2 Fabrication process flow for the chip..... | 161 |
| Figure 6-3 Cross-sectional pictures of the fabricated device. The parylene microfluidic channels are anchored to the silicon substrate, greatly improving its pressure rating.... | 162 |
| Figure 6-4 Comparison of two anchored-channel cross-sections..... | 163 |

| | |
|--|-----|
| Figure 6-5 Epoxy overcoating for device strengthening and passivation..... | 163 |
| Figure 6-6 Bubbling in the photoresist channels during parylene etching | 164 |
| Figure 6-7 Samples with no parylene coating appear intact after baking 10 minutes at 180 °C | 166 |
| Figure 6-8 Samples with parylene coating generate bubbles in the channels immediately after being heated at 170 °C..... | 166 |
| Figure 6-9 Samples with 5 hours of extra baking before parylene coating, baked for 10 minutes at 180 °C..... | 167 |
| Figure 6-10 Silicon needles at the bottom of trench | 168 |
| Figure 6-11 Packaging for the chip..... | 169 |
| Figure 6-12 Pressure vs. flow rate testing result for the on-chip packed column..... | 172 |
| Figure 6-13 Separation result of tryptic digested cytochrome c sample using on-chip reversed-phase gradient separation coupled with online mass spectrometry detection.. | 173 |

List of Tables

| | |
|--|-----|
| Table 1-1 A selected list of properties for parylene N, C, and D | 13 |
| Table 2-1 Milestones in the history of HPLC development | 24 |
| Table 2-2 Typical sensitivity data for common HPLC detectors | 43 |
| Table 2-3 Nomenclature for HPLC systems | 47 |
| Table 3-1 Summary of an on-chip column properties | 85 |
| Table 4-1 Summary of the pressure testing results | 105 |
| Table 5-1 Limiting equivalent ionic conductances in aqueous solution at 25 °C..... | 129 |
| Table 5-2 Downscaling from the Hamilton LC system to the on-chip LC system..... | 138 |

CHAPTER 1

INTRODUCTION

1.1 From IC to MEMS

The last four decades witnessed a revolution in information technology, whose cornerstone is the development of semiconductor integrated circuits (IC). It all started in 1947 when the first transistor (Figure 1-1 (a)) was invented by Bardeen, Brattain, and Shockley at Bell Laboratories, who a decade later shared the Nobel Prize in Physics (1956). Soon, the little transistors replaced the bulky vacuum tubes and became commonplace in everything from radios to telephones. In 1958 and 1959 respectively, Kilby at Texas Instruments and Noyce at Fairchild Semiconductor both independently invented the first integrated circuits. Kilby was awarded the Nobel Prize in Physics (2000) for his part in the invention of the IC (Figure 1-1 (b)). The idea of integration quickly caught people's attention and the IC has evolved at an astonishing pace ever since. In 1965, Gordon Moore predicted that the transistor count on a chip would double every 18

months [1, 2]. This predication is now known as Moore's law. The law has become enormously influential for the semiconductor industry, which continues to develop better, cheaper, and smaller chips following the roadmap set by Moore (Figure 1-1 (c)). The state-of-the-art CPU chip, Intel's Pentium 4 (Figure 1-1 (d)), already integrates 125 million transistors. It is really amazing that those primitive devices (Figure 1-1 (a) (b)) could grow into such a giant dynamic semiconductor industry, which has changed fundamentally how we live, think, and communicate, and will continue to do so for years to come.

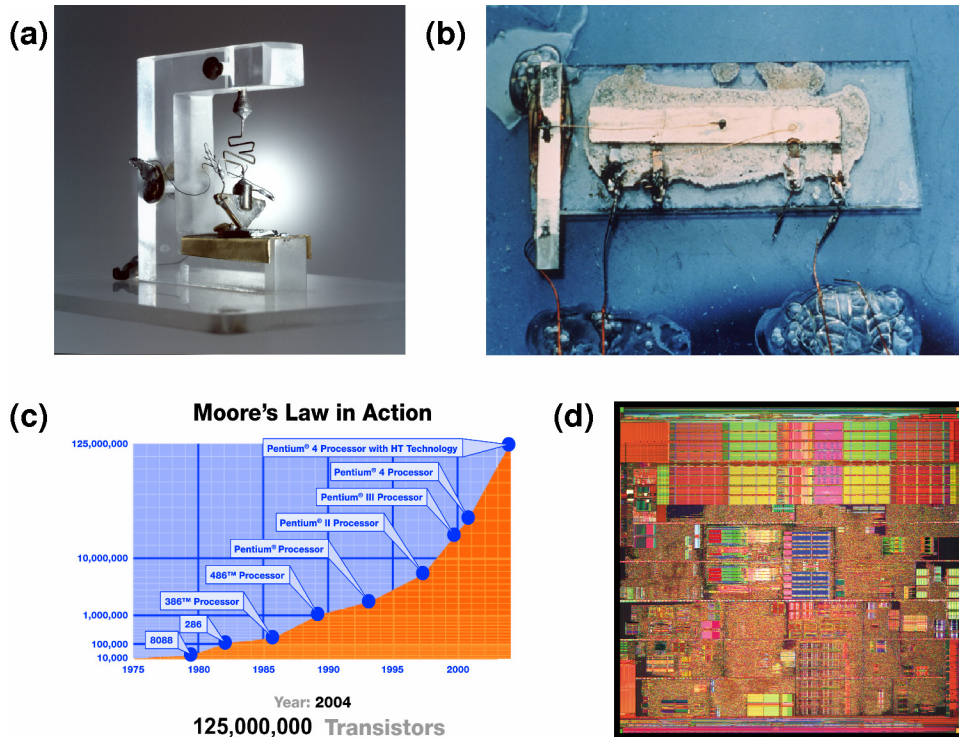


Figure 1-1 (a) The first transistor (Bell Labs); (b) The first integrated circuit (Texas Instruments); (c) Moore's law (Intel); (d) State-of-the-art CPU chip Pentium 4 (Intel).

With the success and knowledge obtained from miniaturization and integration of electronic devices, the potential of accomplishing a similar revolution also emerged for

mechanical and later fluidic devices, which led to the fields of MEMS (Micro-Electro-Mechanical Systems) and μ TAS (Micro Total Analysis Systems).

1.2 Micro-Electro-Mechanical Systems

1.2.1 Introduction

A Micro-Electro-Mechanical System (MEMS) is a microfabricated system that contains both electrical and mechanical components. Its characteristic dimensions, as shown in Figure 1-2, range from 100 nm to millimeters. MEMS are also called micromachines or microsystems technology (MST). MEMS devices serve as one of the bridges connecting the digital world of the integrated circuits with the analog physical world.

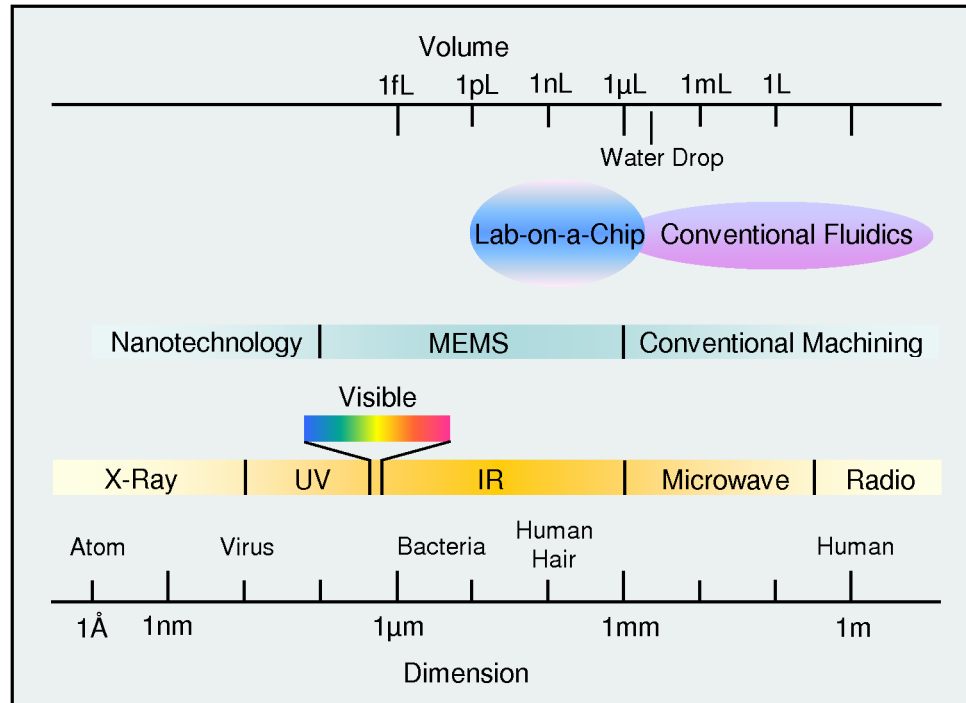


Figure 1-2 Dimensions of MEMS, nanotechnology, and lab-on-a-chip, compared to electromagnetic spectrum and everyday objects.

In 1959, Richard Feynman gave his famous speech titled “There’s plenty of room at the bottom,” in which he mapped out the tremendous potentialities for the miniaturization of machines [3]. In 1965, arguably the first MEMS device, a resonant gate transistor, was demonstrated [4]. In 1982, Kurt Peterson’s groundbreaking paper “Silicon as a mechanical material” [5] summarized many developments to that date, which greatly increased the awareness of MEMS and served as the starting point for realizing Feynman’s dreams. In 1989, researchers at University of California, Berkeley demonstrated the first IC-processed electrostatic micro-motors [6, 7], after which a wide variety of MEMS devices, technologies, and applications blossomed, and the field developed rapidly ever since [8]. Although their complexities are still far from those of state-of-the-art ICs, MEMS devices have shown many hallmarks of ICs such as multi-level stacking (Figure 1-3 (a)) and large-scale integration (LSI) (Figure 1-3 (b)) [9]. MEMS devices also achieved remarkable commercial successes, such as inkjet printer heads from Hewlett Packard, pressure sensors from Honeywell and Motorola, Digital Light Processing (DLP) system from Texas Instruments (Figure 1-3 (c)), and accelerometers from Analog Devices (Figure 1-3 (d)).

1.2.2 Advantages

MEMS technology produces devices that are smaller, better, and cheaper. MEMS chips have significantly smaller footprints than their conventional counterparts. For example, microfabricated needles are minimally invasive and almost entirely painless. By exploiting phenomena that are better or more efficient with downsizing, MEMS devices are often faster, less power-consuming, and more sensitive and selective. Due to

downsizing, in the microscopic world, for instance, gravity is no longer important; surface effects dominant; thermal time constant is minimized; and fluids behave as laminar flows. Moreover, the per-unit cost is low due to MEMS batch fabrication. In addition, MEMS offers new functions that never have been possible before. Its future is even more exciting considering its ability to integrate with ICs.

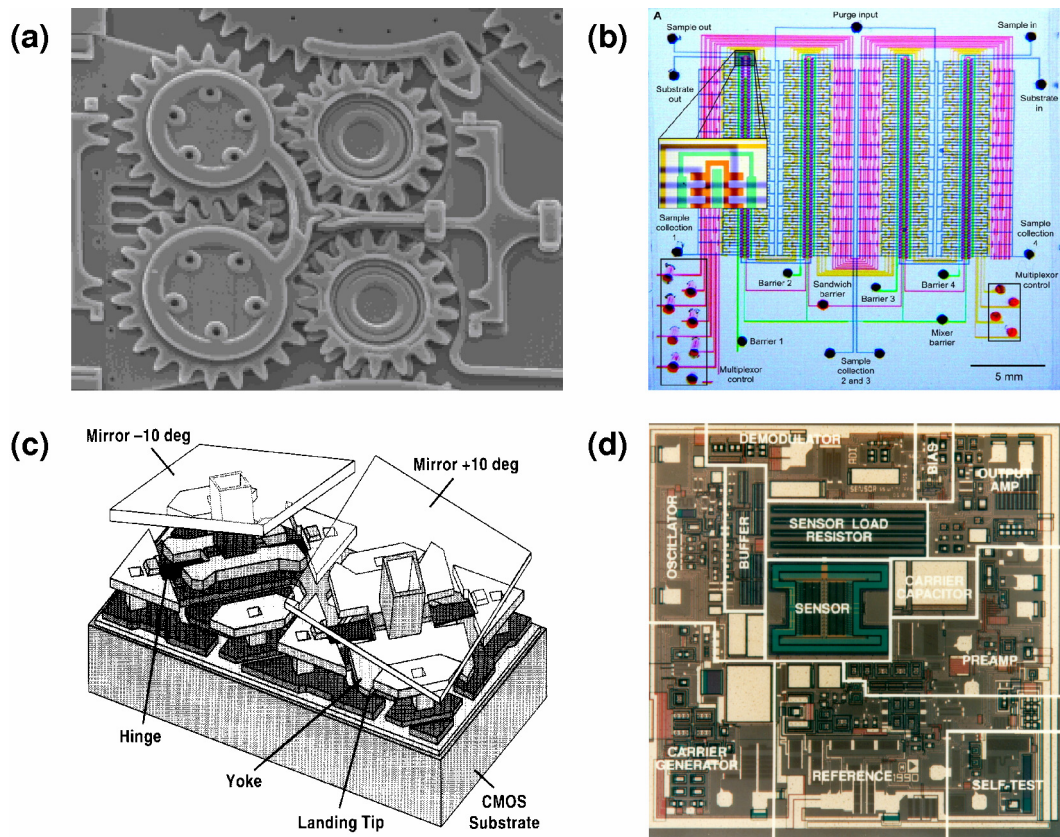


Figure 1-3 Famous MEMS devices. (a) Multi-level MEMS gears (Sandia National Lab); (b) Large-scale integration of miniature pumps and valves; (c) Digital micro-mirror device for digital light processing (Texas Instruments); (d) Monolithic accelerometer (Analog Devices).

1.2.3 Fabrication Technologies

Because of its root in the IC industry, many of MEMS basic processing techniques are borrowed or adapted from those used to produce ICs, such as photolithography, oxidation, diffusion, ion implantation, chemical vapor deposition (CVD), evaporation, sputtering, wet chemical etching, and dry plasma etching [10]. Many microfabrication techniques specifically for MEMS have also been developed over the years, such as KOH, DRIE (deep reactive-ion-etching), LIGA (German acronym for x-ray lithography, electroforming, and molding), wafer bonding, electroplating, and 3D stereo lithography [11]. In recent years, polymer MEMS have become popular, resulting in many new techniques suitable for polymers, for instance soft lithography [12–14].

Multiple basic microfabrication processes are combined to make complete devices in two general ways, bulk micromachining [15] and surface micromachining [16]. As illustrated in Figure 1-4, bulk micromachining uses chemical or plasma selective etching of substrate material, with the help of masking films, to form structures in the substrate. The etching process can be either isotropic such as HNA (hydrofluoric acid + nitric acid + acetic acid), XeF_2 , or anisotropic such as KOH, TMAH (tetra-methyl-ammonium-hydroxide), and DRIE. Surface micromachining, on the other hand, builds devices on top of the substrate, usually with the help of sacrificial materials, to form freestanding or even completely released thin-film microstructures, such as micro-channels and micro-cantilevers (Figure 1-4). Common sacrificial materials are photoresist, polyimide, metals, phosphosilicate glass (PSG), and polysilicon.

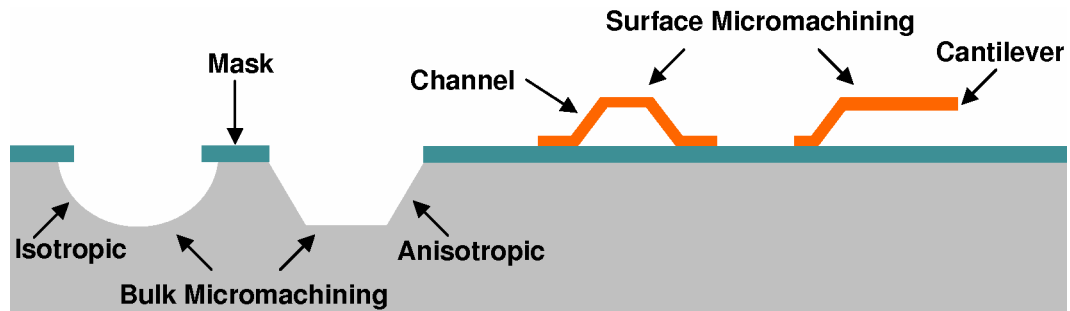


Figure 1-4 Illustration of bulk micromachining and surface micromachining.

1.2.4 From MEMS to μ TAS

Although MEMS started in the mechanical world, the field soon grew rapidly to encompass a wide spectrum of applications in many sub and spin-off fields, such as MOEMS (Micro-Optical-Electro-Mechanical System), RF-MEMS, and μ TAS (Micro Total Analysis Systems). At the present time, μ TAS is the one of the fastest growing subfields, which is highly interdisciplinary by nature, covering areas such as microfluidics, material science, analytical chemistry, and biotechnology.

1.3 Microfluidics, Lab-on-a-Chip, and μ TAS

1.3.1 Introduction

Microfluidics generally refers to the science and technology of manipulating minute amounts of fluids with volumes ranging from micro liters ($1 \mu\text{L} = (1 \text{ mm})^3$) to pico liters ($1 \text{ pL} = (10 \mu\text{m})^3$) (Figure 1-2). Lab-on-a-chip is the miniaturization and integration of the complete functionality of a chemistry or biology lab, such as sample preparation, reactions, separations, and detection, onto a single chip. Microfluidics is the key to the development of lab-on-a-chip, which is also called μ TAS, the miniaturized

microfluidic system that can automatically carry out all the necessary functions to transform chemical information into electronic information. Microfluidics is a more general term than μ TAS.

The concept of μ TAS was first suggested by Manz in 1990 [17], although the first μ TAS device, a miniaturized gas chromatography system, was demonstrated in 1979 [18]. Today, μ TAS has grown tremendously into a large dynamic multidisciplinary field, whose impact could be far-reaching and revolutionary. The field is extensively reviewed in several papers from Manz's group [19–21].

The advantages of μ TAS include significantly reduced size (portability), power consumption, sample and reagent consumption, and manufacture and operating costs (disposability). In addition, μ TAS can achieve better performance in terms of speed, throughput, mass sensitivity, and automation.

It should be noted, however, unlike its integrated circuit analog, which emphasizes continuous reduction of transistor size, μ TAS focuses on making more complex systems with more sophisticated fluid handling capabilities, rather than pushing for the smallest micro-channels possible.

The field of μ TAS finds applications in proteomics and genomics research, high-throughput screening (HTS) of drug candidates, point-of-care (POC) diagnostics, drug delivery, environment monitoring, industrial online analysis, food safety, forensics, bio-defense and many more.

1.3.2 Future Challenges

After over a decade of research and development on μ TAS, it is interesting to discuss its pressing issues and future challenges. The most important ones are sample preparation, world-to-chip interfacing, on-chip chromatographic separation, on-chip feedback control, detection, and total integration.

The integration of sample preparation into microfluidic devices represents one of the main hurdles towards achieving true functional lab-on-a-chip. It becomes more challenging for the enormous variation in samples to be analyzed, and/or the complex raw material in the environment. This problem may have to be handled on a case by case basis. Two reviews on sample preparation in microfluidic systems are given in [22, 23].

Even with preprocessed samples, coupling of the samples, reagents, and conventional macro-scale tubing to the chips, often referred to as “world-to-chip interfacing,” remains a difficult problem. Although the chip may only need a nano liter sample, it is impossible for conventional scale fluidics to handle such a small amount. A much larger volume has to be started with, unless the chip can acquire a nano liter sample from its environment directly. Coupling conventional-scale fluidics with microfluidics is also challenging, especially since no packaging standard is set. Microfluidic chips are usually small and thin, which makes most conventional coupling techniques unrealistic. New coupling methods that are not significantly larger than the chip need to be developed [24]. Especially for high-pressure applications, such as liquid chromatography, reliable coupling with high-pressure ratings is highly desired.

On-chip liquid chromatographic separation with bead-packed column is highly underdeveloped, due to the complexity of individual devices involved and the difficulty

of integration for a complete on-chip system. Liquid chromatography, further discussed in Chapter 2, is the most important separation technique in analytical chemistry. It essentially eliminates highly specific sensing, which is very difficult to achieve.

On-chip feedback control is not widely implemented even today, although its importance is starting to be realized. Conventional transducers are not sensitive enough or practical for monitoring on-chip flows and reactions. It is highly desirable and useful to know the operating conditions of the chip in real time. Devices based on silicon or glass would be better than those based on PDMS (polydimethylsiloxane), since it is much easier to integrate electrodes and circuits on silicon or glass substrates.

Optical detection does not scale down well. With miniaturization of the micro-channels, the usable optical path is greatly reduced, which leads to a significantly reduced optical signal and thus lower sensitivity for optical techniques, such as UV absorbance. Selectivity is also a serious issue. For conventional analysis, selectivity is usually accomplished through chromatography-based separation prior to detection. However, on-chip liquid chromatography is highly underdeveloped, limiting the ability to separate sample compounds on-chip and hence limiting selectivity. Furthermore, many of today's detectors are still off-chip, especially those based on optics and mass spectrometry. When the detector is significantly larger than the chip itself, the whole setup is far from a real "lab-on-a-chip."

Most of the developments in μ TAS so far have been focusing on discrete devices, such as micro-channels, micro-valves, micro-pumps, flow sensors, pressure sensors, and electrochemical sensors. However, total integration is an important trend for μ TAS. Multi-chip packaging and complex fluidic/electrical interconnects are labor-intensive,

inefficient, unreliable, and costly. The integration process is not trivial at all. Firstly, most individual devices are built with incompatible technologies. The desired approach would be to micromachine every part in a compatible way. Secondly, there are few technologies that are sufficiently versatile to make the wide variety of devices needed for the system, while still powerful enough to keep each device optimized. Parylene microfluidics technology, as described in the next section, is a great candidate.

1.4 Parylene Microfluidics Technology

1.4.1 Introduction to Parylene

Parylene (poly-para-xylylene) is the generic name for members of a unique vapor phase deposited thermoplastic polymer series. Discovered in 1947 and commercialized by Union Carbide Corporation in 1965, parylene is used in several industries because of its superior properties. The primary application is PCB (printed circuit board) coating in the electronics industry, where parylene protects the delicate electronic devices against moisture and corrosive environments. Figure 1-5 shows the chemical structures for the three most commonly used parylene types: parylene N, parylene C, and parylene D.

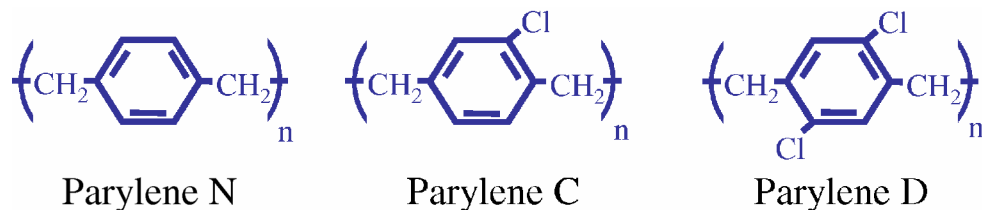


Figure 1-5 Chemical structures of parylene N, C, and D.

Parylene is deposited at room temperature by chemical vapor deposition (CVD). The deposited film is highly conformal and truly pinhole free. It is also an excellent

barrier to gas and moisture. The gas permeability of parylene is more than four orders of magnitude smaller than that of PDMS (polydimethylsiloxane), which is another popular material for microfluidic devices. Moisture vapor transmission is ten times less than silicones.

Parylene is extremely inert to most chemicals and solvents. Based on the manufacturer's study [25], solvents have minor swelling effect on parylene N, C, and D with a 3% maximum increase in film thickness. The swelling is found to be completely reversible after the solvents are removed by vacuum drying. Inorganic reagents, except for oxidizing agents at elevated temperatures, have little effects on parylene. Parylene is also biocompatible (USP Class VI), which means it is safe for long-term human implants.

Parylene exhibits impressive mechanical strength and flexibility in a thin film coating. Its Young's modulus is between silicon and PDMS, so it can be used to make both rigid structures and flexible actuators.

Parylene is an excellent electrical insulator as well as a good thermal insulator. For example, the breakdown voltage for 1 μm thick parylene is over 200 volts, and the thermal conductivity of parylene C is only four times that of air (0.21 $\text{mW}/(\text{cm}\cdot\text{K})$).

Optically, parylene is transparent in the visible light range. It only absorbs light under 280 nm in wavelength, which unfortunately limits its UV applications.

Due to their slightly different chemical structures, the three types of parylene also differ in properties. Parylene N has the best penetration characteristics. However, parylene N also has the slowest deposition rate. Parylene D can withstand higher temperatures than parylene C. Parylene C has a useful combination of electrical and physical properties plus a very low permeability to moisture and other corrosive gases.

Moreover, deposition of parylene C is faster than the other two. Parylene C is the parylene of choice for most conventional and microfluidic applications.

Detailed electrical, mechanical, thermal, barrier, optical, and other properties can be found on a parylene vendor's website [26]. A list of selected properties for parylene N, C, and D are shown in Table 1-1.

| | Parylene N | Parylene C | Parylene D |
|--|------------|------------|------------|
| Breakdown Voltage (V) for 1 μm Film | 276 | 220 | 217 |
| Dielectric Constant at 1 kHz | 2.65 | 3.10 | 2.82 |
| Volume Resistivity ($\times 10^{16}$ $\Omega \cdot \text{cm}$) | 14 | 8.8 | 12 |
| Young's Modulus (GPa) | 2.42 | 2.76 | 2.62 |
| Density (g/cm^3) | 1.1 | 1.3 | 1.4 |
| Index of Refraction | 1.66 | 1.64 | 1.67 |
| Strong UV Absorption (nm) | < 280 | < 280 | NA |
| Water Absorption (% after 24 hours) | < 0.1 | < 0.1 | < 0.1 |
| Melting Temperature ($^{\circ}\text{C}$) | 420 | 290 | 380 |
| Glass Transition Temperature ($^{\circ}\text{C}$) | NA | 80–100 | NA |
| Linear Coefficient of Expansion ($\text{ppm}/^{\circ}\text{C}$) | 69 | 35 | 30–80 |
| Thermal Conductivity at 25 $^{\circ}\text{C}$ ($\text{mW}/(\text{cm}\cdot\text{K})$) | 1.26 | 0.84 | NA |

Table 1-1 A selected list of properties for parylene N, C, and D.

The parylene deposition process and the involved chemical processes are illustrated in Figure 1-6. The process starts with placing parylene dimer (di-para-xylylene), a stable compound in granular form, into the vaporizer, and the substrate to be coated into the deposition chamber. The whole system is pumped down to medium vacuum. The dimer is heated in the vaporizer and sublimates into vapor at around 160 $^{\circ}\text{C}$. The dimer vapor enters the pyrolysis furnace that is maintained at 690 $^{\circ}\text{C}$, where the dimers are cleaved into identical monomers (para-xylylene). In the room-temperature

deposition chamber, the monomers reunite on all exposed surfaces in the form of polymers (poly-(para-xylylene)). The deposition takes place at molecular level. The monomers are extremely active molecules having mean free path on the order of 1 mm (under deposition pressure of around 100 mTorr), which results in superior penetration power and a high degree of conformability to the surfaces being coated. The coated substrate temperature never rises more than a few degrees above ambient. Additional components of the system include a mechanical vacuum pump and associated cold trap. Although parylene N structure is used in Figure 1-6, the process is almost identical for all three common types of parylene, except for some slight differences in pyrolysis temperature and deposition pressure.

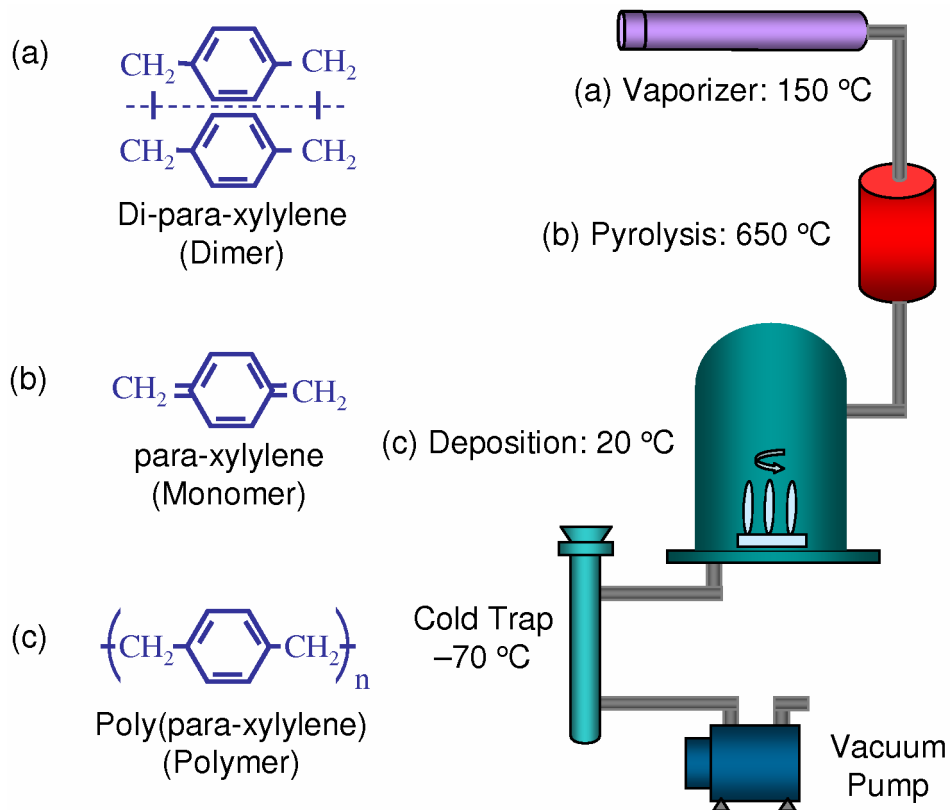


Figure 1-6 Parylene deposition system and the involved chemical processes.

Typical coating thickness ranges from one to tens of microns. It can also be as thin as hundreds of angstroms. The coating thickness can be controlled by the amount of dimer used. The normal deposition rate of parylene C is about 5 μm per hour. The deposition rate is directly proportional to the square of the monomer concentration and inversely proportional to the absolute temperature [26]. Higher deposition rates, however, can result in poor film quality, which often appears as a milky (cloudy) film in contrast to normal clear transparent ones.

1.4.2 Parylene Technology for Liquid Chromatography On-a-Chip

Besides its superior properties, parylene is well suited for μTAS applications because of its ease of integration with other microfabrication techniques.

Parylene's room-temperature deposition makes it post-CMOS compatible, which allows parylene devices to have electrodes, sensors, and even circuits. Parylene's conformal coating enables it to form complicated structures with great step coverage. Moreover, parylene is bio-compatible which makes it suitable for biological sensing applications and implant devices. As an organic polymer, parylene can be easily etched with oxygen plasma, using photoresist or metal as a mask.

Parylene technology is proven to produce a wide variety of devices, including many important microfluidic devices, such as channels, micro-pumps, micro-valves, filters, pressure and flow sensors, mass flow controllers, electrospray nozzles, and gas chromatography columns (Figure 1-7) [27–32]. These microfluidic devices all have compatible fabrication processes, which potentially can all be integrated with a single batch fabrication to make a real micro total analysis system.

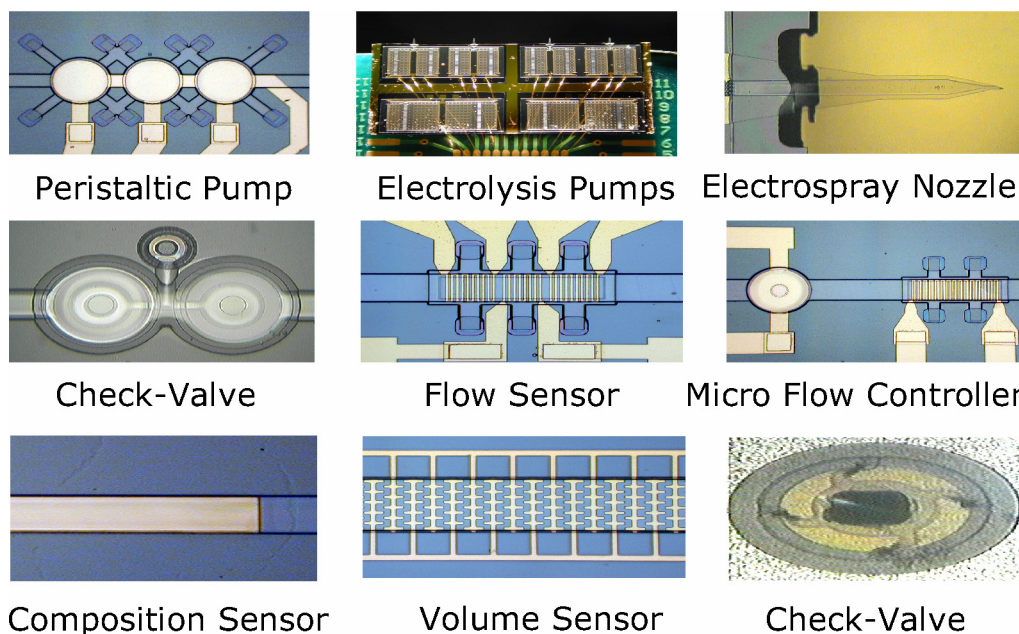


Figure 1-7 Parylene microfluidic devices.

Furthermore, parylene technology is a great candidate for making liquid chromatography (LC) on-a-chip. An LC system is a complicated, highly-coordinated fluidic system that contains reservoirs, tubing, filters, pumps, pressure sensors, flow sensors, valves, mixers, columns, and electro spray nozzle if coupled with mass spectrometry (MS). To miniaturize an LC system, the microfabrication technology has to be versatile and powerful. Parylene technology certainly provides such opportunity for the total integration of an LC system on-a-chip. In addition, as an LC column wall material, parylene's inertness provides unique advantages such as larger pH range and fewer surface functional groups than those of silica.

1.5 Bibliography

- [1] G. E. Moore, "Cramming more components onto integrated circuits" (Reprinted from *Electronics*, p. 114–117, April 19, 1965). *Proceedings of the IEEE*, 1998. 86(1): p. 82–85.
- [2] G. E. Moore, "Cramming more components onto integrated circuits." *Electronics*, 1965. 38(8): p. 114–117.
- [3] R. P. Feynman, "There's plenty of room at the bottom." *Journal of Microelectromechanical Systems*, 1992. 1(1): p. 60–66.
- [4] H. C. Nathanson, W. E. Newell, R. A. Wickstrom, and J. J. R. Davis, "The resonant gate transistor." *IEEE Trans. Electron Devices*, 1967. 14(3): p. 117–133.
- [5] K. E. Petersen, "Silicon as a mechanical material." *Proceedings of the IEEE*, 1982. 70(5): p. 420–457.
- [6] L.-S. Fan, Y.-C. Tai, and R. S. Muller, "IC-Processed electrostatic micromotors." *Sensors and Actuators*, 1989. 20(1–2): p. 41–47.
- [7] Y.-C. Tai and R. S. Muller, "IC-Processed electrostatic synchronous micromotors." *Sensors and Actuators*, 1989. 20(1–2): p. 49–55.
- [8] G. T. A. Kovacs, *Micromachined transducers sourcebook*. McGraw-Hill series in electrical and computer engineering. 1998. Boston: WCB/McGraw-Hill.
- [9] T. Thorsen, S. J. Maerkl, and S. R. Quake, "Microfluidic large-scale integration." *Science*, 2002. 298(5593): p. 580–584.
- [10] S. Wolf and R. N. Tauber, *Silicon processing for the VLSI era*. 2000. Sunset Beach, Calif.: Lattice Press.

- [11] M. J. Madou, *Fundamentals of microfabrication : the science of miniaturization*. 2nd ed. 2001. Boca Raton, Fla.: CRC Press.
- [12] Y. N. Xia and G. M. Whitesides, "Soft lithography." *Annual Review of Materials Science*, 1998. 28: p. 153–184.
- [13] G. M. Whitesides, E. Ostuni, S. Takayama, X. Y. Jiang, and D. E. Ingber, "Soft lithography in biology and biochemistry." *Annual Review of Biomedical Engineering*, 2001. 3: p. 335–373.
- [14] J. C. McDonald, D. C. Duffy, J. R. Anderson, D. T. Chiu, H. K. Wu, O. J. A. Schueller, and G. M. Whitesides, "Fabrication of microfluidic systems in poly(dimethylsiloxane)." *Electrophoresis*, 2000. 21(1): p. 27–40.
- [15] G. T. A. Kovacs, N. I. Maluf, and K. E. Petersen, "Bulk micromachining of silicon." *Proceedings of the IEEE*, 1998. 86(8): p. 1536–1551.
- [16] J. M. Bustillo, R. T. Howe, and R. S. Muller, "Surface micromachining for microelectromechanical systems." *Proceedings of the IEEE*, 1998. 86(8): p. 1552–1574.
- [17] A. Manz, N. Graber, and H. M. Widmer, "Miniaturized total chemical analysis systems. A novel concept for chemical sensing." *Sensors and Actuators, B: Chemical*, 1990. B1(1–6): p. 244–248.
- [18] S. C. Terry, J. H. Jerman, and J. B. Angell, "Gas-chromatographic air analyzer fabricated on a silicon-wafer." *IEEE Transactions on Electron Devices*, 1979. 26(12): p. 1880–1886.

- [19] D. R. Reyes, D. Iossifidis, P. A. Auroux, and A. Manz, "Micro total analysis systems. 1. Introduction, theory, and technology." *Analytical Chemistry*, 2002. 74(12): p. 2623–2636.
- [20] P. A. Auroux, D. Iossifidis, D. R. Reyes, and A. Manz, "Micro total analysis systems. 2. Analytical standard operations and applications." *Analytical Chemistry*, 2002. 74(12): p. 2637–2652.
- [21] T. Vilkner, D. Janasek, and A. Manz, "Micro total analysis systems. Recent developments." *Analytical Chemistry*, 2004. 76(12): p. 3373–3386.
- [22] A. J. de Mello and N. Beard, "Dealing with 'real' samples: sample pre-treatment in microfluidic systems." *Lab on a Chip*, 2003. 3(1): p. 11N–19N.
- [23] J. Lichtenberg, N. F. de Rooij, and E. Verpoorte, "Sample pretreatment on microfabricated devices." *Talanta*, 2002. 56(2): p. 233–266.
- [24] E. Meng, S. Y. Wu, and Y.-C. Tai, "Silicon couplers for microfluidic applications." *Fresenius Journal of Analytical Chemistry*, 2001. 371(2): p. 270–275.
- [25] Specialty Coating Systems, "Solvent resistance of the parylene." *Trade literature*.
- [26] http://www.scscookson.com/parylene_knowledge/specifications.cfm
- [27] L. Licklider, X. Q. Wang, A. Desai, Y.-C. Tai, and T. D. Lee, "A micromachined chip-based electrospray source for mass spectrometry." *Analytical Chemistry*, 2000. 72(2): p. 367–375.

- [28] J. Xie, Y. Miao, J. Shih, Q. He, J. Liu, Y.-C. Tai, and T. D. Lee, "An electrochemical pumping system for on-chip gradient generation." *Analytical Chemistry*, 2004. 76(13): p. 3756–3763.
- [29] X.-Q. Wang and Y.-C. Tai, "Normally closed in-channel micro check valve." *Proceedings of the 13th IEEE International Conference on Micro Electro Mechanical Systems (MEMS 2000)*. Miyazaki, Japan, 2000. p. 68–73.
- [30] J. Xie, X. Yang, X.-Q. Wang, and Y.-C. Tai, "Surface micromachined leakage proof parylene check valve." *Proceedings of the 14th IEEE International Conference on Micro Electro Mechanical Systems (MEMS 2001)*. Interlaken, Switzerland, 2001. p. 539–542.
- [31] J. Xie, J. Shih, and Y.-C. Tai, "Integrated surface-micromachined mass flow controller." *Proceedings of the 16th IEEE International Conference on Micro Electro Mechanical Systems (MEMS 2003)*. Kyoto, Japan, 2003. p. 20–23.
- [32] H. S. Noh, P. J. Hesketh, and G. C. Frye-Mason, "Parylene gas chromatographic column for rapid thermal cycling." *Journal of Microelectromechanical Systems*, 2002. 11(6): p. 718–725.

CHAPTER 2

NANO HPLC

2.1 High-Performance Liquid Chromatography

2.1.1 Introduction

High-Performance Liquid Chromatography (HPLC) is one of the most powerful, versatile, and widely-used separation techniques. It allows separation, identification, purification, and quantification of the chemical compounds in complex mixtures. It is an indispensable tool in analytical chemistry. It has a wide spectrum of applications in fields such as the pharmaceutical industry, proteomics, the chemical industry, environmental laboratories, the food industry, forensic analysis, and clinical analysis. The only limitation for HPLC is that the sample must be soluble in the liquid phase.

Based on the definition given in [1], chromatography in general includes all separation techniques in which analytes partition between different phases that move relative to each other, or where analytes have different migration velocities, such as in electrokinetic chromatography. In most chromatographic techniques, one phase is

stationary, while the other phase is mobile. When this mobile phase is liquid, the chromatographic technique is called Liquid Chromatography (LC). The LC stationary phase can be either solid or surface functional groups bonded on a solid. High-performance liquid chromatography is comprised of those LC techniques that require the use of elevated pressures to force the liquid through a packed bed of stationary phase, which is highly-efficient for separation. The packing material usually consists of particles with dimensions around 10 μm , which creates a large backpressure in the densely-packed bed. Therefore, the technique is also called high-pressure liquid chromatography.

In short, during the elution process, the surface functional groups (stationary phase) on the particles interact with the sample and eluent (mobile phase). When the injected sample plug is carried through the column by the liquid eluent, different sample components interact with the stationary phase differently, partitioning their time in the stationary and mobile phases, and therefore migrate through the column at different speeds, and exit the column at different times. This process is illustrated in Figure 2-1.

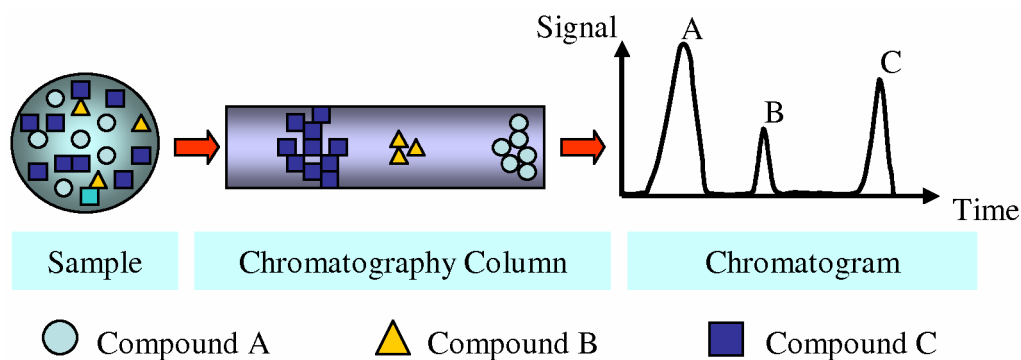


Figure 2-1 Illustration of the chromatographic separation process.

When the solvent composition of the mobile phase is constant, it is called isocratic elution. When a sample mixture contains over 20 compounds, isocratic elution

can be problematic. Early peaks usually have poor resolution and final peaks are broad and flat. Weaker solvents will improve early peaks but worsen the final peaks, while stronger solvents further compress early peaks but improves final peaks. This so-called “general elution problem” can be solved by starting with a weak solvent then gradually increasing solvent strength over time, so that all peaks can be well resolved. The gradient profile can be best determined empirically.

2.1.2 History

Chromatography was invented by a Russian botanist Mikhail Tswett (1872–1919) in 1903 (Figure 2-2) [2]. He employed the technique to separate plant pigments by passing solutions of these species through glass columns packed with finely divided calcium carbonate [3]. The separation appears as colored bands on the column, which is why he named this technique chromatography. The word chromatography is composed of two Greek roots, chroma (color) and graphein (to write).

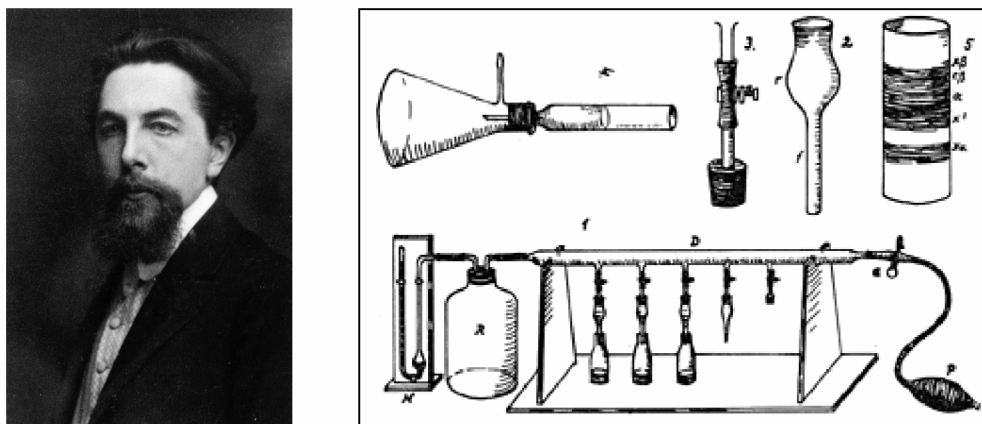


Figure 2-2 The inventor of chromatography, Tswett, and his chromatographic device.

Table 2-1 lists some of the milestones in the development of modern HPLC [4]. In 1941, Martin and Synge developed the theory of partition chromatography and used

mathematics to describe the separation process [5], which became the basis for modern HPLC. They shared the Nobel Prize in Chemistry (1952) for their invention of partition chromatography [6]. Martin also published the first application of gas chromatography with James in 1952. In the same year, gradient elution was demonstrated by Alm. By the late 1960s, LC theories and instrumentations were well established, which led to the first commercially available liquid chromatography system in 1969. Around 1973, packing technologies were advanced so that, for the first time, reproducible high-efficiency columns could be prepared with particles less than 10 μm in diameter. Also in 1973, modification of silica surface via silanization became commercially feasible. These breakthroughs led to the first 10 μm reversed-phase HPLC columns [1]. Since then, HPLC has become one of the most important and fastest-growing techniques in the modern laboratory. The state-of-the-art column liquid chromatography equipment and instrumentation is discussed in a recent review [7].

| | | |
|------|--------------------------------|------------------|
| 1903 | Chromatography Invented | Tswett |
| 1941 | Partition Chromatography | Martin and Synge |
| 1952 | Gas Chromatography | Martin and James |
| 1952 | Gradient Elution | Alm |
| 1969 | First Commercial LC Instrument | |
| 1973 | First Commercial HPLC Column | Waters Corp. |

Table 2-1 Milestones in the history of HPLC development.

2.1.3 Theory

2.1.3.1 Chromatogram and Important Equations

The separated compounds appear as peaks in the chromatogram (Figure 2-3), which is a plot of some function of the compound concentrations versus elution time. Each peak is a Gaussian curve in theory. Retention time of a peak is defined as the time between sample injection and the peak maximum. t_0 is the retention time of the unretained sample, which is the time that the mobile phase takes to travel through the column, also called breakthrough time. If the column length is L_c and the mobile phase linear flow velocity is u , then

$$t_0 = \frac{L_c}{u} \quad (2.1)$$

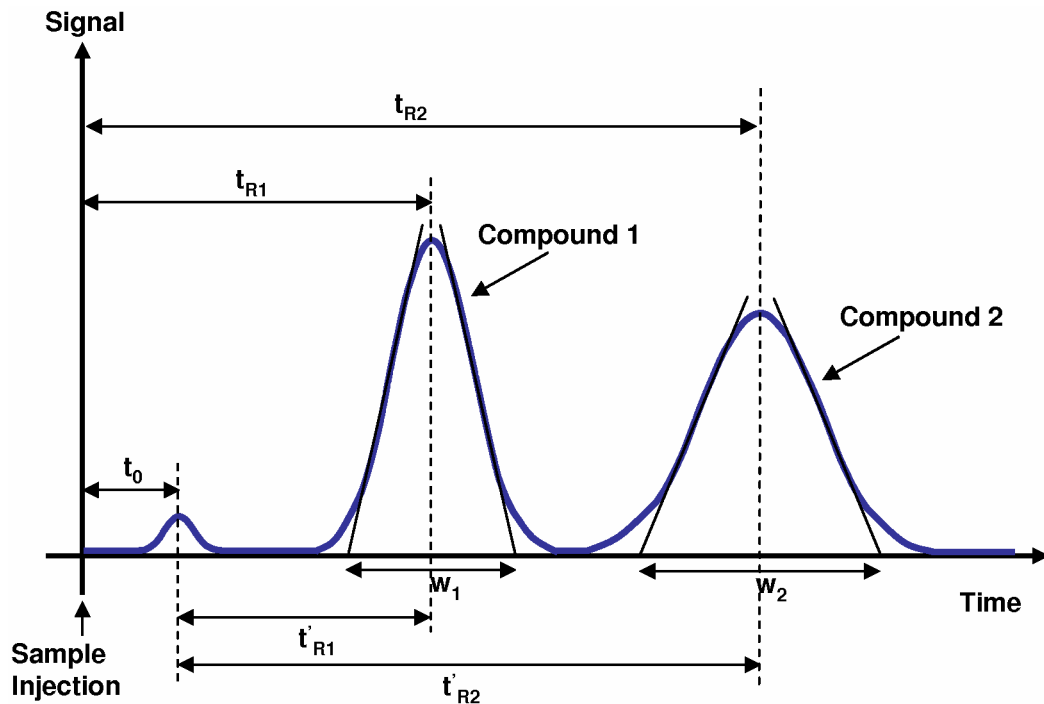


Figure 2-3 Chromatogram and its characteristic features [8].

For most LC separations regardless of column dimension, the optimized linear flow velocity u is on the order of 1 mm/s, as a rule of thumb. The corresponding volumetric flow rate F is:

$$F = \varepsilon u A_c \quad (2.2)$$

where A_c is the column cross-sectional area and ε is the column porosity. For cylindrical columns with inner diameter (ID) of d_c :

$$A_c = \frac{\pi d_c^2}{4} \quad (2.3)$$

The column porosity ε is:

$$\varepsilon = \frac{V_{column} - V_{packing}}{V_{column}} \quad (2.4)$$

where V_{column} is the total volume in the column and $V_{packing}$ is the volume taken up by the solid packing material in the column. The column porosity can also be expressed as the sum of inter-particle porosity and inner-particle porosity.

t_R is the retention time of a retained compound. Two compounds can be separated if they have different retention times. t'_R is the net/adjusted retention time relative to t_0 . Therefore,

$$t_R = t_0 + t'_R \quad (2.5)$$

t_0 represents the time a compound spends in the mobile phase, which is identical for all compounds since compounds only move down the column when they are in the mobile phase. t'_R represents the time spent in the stationary phase. The longer a compound stays in the stationary phase, the later it will be eluted.

To characterize a compound, the retention factor, k , is preferred over the retention time, since the latter also depends on column length and flow velocity. k is given as:

$$k = \frac{t_R'}{t_0} = \frac{t_R - t_0}{t_0} \quad (2.6)$$

k is independent of column length and flow rate and represents the molar ratio of the compound staying preference between the stationary and the mobile phase. Therefore, k can be also expressed as:

$$k = \frac{n_{stationary}}{n_{mobile}} \quad (2.7)$$

where $n_{stationary}$ and n_{mobile} represent the number of molecules of a certain compound in the stationary and mobile phases respectively. Various compounds must have different k values in order to be separated.

The separation factor, α , is defined as:

$$\alpha = \frac{k_2}{k_1} \quad (k_2 > k_1) \quad (2.8)$$

The separation factor shows the chromatographic system's separation power between two compounds, i.e., its selectivity.

As shown in Figure 2-3, w is the peak width. When measured at 13.4% height of a Gaussian peak, w equals four times the standard deviation, σ , of the peak. The resolution, R , of two peaks is defined as the ratio of the two-peak maxima distance to the mean of the two peak widths:

$$R = 2 \frac{t_{R2} - t_{R1}}{w_1 + w_2} \quad (2.9)$$

The more separated and sharp (narrow) the two peaks are, the higher the resolution.

The number of theoretical plates, N , can be calculated from the chromatogram:

$$N = 16 \left(\frac{t_R}{w} \right)^2 \quad (2.10)$$

The equation is correct only if the peak has a Gaussian shape, otherwise, some other approximate equations should be used. Since the calculation of N involves retention time, N can only be derived from isocratic, not gradient, chromatograms. The plate number obtained from a non-retained peak is a measure of the column packing efficiency. Higher N and higher efficiency can be obtained with longer columns, smaller beads, better packing, and better optimized flow velocity. N is proportional to column length, and inversely proportional to bead diameter d_p :

$$N \propto L_c \quad (2.11)$$

$$N \propto \frac{1}{d_p} \quad (2.12)$$

Qualitative and quantitative information about the sample components can be obtained from the chromatogram. The retention time of a compound is always the same under identical chromatographic conditions. Therefore, a compound peak can be identified by comparing to a standard chromatogram with known compounds. The concentration of a compound can be determined by its peak height, which is proportional to the injection concentration. Plots of peak height versus injection concentration, usually linear, can be obtained using samples with known component concentrations.

The concept of reduced/dimensionless parameters allows comparison of different columns. One of the most frequently used parameters is dimensionless flow resistance:

$$\Phi = \frac{\Delta P d_p^2}{L_c \eta u} \quad (2.13)$$

where ΔP is the pressure drop across the column, L_c is the column length, η is the viscosity of the mobile phase. Φ is between 500 (spherical beads) and 1000 (irregular beads) for columns packed with totally porous materials. This equation can also be rearranged to estimate column backpressure:

$$\Delta P = \frac{\Phi L_c \eta u}{d_p^2} \quad (2.14)$$

2.1.3.2 Band Broadening and van Deemter Equation

Chromatographic bands increasingly broaden as the bands move down the column (Figure 2-4). Band broadening reflects a loss of column efficiency. There are four reasons for band broadening.

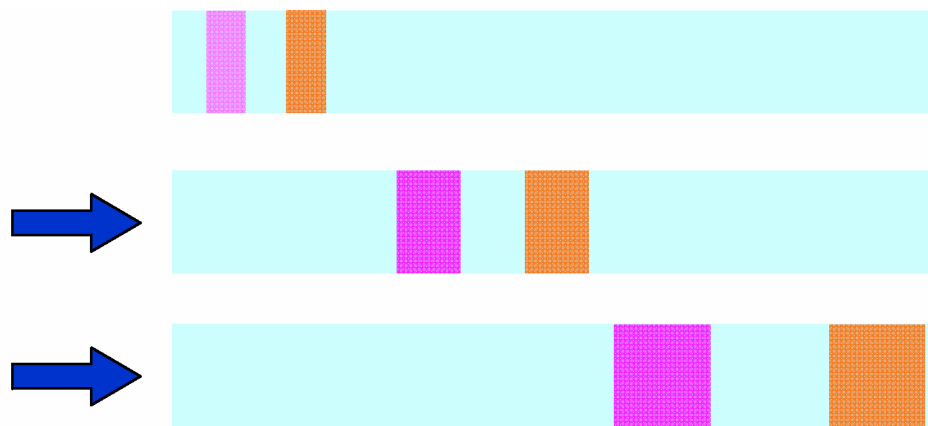


Figure 2-4 Illustration of band broadening during chromatographic elution.

The first is eddy diffusion (multi-path effect) (Figure 2-5 (a)). There are always some sample molecules in the band that go rather straight in the column and exit earlier, while others have many diversions along the way and exit later.

The second is flow distribution of the mobile phase traveling in the channels between the beads (Figure 2-5 (b)). The laminar flow is faster in the channel center and slower on the edge. Both of the above effects can be reduced by using more uniformly-sized beads. However, the mobile phase flow velocity has little effect for either one.

The third cause is longitudinal diffusion of sample molecules in the mobile phase (Figure 2-5 (c)), which happens only when small beads are used, mobile phase velocity is low, and the sample diffusion coefficient in the mobile phase is large. This effect can be minimized by choosing an adequate mobile phase velocity.

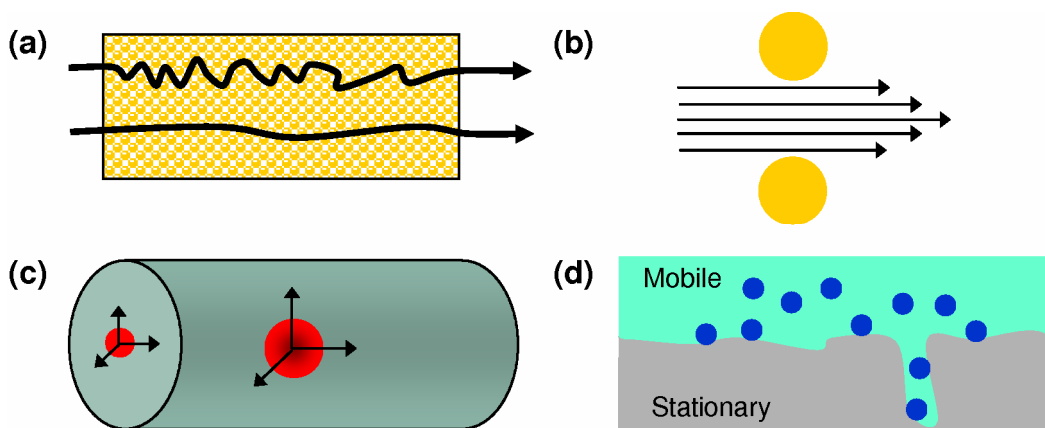


Figure 2-5 Four mechanisms of band broadening.

The fourth cause is the time-consuming mass transfer process between mobile, “stagnant mobile,” and stationary phases (Figure 2-5 (d)). Inside the pores of the beads, molecules move only by diffusion. Therefore, some molecules could be stuck in the pores while others continue to move down the column with mobile phase. In this case, the higher the mobile phase flow velocity, the more broadening effect will be.

In summary, the theoretical plate height H (explained in detail in Section 2.1.3.4), representing the column efficiency, can be plotted against mobile phase velocity u (Figure 2-6), which is called the van Deemter curve. The effect of eddy diffusion and

flow distribution is shown with line 1. The longitudinal diffusion effect is shown with line 2. The mass transfer effect is shown with line 3. And the van Deemter curve is line 4, which is the summary of all four effects. The optimal u is reached when the corresponding H reaches minimum. This H - u relationship can also be expressed with the following van Deemter equation.

$$H = A + \frac{B}{u} + Cu \quad (2.15)$$

where A , B , and C are coefficients for eddy-diffusion and flow distribution effects, longitudinal diffusion effect, and mass transfer effect respectively.

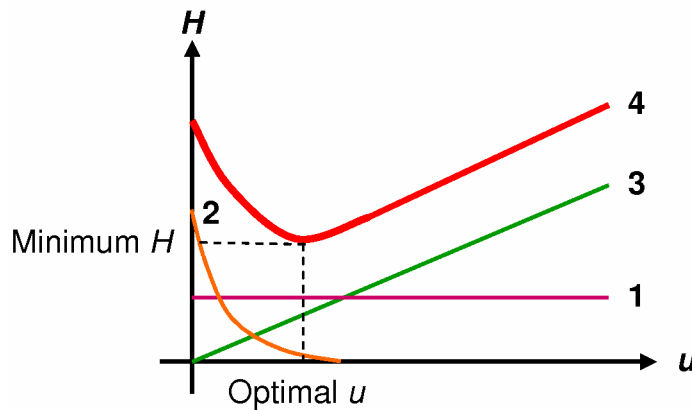


Figure 2-6 Van Deemter Curve.

2.1.3.3 Band Broadening vs. Separation

Even though the band broadening effect exists, the chemical components in a sample can still be separated into non-overlapping bands if the column length is long enough. In a uniformly-packed column, the band width increases with the square root of the length it has traveled down the column, while the distance between two bands is

proportional to the traveled length. This is the fundamental reason why chromatography works [1].

Chemical compound concentration is not uniform in a band (peak). The band is rather a statistical distribution of molecules. The width of the band is always proportional to the standard deviation of the distribution, σ , with the proportionality factor depending on the distribution type. For typical chromatographic bands that are Gaussian distributed, the peak width measured at 13.4% of peak height is 4σ . The band standard deviation increases with the square root of the time spent in the column. Therefore, as equation (2.16) shows, the band width W increases with square root of L , the length traveled.

$$W \propto \sigma \propto \sqrt{t} = \sqrt{\frac{L}{u}} \propto \sqrt{L} \quad (2.16)$$

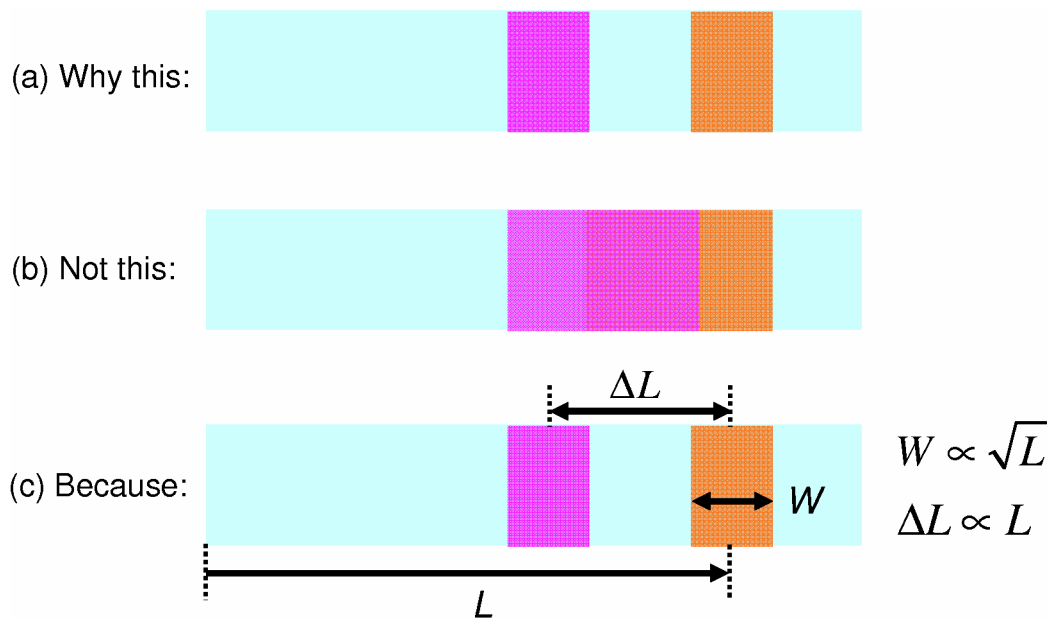


Figure 2-7 Band broadening effect vs. separation effect.

While the distance between two bands, ΔL , approximately can be expressed as:

$$\Delta L = (t_{R1} - t_{R2}) \frac{L}{L_c} u = (k_1 - k_2) L \propto L \quad (2.17)$$

2.1.3.4 Height Equivalent to a Theoretical Plate

In some sense, the height equivalent to a theoretical plate (HETP), H , can be imagined to be the distance over which chromatographic equilibrium is achieved [8]. The smaller the H value, the higher the column efficiency. However, the plate model is not a very good presentation of chromatographic column; plate height represents column efficiency for historic reasons only, and not because it has physical significance [3].

Chromatographic band (peak) width can be described by its variance σ^2 . As stated in the previous section, σ increases with the square root of the length traveled. Therefore, the peak variance increases linearly with the length it has traveled (Figure 2-8). The smaller the slope, the slower the peak widens, the higher the column efficiency. The slope (variance per unit length) is defined to be HETP:

$$H \equiv \frac{\sigma^2}{L} \quad (2.18)$$

H can also be calculated as:

$$H = \frac{L_c}{N} \quad (2.19)$$

The reduced/dimensionless plate height, h , is defined as:

$$h = \frac{H}{d_p} \quad (2.20)$$

h represents the number of layers of stationary phase packing over which a complete chromatographic equilibrium is obtained. A column with good packing usually has h from 2 to 5.

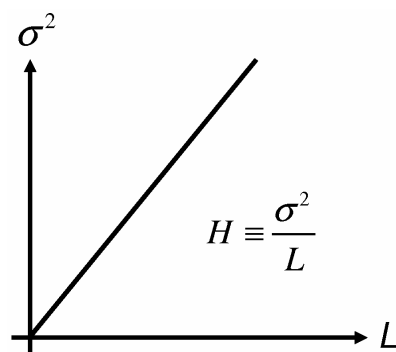


Figure 2-8 Definition of HETP.

2.1.4 Instrumentation

A typical HPLC instrument has the following parts: solvent reservoirs, high-pressure pumps, sample injection device, separation column, and detector (Figure 2-9). Some of the optional parts are guard column, thermostat oven, and fraction collector. Since this thesis work emphasizes column and detector, these two parts will be discussed in more detail below.

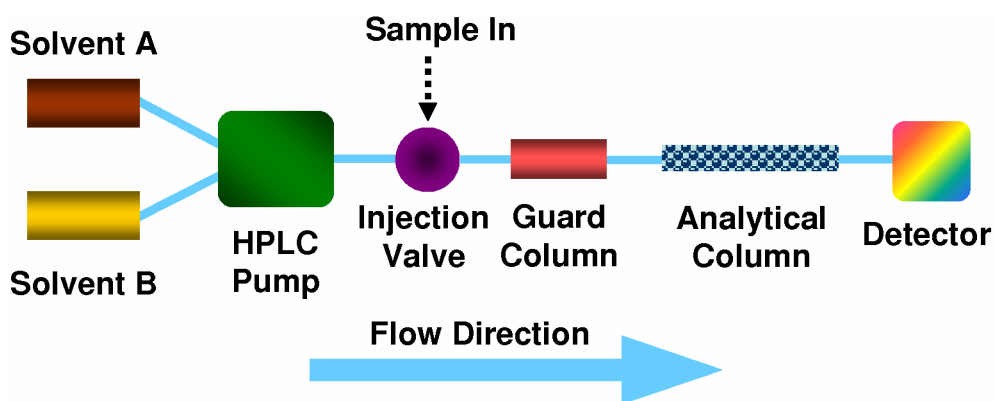


Figure 2-9 Schematics for a typical HPLC system.

2.1.4.1 Solvents

Solvents must be HPLC-grade. They have to be degassed before entering the column, otherwise gas bubbles will appear in the detector where the pressure is low. Commercial HPLC systems usually have on-line degassers in their pumping units. The most preferred organic solvent is now acetonitrile rather than methanol mainly because the latter is more viscous, and thus generates higher backpressure. Methanol viscosity is 0.6 cP at 20 °C, while that of acetonitrile is 0.37 cP. Acetonitrile is, however, much more expensive than methanol.

2.1.4.2 Pumps

An HPLC pump has to be able to generate thousands of psi pressure, and provide high flow accuracy and precision. The delivered flow rate must be unaffected by backpressure change during separation. For example in gradient separations, the ratio between solvents in the mobile phase changes, which leads to a total effective viscosity change, and therefore a backpressure change. Commercial HPLC pumps are mostly piston pumps. Recently, a new pump for nano HPLC applications has appeared on the market, which uses compressed air as the pressure source and a flow sensor to perform feedback control to generate precise nano liters per minute flow rates [9].

2.1.4.3 Sample Injectors

An injection valve is used for sample injection into the column with an accurate and precise amount of sample. Figure 2-10 illustrates the working mechanism for a six-port sample injection valve. In Figure 2-10 (a), the sampling loop is connected to the

sample injection inlet, from which sample is loaded into the loop. Excessive amount of sample is usually loaded, in order to make sure the loop is completely filled. Then the internal rotor seal is rotated to bring the sampling loop online with the pump and column (Figure 2-10 (b)) to inject sample into the column.

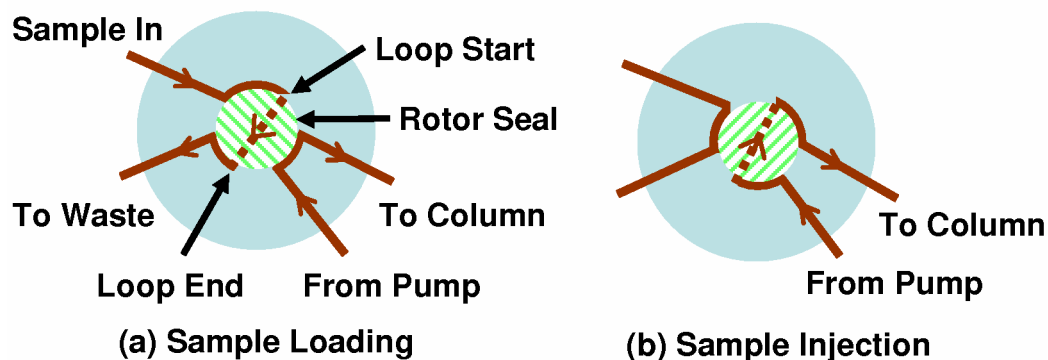


Figure 2-10 Injection valve working mechanism.

2.1.4.4 Chromatographic Columns

2.1.4.4.1 Column Dimension

Column length and inner diameter (ID) are two of the most important column properties. The separation power in terms of number of plates is proportional to column length. However, backpressure and analysis time will also rise proportionally to column length increase. For gradient separation, the column length is less a factor for resolution since the separation is controlled by gradient rather than the length of the column. Narrower columns require less sample injection, consume less mobile phase, and have better sensitivity when the same amount of sample is injected. However, wider columns permit higher sample loadability.

2.1.4.4.2 Column Packing Physical Properties

HPLC columns are mostly densely-packed with micro-scale beads. The aim of the beads is to carry the stationary phase and to generate high surface area. As shown in Figure 2-11, the beads used in HPLC column packing differ in shape, size, pore size, and surface area (porosity).

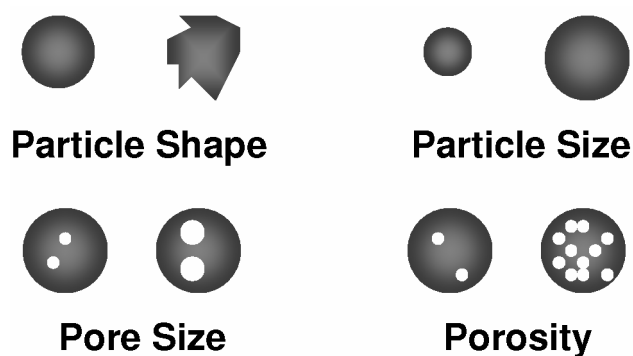


Figure 2-11 Physical properties of liquid chromatographic beads.

The shape of HPLC beads is either spherical or irregular. The vast majority of all columns uses spherical beads, since they provide more uniform and dense packing, better flow profiles, less backpressure, and higher efficiency. Irregular beads often provide more surface area and higher capacity.

The size of most commercial HPLC beads is between 3 μm and 10 μm in diameter, while 1 μm diameter beads are also being explored. Smaller beads provide smaller plate height, which is proportional to bead diameter. This comes with the expense of significantly higher backpressure, which is inversely proportional to the square of bead diameter. Therefore, the trend is to increase resolution rather than continue to reduce particle size.

Pore size is the average dimension of the channels inside the porous beads. The bead internal structure is fully porous and can be best compared to a sponge with a rigid structure. Within the pores, the mobile phase and the analytes do not flow but move only by diffusion. The pore size can range from 60 Å to over 10,000 Å. Molecules smaller than the pore size can enter the pores and fully utilize the internal stationary phases. Larger molecules may be kept outside the pores and thus have little retention. In practice, molecular weight is used instead of size.

The bead surface area is determined by the pore size and abundance of pores in the bead. Higher porosity beads with smaller pores have larger surface area. For example, the surface area of a column packed with 5 µm non-porous beads is only 0.02 m²/mL, while that of a totally porous-bead-packed bed is 150 m²/mL [1]. Pores that are too small, however, are detrimental to column efficiency, since they are difficult to access. For general purpose columns, 10 nm pores are often used. For large molecules like proteins, 100 nm pores are the best choice. For beads without bonded surface functional groups, larger surface area means more capacity, longer retention, and generally higher resolution. For bonded beads, both surface area and bonding density should be considered. There are also non-porous bead columns, which can eliminate band broadening caused by poor mass transfer into the stagnant mobile phase within the pores, and can reduce undesired loading capacity in some cases.

2.1.4.4.3 Base Material and Bonded Phases

The base material of the beads is generally a metal-oxide, such as silica and alumina, or a polymeric material, such as polystyrene-divinylbenzene (PS-DVB). Silica

is the most popular base material for HPLC column packing, while polymeric materials are gaining popularity. Silica beads are produced by a number of different syntheses such as complete hydrolysis of sodium silicate, or the polycondensation of emulsified polyethoxysiloxane followed by dehydration [8]. A silica bead has silanol (-OH) groups on its surface, which can be chemically modified (replaced) with desired stationary phases. A number of reactions can be used. Figure 2-12 gives one example, where the silanol group is reacted with an alcohol, ROH. R may be an alkyl chain or other functional group.

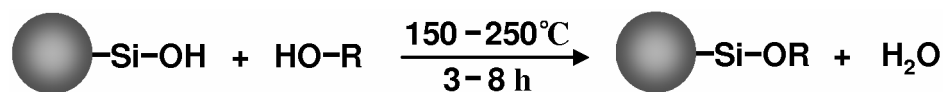


Figure 2-12 Chemical modification of silica surface.

ODS (octadecylsilane), in which $\text{R} = -(\text{CH}_2)_{17}\text{CH}_3$, is the most common type used in HPLC columns. It is also called C18 since there are eighteen carbon atoms in this alkyl chain (Figure 2-13). It is very non-polar and is used in reversed-phase (RP) HPLC, as explained in Section 2.1.4.4.4. Similarly, C8 ($\text{R} = -(\text{CH}_2)_7\text{CH}_3$) and C4 ($\text{R} = -(\text{CH}_2)_3\text{CH}_3$) are also used in RP-HPLC. Since they have shorter alkyl chains than C18, they are less non-polar and require less run time for separations.

After the functional group bonding process, the silica bead may also be end-capped, which bonds short hydrocarbon chains to free silanol groups still on the base silica surface. End-capped beads provide more predictable separations since the effects from free silanol groups are mostly removed.

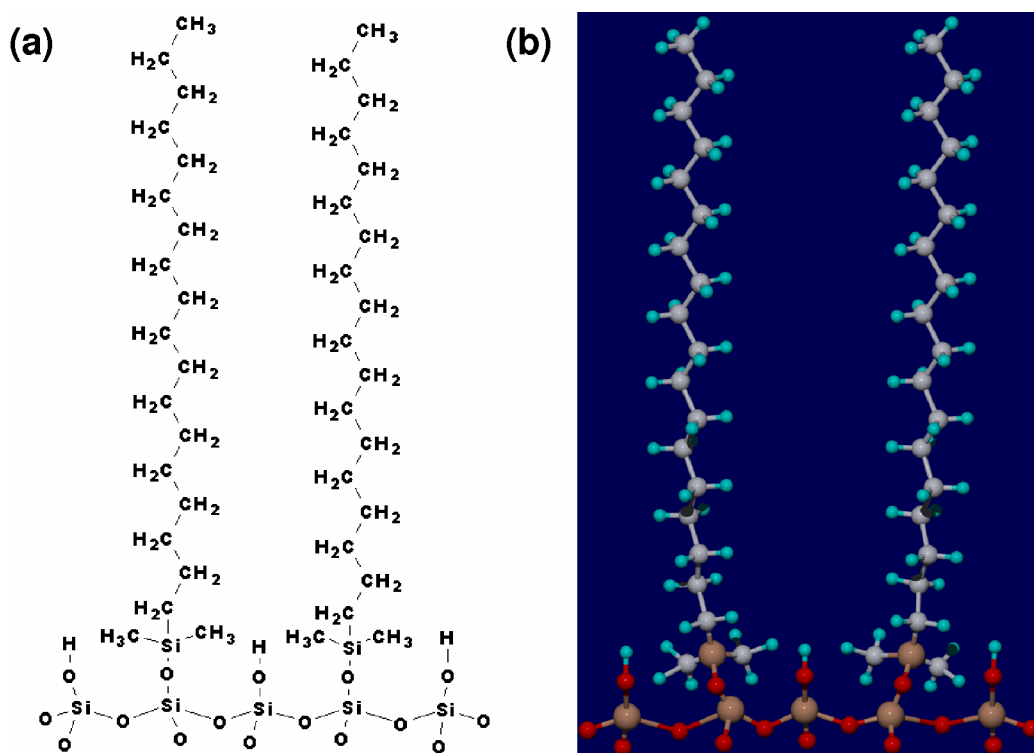


Figure 2-13 Chemical structure and 3D illustration of C18 functional groups on silica surface.

Compared to silica beads, polymer materials have wider pH range. Silica can only tolerate mobile phases having pH 2 to 7.5, while polymers are usually good between pH 2 to 12, sometimes even 0 to 14. Strong acids and bases can not be used for silica-based columns. Polymer-based columns, on the other hand, can be thoroughly cleaned with strong acids or bases to have a longer lifetime than silica-based columns. Moreover, the polymer material surface is free of silanol group, which can sometimes affect separation.

One disadvantage of polymers is they are softer than silica. They can swell in non-polar solvent and shrink in aqueous solvent. In addition, when compared to silica-based columns, polymer columns take longer time to equilibrate when a new mobile phase is introduced.

2.1.4.4.4 Separation Mechanisms

The most common types of LC, based on the separation mechanisms in the column, are normal-phase, reversed-phase, ion, size-exclusion, hydrophilic interaction, and hydrophobic interaction.

Normal-phase LC employs a polar (water-soluble, hydrophilic) adsorbent such as silica, and a non-polar (fat-soluble, hydrophobic) mobile phase based on hydrocarbons such as petrol. It is also often called adsorption chromatography and was the first type of LC technique developed. However, two reasons greatly limit its use. Firstly, silica is hydrophilic, any trace amount of water in the solvent could change its surface property, thus change elution time. Second, many interesting analytes, such as amino acids, peptides and nucleotides, are so polar that they do not easily dissolve in non-polar solvents, and therefore can not be analyzed by normal-phase.

The solution to these two problems is to modify the silica surface to be hydrophobic (non-polar), and use polar solvents for elution, which is known as reversed-phase (RP) LC. RP-LC is the most popular type of LC today. Non-polar compounds are eluted later than polar compounds. Water as a mobile phase cannot interact with the non-polar (hydrophobic) station phase. Therefore, water has little elution power. Non-aqueous solvents, such as acetonitrile and methanol, are less polar than water. Therefore, they have better elution capability. The more solvent content in the mobile phase, the faster the separation.

Ion chromatography utilized ion-exchange interactions of charged analytes, eluent (mobile phase) ions, and charged functional groups on the stationary phase. Eluent ionic strength and pH can affect the elution. This is discussed in detail in Section 5.1.2.

Size-exclusion chromatography is a separation based on size, i.e. according to molecular mass, rather than any interaction phenomena. Larger analytes have limited access to stationary phase in the pores of the packing. Therefore, larger molecules are eluted earlier than smaller ones.

Hydrophilic interaction chromatography is an extension of normal-phase chromatography where very polar analytes and aqueous mobile phases are used. Stationary phases are still the same.

Some protein separations need significantly less-hydrophobic stationary phase to prevent the proteins from being denatured by common RP-HPLC solvents. This technique is called hydrophobic interaction chromatography, which is an extension of reversed-phase chromatography.

2.1.4.5 Detectors

A successful HPLC analysis relies not only on the mixture separation delivered by the chromatographic process, but also on the visualization of the separated compounds provided by the detector. For the earliest chromatography, the separation is literally “visualized” by a rainbow of colors. Over the years, a whole spectrum of detectors exploiting all kinds of physical and chemical properties has been developed. Detailed discussions are given in [10]. As the separated compounds exit the column and pass through the detector cell, changes on the background signal are sensed by the detector and recorded on a chromatogram. Among all the detection methods, UV-visible absorbance, fluorescence, refractive index (RI), electrochemical/conductivity, and mass spectrometry (MS) are the most common ones.

The choice of the appropriate detector for an application depends mainly on the analytes of interest and the desired sensitivity. Table 2-2 summarizes the sensitivity for the most common HPLC detectors [3, 10–12]. The sensitivity data are dependent on the compound, instrument, and HPLC conditions. Those given in the table are only typical values. Other important detector properties include selectivity, response time, and detector cell volume. The selectivity determines how well it can discriminate a compound from others or from the background. The detector also has to be fast enough to allow real-time detection. If more time is required to achieve a desired sensitivity, the analyte fractions may have to be collected and analyzed later. Since trace levels of chemicals are to be determined, the volume of the detector cell needs to be small enough that the separated peaks do not distort or overlap in the detector.

| HPLC Detectors | Typical Concentration Sensitivity | Typical Mass Limit of Detection |
|--|-----------------------------------|---------------------------------|
| Refractive Index | 10 ppm | 1 ng |
| UV/Visible | 1 ppb | 10 pg |
| Conductivity (non-suppressed and suppressed) | 10 to 0.1 ppb | 1 to 0.1 ng |
| MS | N/A | < 1 pg |
| Fluorescence | 10 ppt | 10 fg |

Table 2-2 Typical sensitivity data for common HPLC detectors.

UV-visible absorbance detector measures the loss of ultraviolet or visible light as the light passes through the HPLC column effluent. The chemicals of interest must contain chromophores that absorb UV or visible light, such as conjugated double bonds and aromatic rings. The flow cell is usually arranged in a “Z” pattern, in which the flow

path is maximized to maximize absorbance that is proportional to the flow path in the detector cell. The absorbance rather than the transmittance is recorded, because the former, not the latter, is linear with sample concentration. The absorbance method is simple and reliable. However, it is less sensitive than fluorescence, electrochemical, and mass spectrometry detections. And it is not a universal method for all analytes.

Fluorescence detection captures the fluorescence emission at a higher wavelength generated by a lower excitation wavelength. The analytes must have fluorophores, which are compounds that fluoresce. This method has much better sensitivity and selectivity than most other methods. Its sensitivity comes from the fact that most background solvents do not fluoresce and the analytes usually strongly fluoresce. There are two reasons for its selectivity. Firstly, not all organic molecules fluoresce. Secondly, fluorescence detection uses two distinct wavelengths as opposed to one in absorbance method, which greatly reduces the chance of interfering peaks. One important disadvantage of fluorescence detection is the limited number of compounds that fluoresce, although some of them can be chemically derivatized to have fluorescent “tags.” Another drawback is that the fluorescent response can be affected by solvent type, temperature, and pH.

Refractive index detection is a universal method, since the refractive index difference between any two liquids is on average about a million times larger than the detection limit of current RI detectors. It is often used for compounds that do not have strong UV chromophores, fluorophores, electrochemical activity, or ionic conductivity. One major disadvantage, however, is the lack of sensitivity. Since the refractive index is

a property of the bulk solution, any change in temperature, pressure, or composition can affect the baseline stability. Therefore, gradient elution should be avoided.

Electrochemical detectors measure the electrochemical properties of the HPLC column effluents. It has good sensitivity and can be used for an extensive list of analytes. The most common type of electrochemical detectors is the conductivity detector, which measures the electrical conductance. It is especially used for ion chromatography where the analytes are ionic and have weak UV absorbance. Non-suppressed conductivity detection measures sample signals directly on top of baseline signal generated by the mobile phase. Suppressed detection removes the background after separation but prior to detection. The sensitivity of suppressed conductivity detection is one to two orders of magnitude better than non-suppressed one, according to the data in Table 2-2. One main issue of conductivity detection is the temperature effect on the ion mobility, and thus on the conductivity. Conductivity of an ionic solution rises about 2% for every degree increase in temperature [13]. Therefore, the detector cell temperature must be carefully maintained and/or temperature compensation must be used. More details of conductivity detection are presented in Section 5.2.2.

HPLC-MS seems to be the ideal merger for separation and detection. Mass spectrometry is one of the most sensitivity detection methods for HPLC. It is universal and can be used for specific compound identification and quantitative determination. MS has superior selectivity and it can easily discriminate against interference from background or other eluted materials. In a mass spectrometer, compounds are vaporized, ionized, separated according to their mass-to-charge ratio (m/z), and detected. Electrospray ionization (ESI) [14] is one of the most common ionization techniques,

especially for high molecular weight samples used in proteomics. Other notable interfacing techniques are atmospheric pressure chemical ionization (APCI) and matrix-assisted laser desorption ionization (MALDI). The interfacing requirement is one factor limiting the use of MS. Another practical reason is that mass spectrometers are still very expensive. Furthermore, since MS demands a rather low flow rate on the order of 100 to 1000 nL/min, it raises challenges on the LC side, which is actually one of the main reasons for the development of nano HPLC.

2.2 Nano HPLC

2.2.1 Definition

The recent developments in proteomics, in particular, have been demanding the reduction of LC column IDs, to accommodate dwindling sample amount and the need for increasing sensitivity. In addition, the field of lab-on-a-chip demands on-chip liquid chromatography separation for other chip-based chemical analysis, just in the same way that LC is highly desired and utilized in conventional-scale analytical chemistry applications. Performing separation prior to detection essentially eliminates the need for highly specific sensing, which is difficult to achieve on-chip.

Based on the definition given in Table 2-3 [15], many columns used for proteomics applications today can be called nano HPLC columns. Inherently, most on-chip microfluidic columns also fit in the nano HPLC category. It should be noted, however, that on-chip columns usually have rectangular cross-sections, unlike the conventional cylindrical columns.

Nano HPLC is sometimes also referred to as “nanobore HPLC” or “nano-scale HPLC” in the literature.

| Description | ID Dimension | Flow Rate (Velocity 1–10 mm/s) |
|--------------------|------------------------|--|
| Open Tubular LC | < 25 μm | < 25 nL/min |
| Nano HPLC | 25–100 μm | 25–4000 nL/min |
| Capillary HPLC | 100–1000 μm | 0.4–200 $\mu\text{L}/\text{min}$ |
| Micro HPLC | 1.0–2.1 mm | 50–1000 $\mu\text{L}/\text{min}$ |
| Normal HPLC | 4.0–5.0 mm | 1.0–10.0 mL/min |
| Preparative HPLC | > 10 mm | > 20 mL/min |

Table 2-3 Nomenclature for HPLC systems.

It is interesting to note that nano HPLC does not mean the column ID is on the nanometer scale, but rather the flow rate is on the scale of nano liters per minute (nL/min). Similarly, micro HPLC means the flow rate is on the scale of $\mu\text{L}/\text{min}$, while normal HPLC has its flow rate between 1 to 10 mL/min. The operating flow rates for each category are calculated based on the column ID and optimal flow velocity, which is usually on the order of 1 mm/s.

2.2.2 Miniaturization Benefits

First, the use of narrower columns reduces solvent consumption significantly. Since the optimal linear flow velocity for LC separation is independent of column ID, the actual eluent volumetric flow rate scales with column cross sectional area. The retention volume V_R , which is the volume of the mobile phase necessary to elute a peak with retention factor k , is proportional to column cross-sectional area:

$$V_R = F \times (k+1)t_0 = (k+1)\varepsilon L_c A_c \propto A_c \quad (2.21)$$

For cylindrical columns, this means it is proportional to column ID square:

$$V_R \propto d_c^2 \quad (2.22)$$

When column ID shrinks, theoretically [8], the separation efficiency remains nearly unchanged given the same packing quality of the columns. Thus the separated peak width is almost independent of column ID. Another way to understand it is to imagine the column with smaller ID was taken out from the central rod of the larger column (Figure 2-14). Since sample band (peak) width is the same across the column cross-section, the smaller column should produce the same peak width as the larger one.

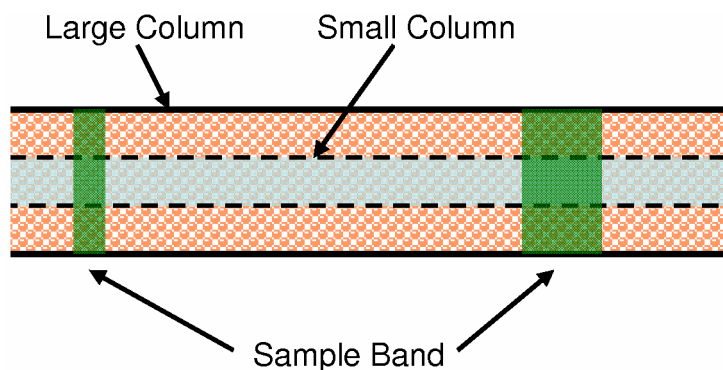


Figure 2-14 Peak width remains nearly unchanged with column ID reduction.

As a result, when the same amount of sample is injected, the peak maximum concentration, c_p , scales inversely with column ID square,

$$c_p = \sqrt{\frac{N}{2\pi}} \frac{V_i}{V_R} c_i \propto \frac{1}{V_R} \propto \frac{1}{d_c^2} \quad (2.23)$$

where V_i is the injection volume, and c_i is the injection concentration. Since most HPLC detectors, such as UV absorbance, fluorescence, mass spectrometry, and conductivity

detectors, are concentration-sensitive instead of mass-sensitive, the detector response shown as peak height scales the same way. Therefore, higher sensitivity and/or less sample requirement can be obtained with column ID miniaturization.

This effect of column ID and bead diameter reduction is illustrated in Figure 2-15. Columns 1 and 3 have the same packing quality but different ID. For the same injection, the peak from column 3 has the same width but much more height than that from column 1. The same holds for columns 2 and 4.

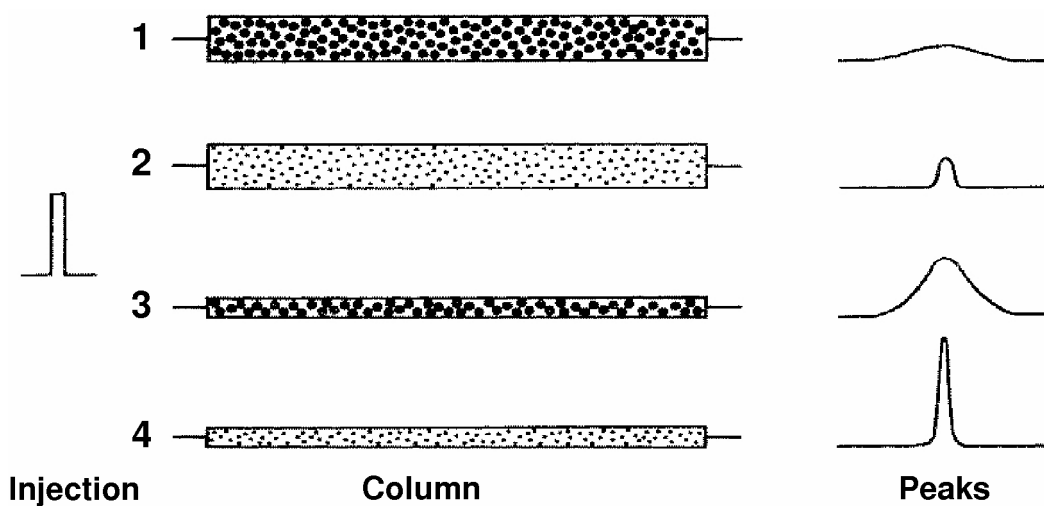


Figure 2-15 Effects of column ID and bead diameter reduction on separation performance.

Since most HPLC detectors are concentration dependent, the number of sample molecules in the peak is proportional to the peak area times column cross sectional area. Therefore although injected sample amount are the same for 3 and 1, the peak area in 3 is larger than that in 1, because column 3 is narrower than 1. The same holds for columns 2 and 4.

Comparing column pairs with the same ID but with different bead diameters, the peak height from column 2 is about the same as that from column 1, while the peak width

is much narrower due to better separation efficiency of the smaller packing materials (Figure 2-15). The same holds for columns 3 and 4.

Furthermore, the miniaturized column does not have the burden of elevated pressure requirements, although its flow resistance is significantly increased. The reason is the optimal operating pressure is proportional to the optimal linear flow velocity (equation (2.14)), which is independent of column diameter.

Finally, a miniaturized LC system will be significantly cheaper than its conventional counterpart. In addition, it will be significantly smaller even compared to today's most compact desktop LC systems. These new features could enable portable and/or disposable LC systems that could be used for field tests, networked sensing, real-time environmental monitoring and so on, which would be impossible with today's bulky lab LC instruments. LC chips can also be incorporated with other chemical and biological sensors to make them more selective and sensitive. Moreover, mass parallel LC separations could be possible with LC chips, which would greatly reduce drug discovery time and cost.

2.3 Review of Nano HPLC Chips

Despite the benefits of miniaturized LC systems, on-chip classic pressure-driven LC technology is actually considerably under-developed [15–25], compared to chip-based capillary electrophoresis (CE) with its abundant publications.

As another popular separation technique, CE has its limitations and drawbacks compared to LC. Firstly, CE relies on charged analytes moving in an electric field, which is not suitable for analytes that are barely conducting or dissociate in high electric field.

LC, on the other hand, is a rather general method. Almost any, if not all, samples that are soluble in liquid phase can be separated using LC. Secondly, LC does not need the high voltages employed for CE, mostly on the order of kilovolts, which is not suitable for many practical applications. Thirdly, for CE, the resistive heating across the column is also a concern. Fourthly, on-chip CE demands the use of a tiny plug of injected sample, which mostly has to be done on-chip, raising the micro-system complexity considerably. In contrast, LC systems can tolerate much larger injection volumes, which could be from off-chip, since the sample will concentrate on the LC column inlet, given adequate capacity of the column.

One main factor limiting the development of LC on-a-chip is the lack of available technologies to integrate various components of an LC system, especially for the heart of the LC system, the separation column [16, 17]. Although the packing of the on-chip column with beads seems to be desirable and straightforward, until recently, most chip-based LC columns with few exceptions [18] were made using alternative methods. These include open-tubular [19], surface-activated micromachined posts [20], continuous monolithic bed formed by in-situ polymerization [21], and column coated with nanoparticles [22].

For all the chips presented in this thesis, columns are all fabricated by either integrating LC beads into the column during fabrication or packing columns with beads after fabrication. There are two important advantages of using conventional beads over alternative methods. Firstly, without introducing new surface chemistry, the well-established separation knowledge can be utilized. Secondly, there is more flexibility to

perform various types of LC separations and/or to optimize particular separations, by choosing from a variety of commercially available beads and stationary phases.

Recently, Nanostream Inc. revealed their micro parallel LC cartridge, which is made of polymeric material and has 24 bead-packed microfluidic columns allowing 24 samples to be analyzed in parallel. The samples are injected from off-chip using an auto sampler and detected with 24 UV absorbance detectors off-chip. Also recently, researchers from Agilent presented their chip-based fritless LC column with electrospray ionization (ESI) nozzle [15, 23]. The chip is made of two polyimide layers bonded together, while the ESI nozzle is fabricated by laser ablative trimming of the bonded chip. The column is packed with C18 beads using a tapered outlet rather than frit, utilizing a so-called “keystone effect” [26]. Samples are injected from off-chip using an injection valve attached to the back of the chip. A mass spectrometer is used as the detector. The most complete LC chip so far is a device from our research group [24] that has on-chip gradient pumping, sample injection, column, and electrospray nozzle. Its 1 cm long column is packed after chip fabrication. A mass spectrometer is used as the detector. Some packaging is required to form the solvent and sample reservoirs for the chip.

The goal of this thesis is to develop technologies and devices to address the important and challenging issues of previous LC chips. Firstly, there is no device to date that integrates bead column during chip fabrication, which directly prevents real batch fabrication of LC chips (Chapter 3). Secondly, the needs for high-pressure rating and efficient high-pressure generation on-chip are still unmet, especially for parylene micro devices, which has to be solved in order to perform real high-performance/pressure liquid chromatography on-a-chip (Chapter 4). Chapter 5 presents the first integrated ion

chromatography chip, which demonstrates on-chip sample injection, column separation, and conductivity detection for multi-ion sensing. And Chapter 6 demonstrates a high-pressure LC-ESI/MS microchip, which is integrated with 6.5 cm long column, filter for packing beads, and electrospray nozzle for coupling to mass spectrometry detection. Finally, Chapter 7 concludes the thesis.

2.4 Bibliography

- [1] U. D. Neue, *HPLC columns: theory, technology, and practice*. 1997. Wiley-VCH.
- [2] L. S. Ettre, "M.S. Tswett and the invention of chromatography." *LC GC North America*, 2003. 21(5): p. 458.
- [3] D. A. Skoog, *Fundamentals of analytical chemistry*. 8th ed. 2004. Belmont, CA: Thomson-Brooks/Cole.
- [4] B. A. Bidlingmeyer, *Practical HPLC methodology and applications*. 1992. New York: Wiley.
- [5] A. J. P. Martin and R. L. M. Synge, "A new form of chromatogram employing two liquid phases." *Biochemical Journal*, 1941. 35: p. 1358–1368.
- [6] Nobel Prize in Chemistry 1952, <http://nobelprize.org/chemistry/laureates/1952/index.html>
- [7] W. R. LaCourse, "Column liquid chromatography: Equipment and instrumentation." *Analytical Chemistry*, 2002. 74(12): p. 2813–2831.
- [8] V. Meyer, *Practical high-performance liquid chromatography*. 3rd ed. 1998. Chichester; New York: Wiley.
- [9] Eksigent, <http://www.eksigent.com/hplc/nano/>
- [10] D. Parriott, *A practical guide to HPLC detection*. 1993. San Diego: Academic Press.
- [11] B. Limpert, L. Consulting, and Bellingham, *Alltech HPLC Detector Seminar Booklet*. 1995.
- [12] Alltech Associates, www.AlltechWEB.com

- [13] J. S. Fritz and D. T. Gjerde, *Ion chromatography*. 3rd, 2000. Weinheim, Germany; New York: Wiley-VCH.
- [14] C. M. Whitehouse, R. N. Dreyer, M. Yamashita, and J. B. Fenn, "Electrospray interface for liquid chromatographs and mass spectrometers." *Analytical Chemistry*, 1985. 57(3): p. 675–679.
- [15] G. Rozing, "Trends in HPLC column formats—microbore, nanobore and smaller." *LC GC Europe*, 2003. 16(6A): p. 14–19.
- [16] A. de Mello, "On-chip chromatography: The last twenty years." *Lab on a Chip*, 2002. 2(3): p. 48n–54n.
- [17] C. M. Harris, "Shrinking the LC landscape." *Analytical Chemistry*, 2003. 75(3): p. 64a–69a.
- [18] G. Ocvirk, E. Verpoorte, A. Manz, M. Grasserbauer, and H. M. Widmer, "High-performance liquid-chromatography partially integrated onto a silicon chip." *Analytical Methods and Instrumentation*, 1995. 2(2): p. 74–82.
- [19] A. Manz, Y. Miyahara, J. Miura, Y. Watanabe, H. Miyagi, and K. Sato, "Design of an open-tubular column liquid chromatograph using silicon chip technology." *Sensors and Actuators B-Chemical*, 1990. 1(1–6): p. 249–255.
- [20] B. He, N. Tait, and F. Regnier, "Fabrication of nanocolumns for liquid chromatography." *Analytical Chemistry*, 1998. 70(18): p. 3790–3797.
- [21] C. Ericson, J. Holm, T. Ericson, and S. Hjerten, "Electroosmosis- and pressure-driven chromatography in chips using continuous beds." *Analytical Chemistry*, 2000. 72(1): p. 81–87.

- [22] J. P. Murrphy, M. C. Breadmore, A. M. Tan, M. McEnery, J. Alderman, C. O'Mathuna, A.P. O'Neill, P. O'Brien, N. Advoldvic, P.R. Haddad, and J.D. Glennon, "Ion chromatography on-chip." *Journal of Chromatography A*, 2001. 924(1-2): p. 233-238.
- [23] K. Killeen, H. Yin, D. Sobek, R. Brennen, and T. v. d. Goor, "Chip-LC/MS: HPLC-MS using polymer microfluidics." *Seventh International Conference on Micro Total Analysis Systems (microTAS 2003)*. Squaw Valley, California, USA, October 5-9, 2003. p. 481-484.
- [24] J. Xie, J. Shih, Y. Miao, T. D. Lee, and Y.-C. Tai, "Complete gradient-LC-ESI system on a chip for protein analysis." *Proceedings of the 18th IEEE International Conference on Micro Electro Mechanical Systems (MEMS 2005)*. Miami Beach, Florida, 2005. p. 778-781.
- [25] Q. He, C. Pang, Y.-C. Tai, and T. D. Lee, "Ion liquid chromatography on-a-chip with beads-packed parylene column." *Proceedings of the 17th IEEE International Conference on Micro Electro Mechanical Systems (MEMS 2004)*. Maastricht, Netherlands, 2004. p. 212-215.
- [26] G. A. Lord, D. B. Gordon, P. Myers, and B. W. King, "Tapers and restrictors for capillary electrochromatography and capillary electrochromatography mass spectrometry." *Journal of Chromatography A*, 1997. 768(1): p. 9-16.

CHAPTER 3

BEAD INTEGRATION TECHNOLOGY AND AN LC-ESI/MS CHIP

3.1 Introduction

As mentioned in Chapter 2, one of the most challenging parts involved in the development of on-chip liquid chromatography is the bead separation column. Conventionally, LC columns are packed by a so-called “slurry-packing technique,” in which beads prepared in slurry are externally packed into the column. Naturally, some researchers use the same method to pack on-chip micro-channels [1–5]. Unfortunately, although it seems to be straightforward to pack a fabricated micro-channel, the packing process is laborious, time-consuming, and only one column can be packed at a time. Some alternative methods [6–9] that avoid packing have also been proposed. These novel packing-less columns are useful for some applications. However, they also have serious disadvantages such as limited separation knowledge base, separation mechanisms, and

applications. A detailed discussion is given in Section 2.3. The conclusion is on-chip bead-packed column that miniaturizes its conventional-scale counterpart is the desired approach for on-chip LC. The fabrication of the bead column, however, needs to be greatly simplified. Therefore, this chapter discusses the development of a new in-process bead-delivering technique to make integrated bead columns. This method offers the advantages of batch fabrication, easy integration with other devices, and little dependence on bead type.

The chapter starts with a discussion of many aspects in dealing with beads. The second part develops a novel technique to integrate beads into micromachined devices. Finally the third part demonstrates an application of this technique, which is a liquid chromatography–electrospray ionization (LC-ESI) chip with integrated LC bead column, particle filters, and electrospray nozzle for coupling to on-line mass spectrometry detection. The combination of liquid chromatography and mass spectrometry (LC-MS) is a very powerful merger for separation and detection. Microchips with LC-ESI/MS capabilities are highly desired, especially in the field of proteomics. We have successfully demonstrated similar parylene freestanding ESI nozzles before [10, 11]. This work for the first time truly integrates the LC bead column with ESI nozzle.

3.2 Working with Beads

3.2.1 Various Terms and Properties

In the literature, the terms “particles,” “beads,” and “microspheres” are often used. Generally speaking, “particles” are usually irregular in shape and non-uniform in size. “Beads” are more spherical and more uniform. “Microspheres” are the most spherical and

uniform of the three. However, the distinction is not so clear cut. Therefore, the three terms are often used interchangeably. In the field of liquid chromatography, the term “bead” is mostly used to describe the packing material in the separation column.

There are a wide variety of beads commercially available. Their sizes can range from several nanometers to millimeters. The base material can be silica, alumina, polystyrene (PS), and many others. There are a number of choices for surface chemistries and bulk properties as well, such as hydrophobicity, fluorescence, and magnetism. The beads can also come in a rainbow of colors. Some major vendors for all general and special beads are Bangs Laboratories (Fishers, IN), Duke Scientific (Palo Alto, CA), and Polysciences (Warrington, PA). Liquid chromatographic beads are available from vendors such as Alltech Associates (Deerfield, IL), Hamilton (Reno, NV), and Grace Vydac (Hesperia, CA).

3.2.2 Aggregation

The interactions between particles, especially surface forces, are proportional to the first power of particle size. As a comparison, gravitational force is proportional to the mass, thus to the cube of particle size. Hydrodynamic forces caused by flow depend roughly on the square of particle size. Therefore, when the particle dimension reaches the micron level, surface forces become dominant. Aggregation is often seen for suspended micro-particles, which aggregate by collision and are held together by surface forces [12].

The leading cause for aggregation of polymeric particles is hydrophobic interaction. The particles are likely to form aggregates in aqueous solution to reduce their total surface area, and thus lower their surface energy. Silica beads are more hydrophilic

because of their surface hydroxyl groups. For them, the main cause of aggregation is charge interactions. Furthermore, higher temperature or particle concentration increases the likelihood for the particles to contact, thus creates more opportunities for aggregation.

To break aggregates and homogenize the suspended particles, two methods are commonly used, sonication and vortexing. In addition to these two physical methods, the addition of suitable molecules can often effectively reduce the hydrophobicity or surface charges of the particles, thus reversing the aggregation. The choice of the right solvent is often the best way to avoid particle aggregation.

3.2.3 Packing and Porosity

The packing quality and porosity of chromatographic columns are two of the most important factors for column performance. Therefore, it is worthwhile to discuss bead packing and porosity. Let us start with a simple case, packing of uniformly-sized solid spherical beads. Two types of packing are the most common, BCC (Body-Centered Cubic) and FCC (Face-Centered Cubic). For BCC packing (Figure 3-1 (a)), there are two beads per unit cell. The coordination number is eight, meaning each bead has eight closest neighboring beads. The porosity for BCC is 0.32. Examples of BCC materials are chromium (Cr) and tungsten (W). For FCC packing (Figure 3-1 (b)), there are four beads per unit cube. The coordination number is twelve. The porosity is 0.26. Examples of FCC materials are aluminum (Al), copper (Cu), and platinum (Pt). For all types of packing of solid spherical beads, only inter-particle porosity exists, and the porosity of 0.26 obtained for FCC is actually the smallest possible. Although dense packing is desired for chromatographic columns, the commercial non-porous-beads can only obtain column

porosities of about 0.4. One reason is that chromatographic beads have considerable variations in size and shape. The other reason is that the packing process is not able to replicate the uniform crystal structures.

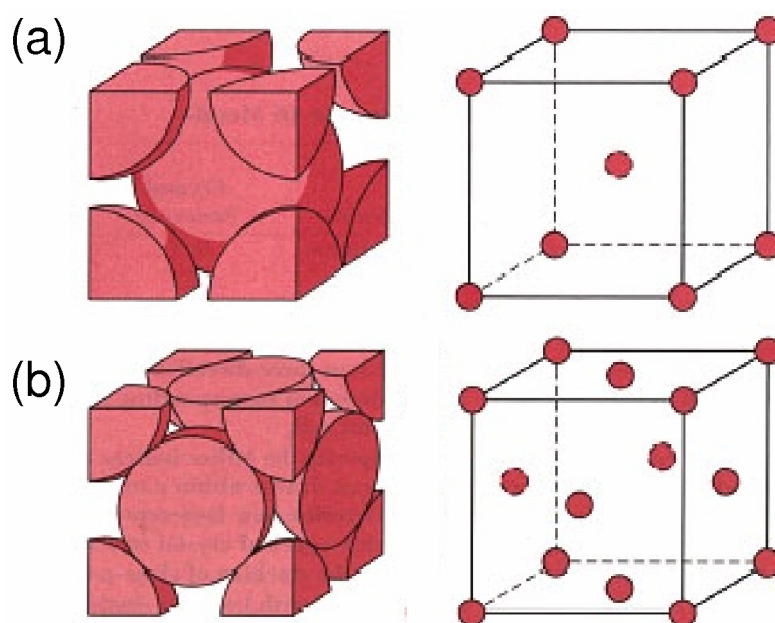


Figure 3-1 Two common particle packing structures (a) BCC; (b) FCC.

In addition to dense packing, high porosity is also desired for HPLC columns. Higher porosity means more surface area, more efficient separation, and less flow resistance. However, high porosity resulting from loose packing is undesirable since it creates dead volumes that cause excessive band broadening. Closely-packed porous-bead columns can solve this dilemma since inner-particle porosity is added to the inter-particle porosity. Commercial porous-bead columns have total porosities around 0.7 to 0.8, which means as little as only 20% of the volume inside the column is occupied by solid material.

3.2.4 Applications in MEMS

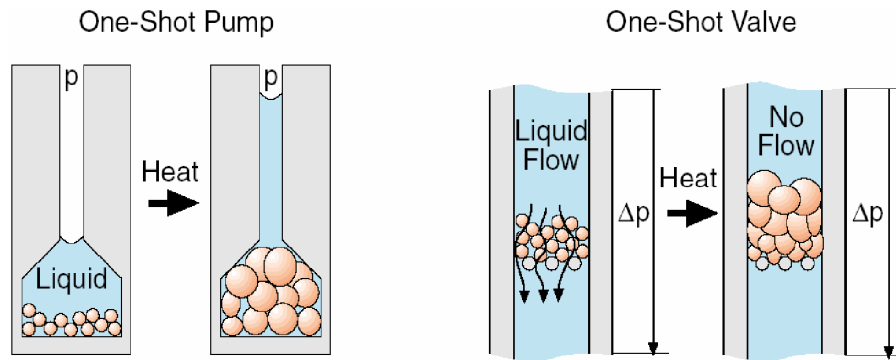


Figure 3-2 One-shot pump and valve using expandable microspheres.

A wide variety of interesting applications of micro and nano particles in MEMS are already available. For example, fluorescent and dyed particles are frequently used in microfluidic devices for flow visualization [13]. Magnetic micro-beads can be manipulated in micro devices for transportation of chemical reagents and cells [14]. Using thermally expandable microspheres, one-shot micro-valve and micro-pump (Figure 3-2) have been demonstrated [15]. The valve can be used for normally-open (NO) applications. The pump can be used for chemical release. They are one-shot only since the expansion is irreversible. Using silica bead-packed capillaries with electrokinetic pumping, pressures over 8000 psi have been achieved [16]. The pressure is proportional to the voltage applied, and inversely proportional to square of the bead diameter. Moreover, microspheres with special coatings have been demonstrated for multi-analyte sensor arrays for the analysis of complex fluids (Figure 3-3) [17]. Each bead in the array acts like a taste bud. When combined, these beads form an array for detection of a variety of important classes of analytes, including acids, bases, metal cations, metabolic cofactors, and antibody reagents.

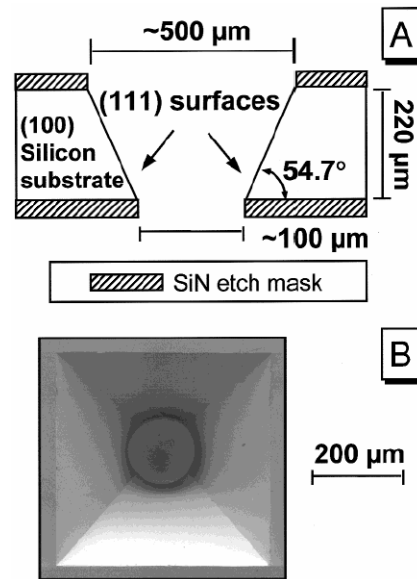


Figure 3-3 Multi-analyte sensor using specially-coated beads.

However, none of these applications directly integrates particles into the device. Instead, the particles are usually injected into the device through access holes or placed by micromanipulators after device fabrication.

3.3 Integrating Beads into Micromachined Device

3.3.1 The Method

MEMS devices are integrally fabricated with included beads by starting with a mixture of a sacrificial material and beads and disposing the mixture onto a substrate. A MEMS structure is fabricated on the substrate including at least part of the mixture, so that at least some of the mixture is enclosed in the MEMS structure. Finally, the sacrificial material is removed, leaving at least some of the beads substantially free and enclosed in the MEMS structure.

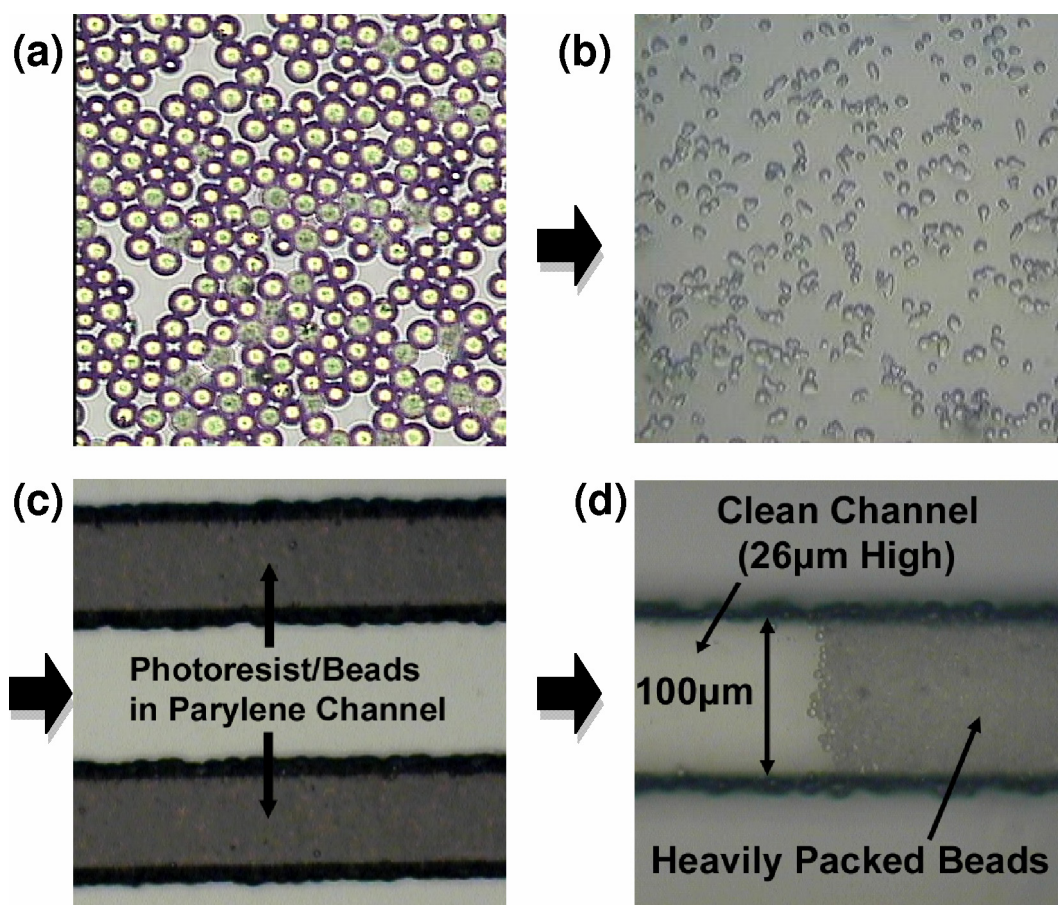


Figure 3-4 Pictures illustrating the major steps for integrating beads into parylene channel.

The major steps for integrating beads into a typical parylene device are shown in Figure 3-4. First the beads (Figure 3-4 (a)) are mixed with photoresist. The mixture is spin-coated (Figure 3-4 (b)) and photo-patterned. Parylene is coated (Figure 3-4 (c)) on top to form channels and filters, where filters are channels with height smaller than the bead diameter. After photoresist removal by acetone, the beads are free to move in the channel but trapped by filters at ends of the channel. Figure 3-4 (d) illustrates a densely-packed column with 5 μm diameter silica C18 LC beads. The column is 100 μm wide and 26 μm high. The process flow for the device is shown in Figure 3-5. Despite a few

novel aspects, the bead integration process is still mainly a photolithography process, which allows its easy integration with other processes and/or devices.

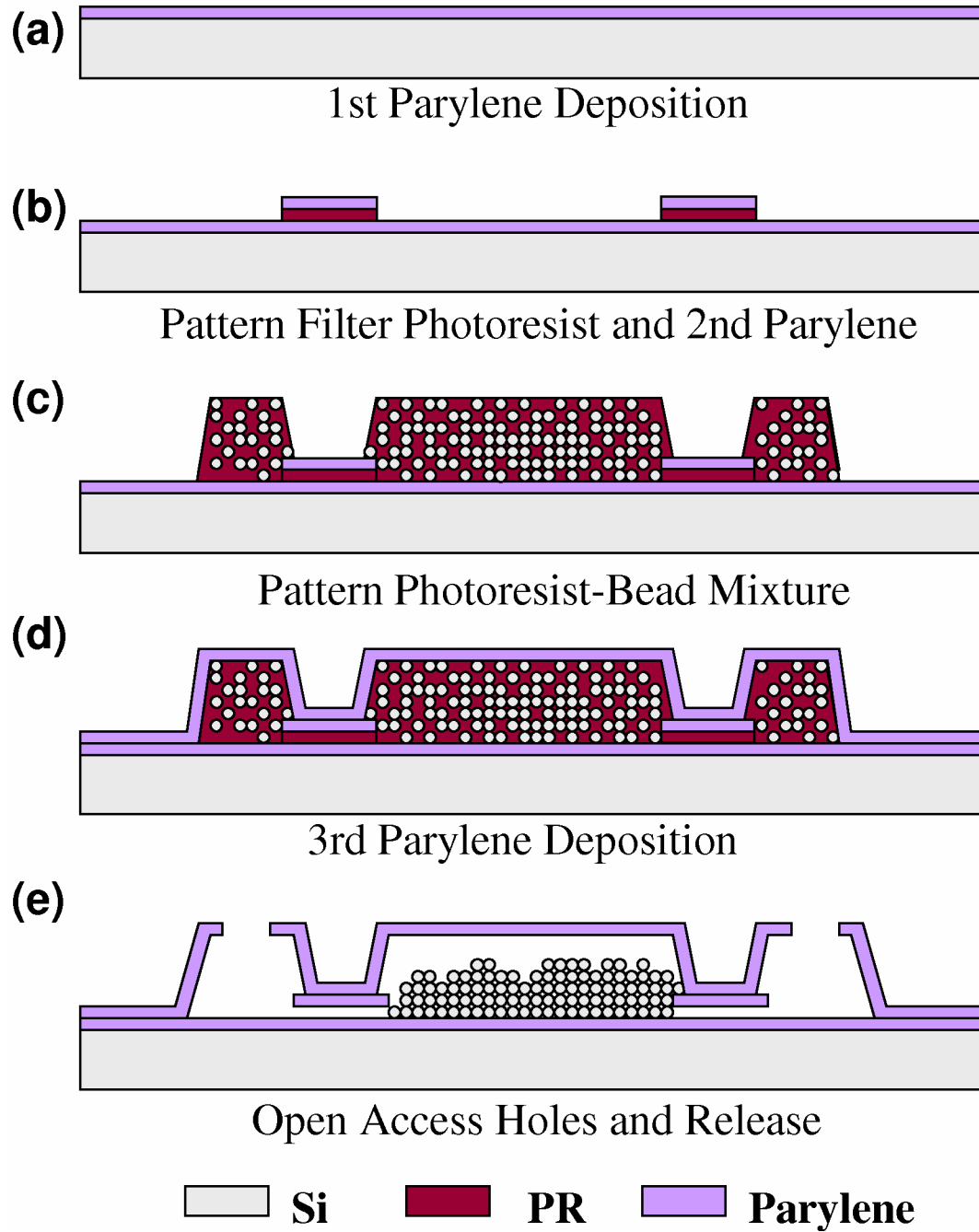


Figure 3-5 Process flow for the testing device for bead integration technology.

3.3.2 Mixing and Spin-Coating

The fabrication process starts with mixing particles, such as LC beads, with a sacrificial material, such as photoresist. By measuring the weight and knowing the density of the particles, the total volume of the particles, and thus the volume mix ratio between the sacrificial material and particles, can be determined. Then to remove the bubbles generated by mixing, the mixture can be degassed by any degassing technique, such as vacuum or centrifuge. After that, the mixture is applied onto the wafer substrate by standard spin-coating or any other appropriate coating processes, such as squeegee.

A low-spin-rate effect is found to create web-like non-uniform bead distribution in the spin-coated film. As Figure 3-6 shows, the beads are dense in some areas while sparse in others. The hypothesis is the spin-rate is not high enough to create enough force during spinning to break the bead aggregates and distribute the beads uniformly.

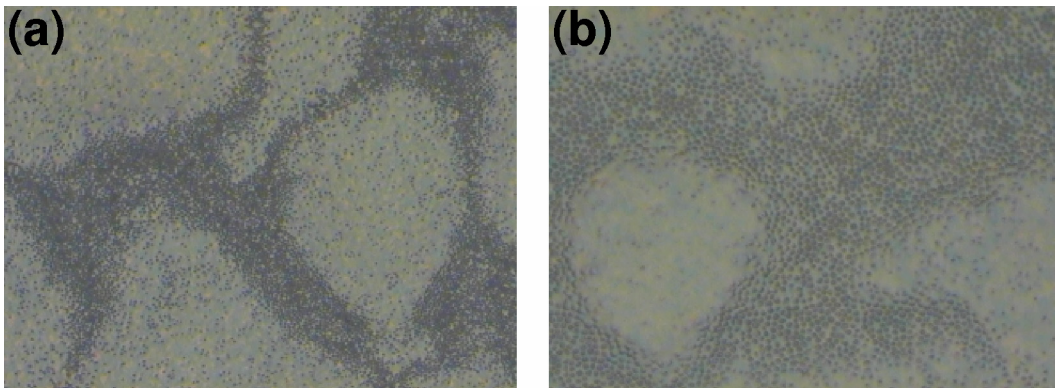


Figure 3-6 Spin rate effect on the coated photoresist-bead film.

The thickness of the spin-coated mixture film depends on the spin rate, type of bead and photoresist, and mixing ratio. The higher the bead content in the mixture, the thicker the resulting film becomes, which is due to the increase in effective viscosity of the mixture. It is found that substantially thicker films can be achieved by adding enough

particles to the mixture before spin-coating. For example in Figure 3-7, the bead ratio in (b) is 3.5 times of that in (a). The film thickness in (b) is 44 μm compared to 12 μm in (a). In addition, the film thickness can be further increased by multiple spin coatings. This enables many thin-film materials to be extended to thick-film applications.

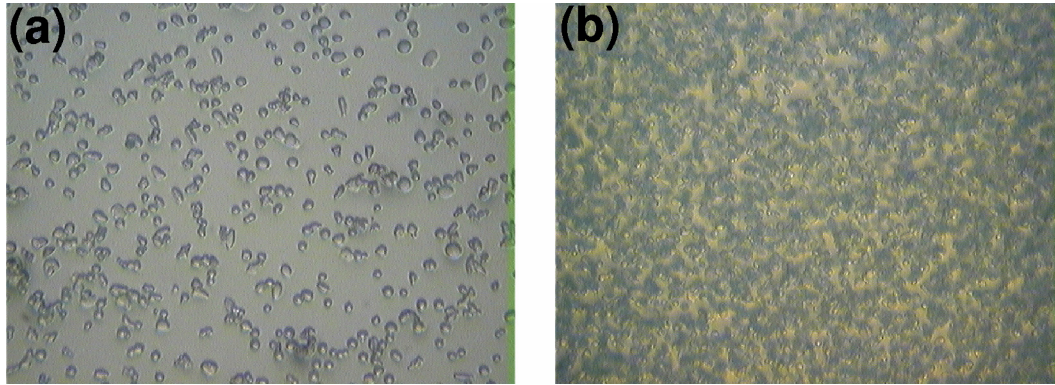


Figure 3-7. Spin-coated photoresist-bead film and the mixing ratio effect.

3.3.3 Patterning

Patterning of the mixture can be achieved with either photo-patterning or etching with a patterned mask on top of the mixture film. When photoresist is utilized as the sacrificial material, a standard photolithography process can be conveniently used.

In order to successfully pattern the bead-embedded thick photoresist film, multiple exposure-developing cycles are often necessary. It is different from simply increasing exposure and developing time, in which only the film top part gets overexposed, since the beads may block the bottom part from exposure. By developing away the exposed top part before the next exposure, the bottom parts of the film can then be fully exposed. By repeated exposure and developing, the mixture film can be patterned with ease. Finally, ultrasonic cleaning can be used to detach and remove any particles still sticking to the substrate. Figure 3-8 shows a patterned bead-photoresist film.

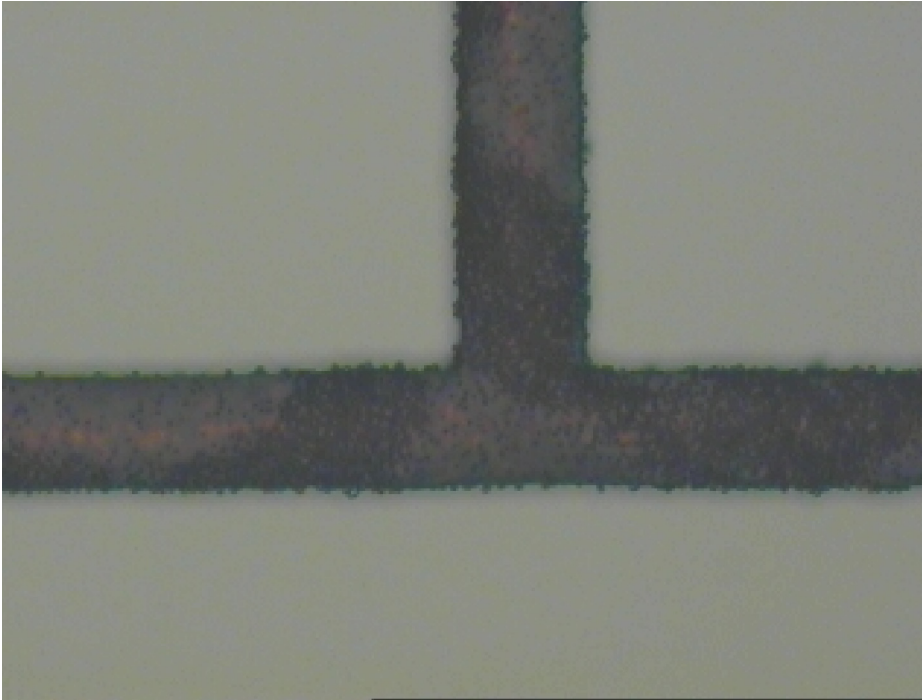


Figure 3-8 Patterned bead-photoresist mixture film.

3.3.4 Parylene Coating

The photo-patterning process can leave a bumpy surface after developing. This is due to beads either exposed on or removed from the top surface during developing. Some SEM (Scanning Electron Microscope) pictures are shown in Figure 3-9. Figure 3-9 (a) and (c) are from one sample with the beads sticking out on the patterned film, while Figure 3-9 (b) and (d) are from another sample where most beads are removed from the photoresist top surface. Therefore, the photo-patterned structure surface roughness is about twice the bead diameter.

Those beads that are exposed after photo-patterning tend to stick to subsequently conformally-deposited parylene and do not release from parylene even after photoresist removal. Figure 3-10 (a) shows one example where the beads are trapped in the top

parlylene even after photoresist is removed from the chamber. The out-of-focus Au stripes at the chamber bottom can be used to confirm the beads are really sticking at top. To prevent bead sticking to the top parlylene, a buffer photoresist layer can be spin-coated on top of the mixture film and patterned together with the mixture. The result can be seen in Figure 3-4 (d) where essentially no beads stuck to the top parlylene.

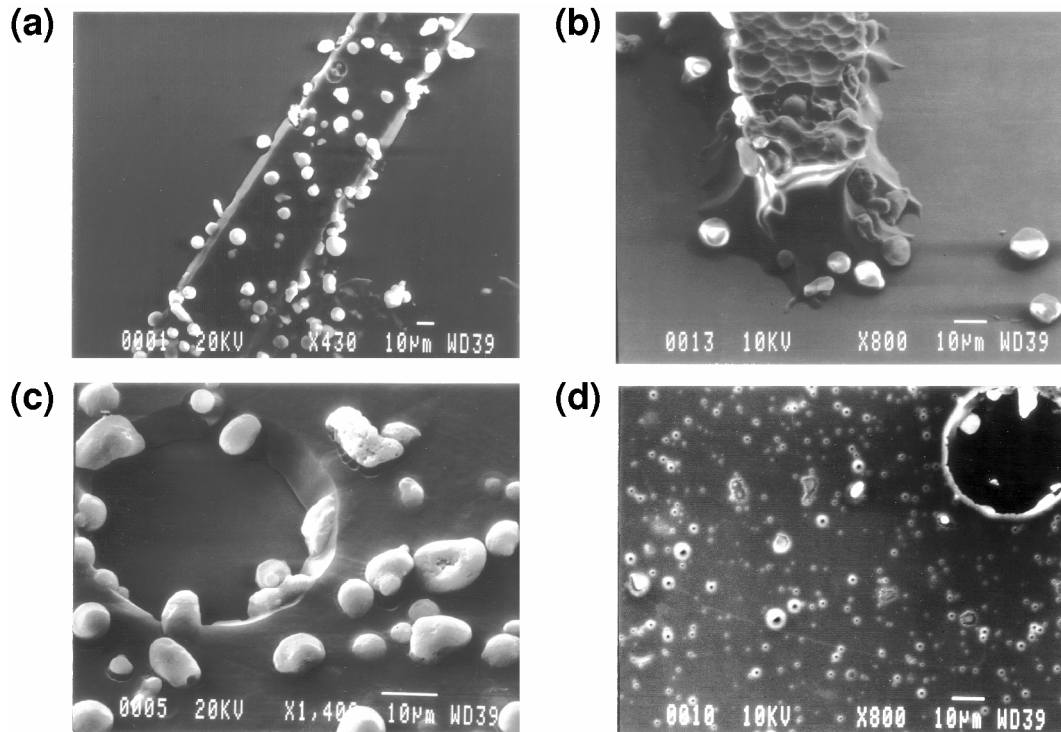


Figure 3-9 Scanning electron microscopic pictures of patterned bead-photoresist films.

Similarly, bead/photoresist scums can also stick to the bottom substrate after developing, which is sometimes hard to remove even with ultrasonic agitation (Figure 3-10 (b)). The solution is a bottom buffer photoresist layer spun before the mixture film, which prevents direct bead-to-substrate contact. In summary, the bottom buffer photoresist, the beads/photoresist mixture, and the top buffer photoresist should be spin-coated sequentially and patterned all together.

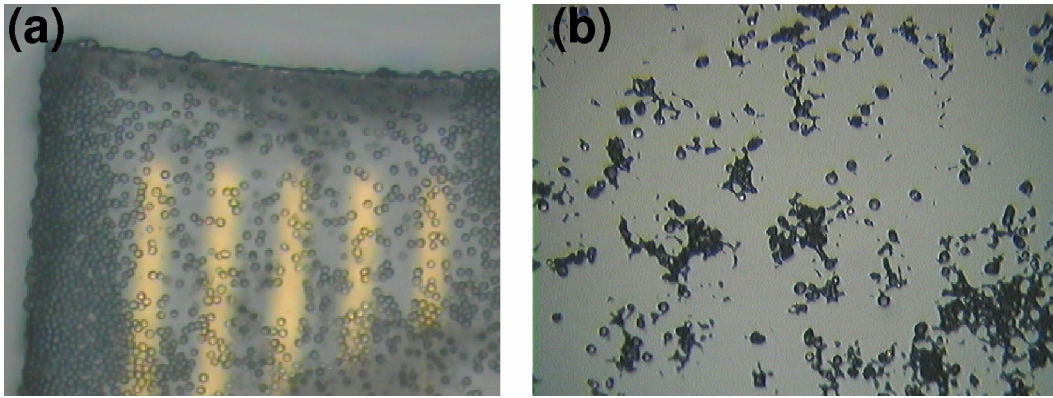


Figure 3-10 Beads sticking to subsequent parylene cover or to the substrate.

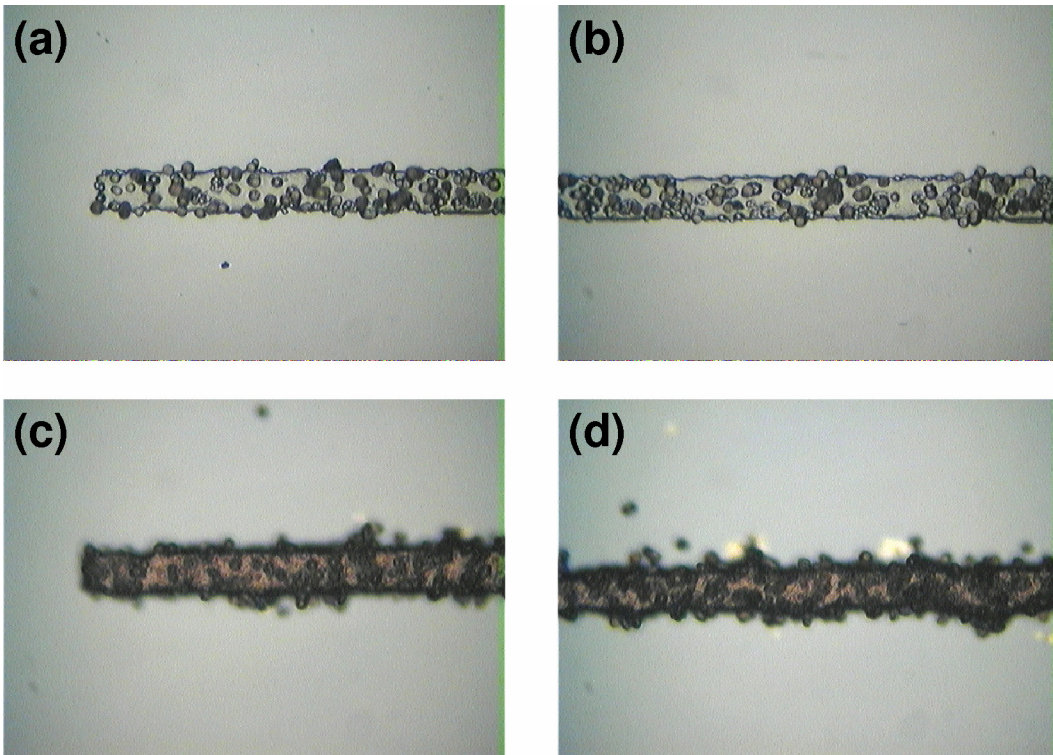


Figure 3-11 Parylene thickness effect.

In the case where no buffer photoresist layers are used, the thickness of the parylene film is found to be important as well. When the parylene film is very thin, for example 1 μm , the film cannot provide pinhole-free protection for the bead-photoresist

mixture underneath. When such a device is immersed in acetone, the photoresist can be stripped within minutes. Figure 3-11 (a) and (b) shows an example where photoresist is removed from 1 μm thick parylene “encapsulated” micro-channel. Figure 3-11 (c) and (d) shows another device with 3 μm thick parylene encapsulation, in which the photoresist is intact even after a long time in acetone. The hypothesis is the bumpy surface and the porous beads make parylene inaccessible to some tiny pores. Thus the parylene fails to fill some pores when it is too thin, leaving some pinholes around the pores.

3.3.5 Releasing

After the structural parylene is etched to open access to the mixture layer, the sacrificial material can be removed by a corresponding etchant or solvent, such as photoresist stripper or acetone when sacrificial photoresist is used. The particles are kept inside the structures by on-chip filters, which usually are designed to restrict one dimension, such as height, of the flow channel to prevent particles from leaving or entering the fluidic system. Figure 3-4 (d) shows a micro-channel with beads released but still confined in the channel.

With the embedded beads, however, this seemingly straightforward process can have complications. One phenomenon observed is bead-photoresist aggregation, which prevents the photoresist from being removed. Figure 3-12 shows two devices both having this problem. Figure 3-12 (a) shows blocks of bead-photoresist aggregates still in the device, although some parts are clean. The problem shown in Figure 3-12 (b) is even worse. The whole micro-channel seems like a big aggregate in which nothing can be removed. This phenomenon usually appears for high bead content in the mixture and high

baking temperature. One hypothesis is polymer-assisted particle flocculation (Figure 3-13) [12], where the photoresist polymer helps the beads to form almost irreversible aggregates. Flocculation refers to the type of aggregation that arises from inter-particle bridging by ligands or macromolecules. In some cases, even without photoresist as a binder, beads can still fuse together at high temperatures. Therefore, to avoid aggregates, the bead ratio should not be too high and processing temperature must always be kept low, for example 60 °C to 80 °C.

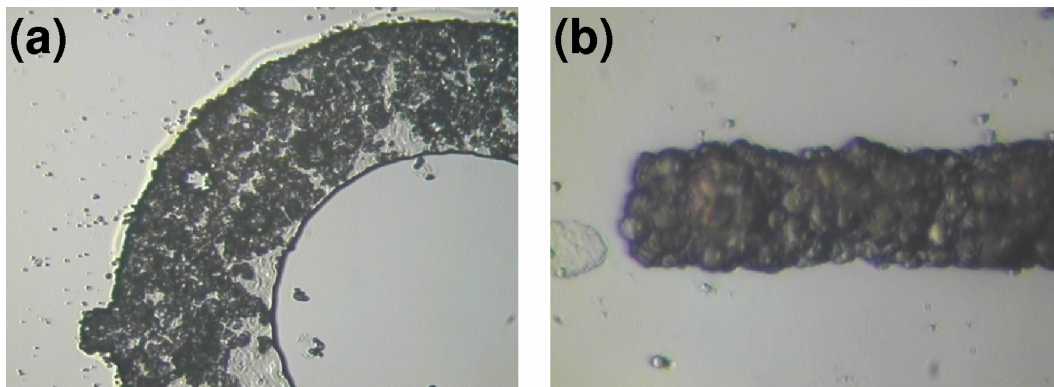


Figure 3-12 Photoresist releasing issue.

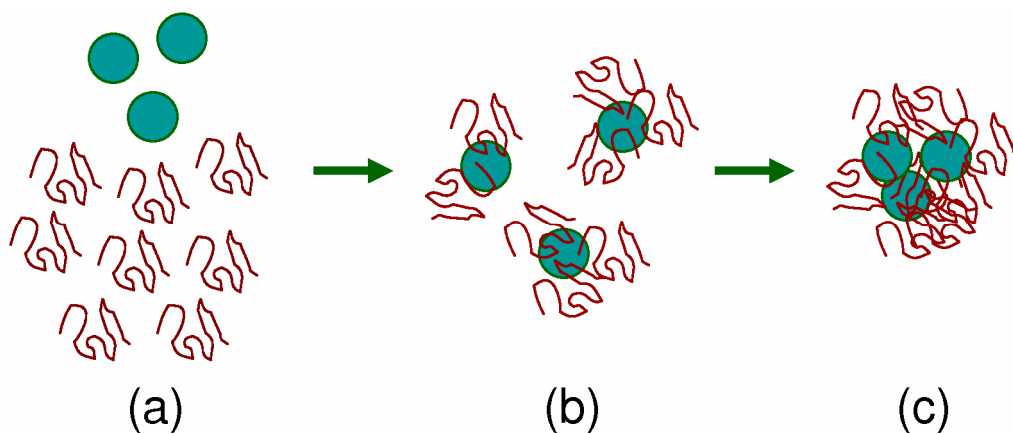


Figure 3-13 Polymer-assisted particle aggregation.

3.4 LC-ESI/MS Chip with Integrated Bead Column

3.4.1 Introduction

The LC-ESI/MS microchip presented here is microfabricated on a silicon wafer through a single batch fabrication. The liquid chromatography column, bead filter, and electrospray ionization (ESI) nozzle are all integrated on-chip with a process that is compatible with CMOS integrated circuit technology. To make the chip, the bead integration technology developed in the previous section is incorporated with a parylene ESI nozzle process similar to the one used in [10].

3.4.2 Design

This microchip has a wafer backside access hole as fluidic inlet. Solvents and sample flow through the integrated LC column packed with LC beads, and then enter the electrospray nozzle with minimum dead volume in between, which greatly reduces post-column peak broadening. The freestanding nozzle couples the chip to a mass spectrometer for on-line detection and analysis. The inlet bead-filter is comprised of multiple independent channels all having a height smaller than the bead diameter (Figure 3-14 (a), (c)). The redundancy of filter channels is to guarantee the column inlet remains open even when some of the filter channels have problems, such as stiction. Since the nozzle height is smaller than the bead diameter, it is also used as outlet bead filter (Figure 3-14 (b), (d)). The on-chip packed column length is 8 mm. The cross section of the column is 100 μm wide and 25 μm high, and shares the same cross-sectional area as a 56 μm ID capillary. The filter/frit is a 3 μm high channel leading to the ESI nozzle. The ESI nozzle freestanding overhang is 600 μm in length (Figure 3-14 (e)). The nozzle opening

is 15 μm wide by 3 μm high. The column beads are from Grace Vydac (Hesperia, CA). They are 5 μm diameter particles with 300 \AA pores and coated with C18 groups, which is one of the most popular types for reversed-phase LC columns.

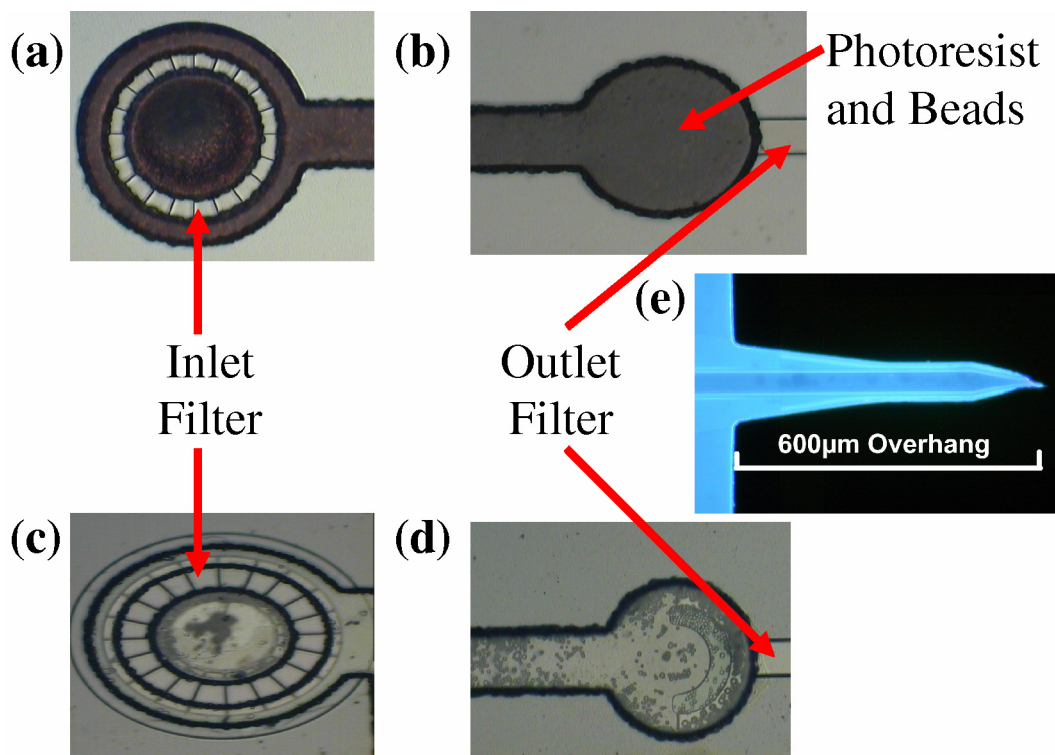


Figure 3-14 Fabricated device pictures of the LC-ESI chip.

3.4.3 Microchip Fabrication and Packaging

3.4.3.1 Fabrication Process

The process used to fabricate the integrated LC-ESI chip is illustrated in Figure 3-15. It starts with growing a 1.7 μm SiO_2 layer on both sides of a 4-inch silicon wafer by thermal oxidation. Then using a delay-mask technique described below, two-level backside holes are created with DRIE, leaving only a 50 μm thick diaphragm (Figure 3-15 (a)).

First, the backside oxide is patterned and etched with buffered HF (Transene, Danvers, MA) which defines the 150 μm diameter small hole. Then an 8 μm photoresist AZ4620 (Clariant, Somerville, NJ) layer is patterned on the backside to define the 360 μm diameter big hole, which is concentric with the small hole. DRIE is performed to etch the small hole 200 μm deep into the silicon wafer backside using the small-hole oxide as a mask. After etching the backside oxide using the big-hole photoresist as a mask, DRIE is performed again to etch the backside until only a 50 μm thick diaphragm is left. The big hole is “delayed” compared to the small hole, which creates a two-level structure used as a fluidic access port. The two-level structure can be used as a tubing stopper when coupling tubing is directly inserted into the chip.

The frontside oxide is patterned to open areas for the fluidic access hole and for nozzle release. Then a 3 μm thick parylene C (Specialty Coating Systems, Indianapolis, IN) film is conformally deposited on the frontside only. The wafer backside is covered during the parylene deposition. A 3 μm thick photoresist layer is spin-coated and patterned for the inlet filters and nozzle. A second 3 μm thick parylene layer is deposited on the frontside, and patterned all the way through the bottom photoresist and first parylene layer to the substrate (Figure 3-15 (b)).

Photoresist AZ4620 is used to mix with the beads at 1:10 (bead:photoresist) volume ratio. The mixture is spin-coated at 2.5 krpm after a 2.5 μm thick bottom buffer photoresist coating, which is followed by a 5 μm thick top buffer photoresist coating. This mixture film is patterned by multiple exposure-developing cycles. The wafer is further cleaned in an ultrasonic tank for a short period of time.

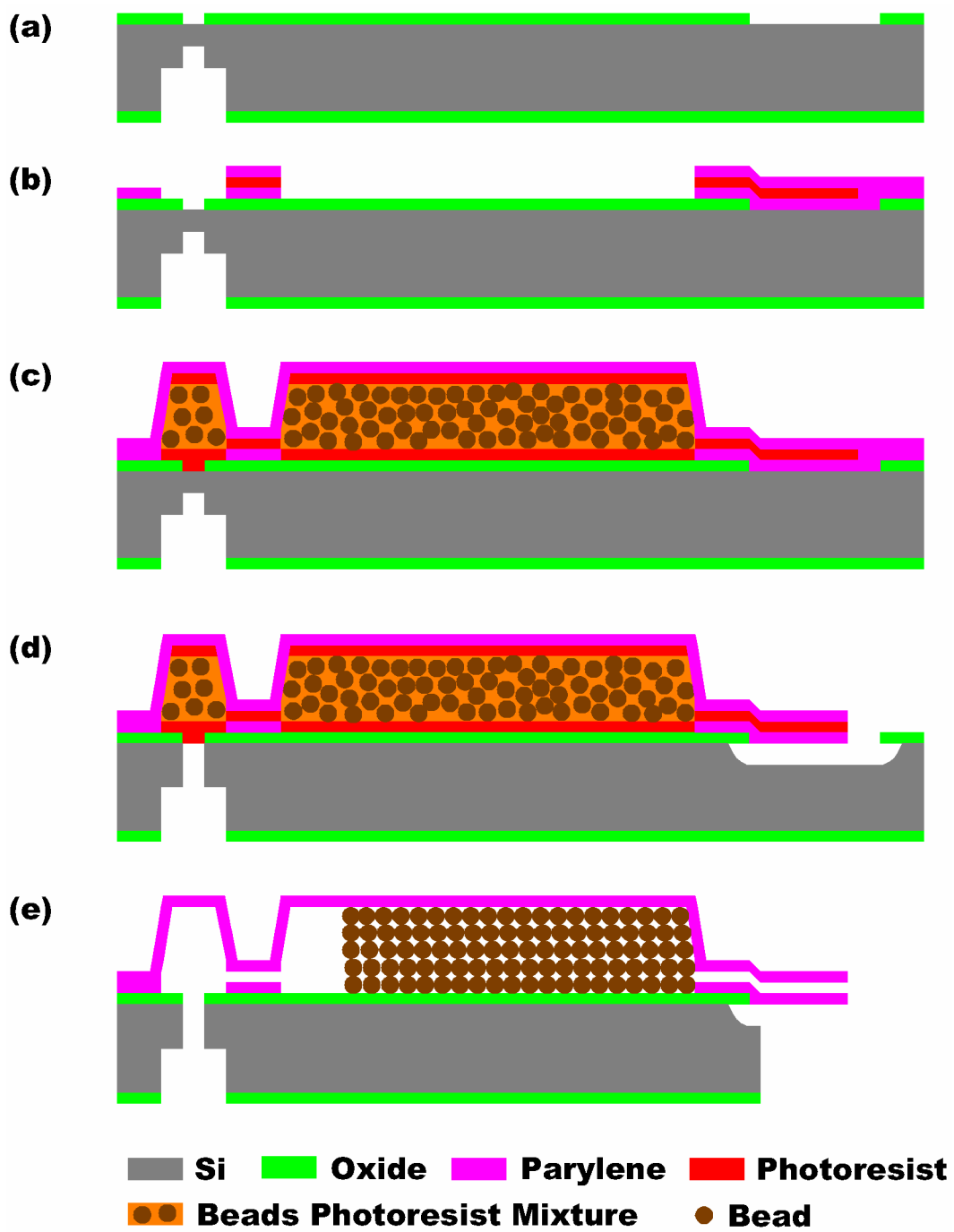


Figure 3-15 Fabrication process flow for the liquid chromatography – electrospray ionization (LC-ESI) chip with integrated bead-column.

The third 5 μm thick parylene layer is deposited to cover the wafer frontside (Figure 3-15 (c)), and patterned with a thick photoresist mask to open the nozzle. DRIE is performed again on the backside to open the access hole. The frontside substrate silicon underneath the nozzle and along a trench perpendicular to the nozzle is etched with BrF_3 gas-phase silicon etching, in order to make the nozzle freestanding. Pre-patterned frontside oxide is used as the mask. The etching depth is 150 μm . Then, the channels are released by dissolving the channel sacrificial photoresist in warm acetone. The freed beads automatically pack to the nozzle end during drying, since the nozzle end is a much smaller opening compared to the column inlet. The column can be further packed with an off-chip pressurized flow. Finally, the nozzle is freed by detaching a piece of the chip along the across-chip trench (Figure 3-15 (e)). To further strengthen and passivate the device, an optional epoxy overcoating layer can be applied to the device.

Figure 3-14 shows various parts of a fabricated LC-ESI chip, both before (Figure 3-14 (a), (b)) and after photoresist removal (Figure 3-14 (c), (d), (e)). Both the multiple inlet filters and outlet filter/nozzle can be clearly seen in the pictures. After photoresist removal, it can be seen that the beads are released in the channel. Figure 3-14 (e) shows a fluorescent picture of the freestanding parylene ESI nozzle. The freestanding part is 600 μm long. The nozzle opening is 15 μm wide by 3 μm high.

3.4.3.2 Photoresist Releasing Issue

The main challenge for this device and other long-channel devices is the photoresist releasing process. Firstly, the micro-channel is long and packed with beads. Therefore it takes a long time for acetone to diffuse deep into the channel to dissolve

photoresist. A detailed discussion of photoresist as a micro-channel sacrificial material by dissolution in acetone is given in [18]. One effective way to reduce the diffusion time is to increase the diffusion constant by increasing temperature of the acetone solution, which also increases the dissolution rate. However, heating temperature is limited by the acetone boiling point of 56.5 °C and safety concerns since acetone is flammable. It is found that ST-22 standard photoresist stripper is much less effective in the micro-channel releasing process than acetone, although ST-22 provides a cleaner surface than acetone for photoresist film stripping. It is because ST-22 is much more viscous and the diffusion constant is much lower. IPA (isopropyl alcohol), another common solvent for removing organic residues, is much less effective for dissolving photoresist than acetone even when heated close to its boiling temperature of 82.5 °C.

Secondly, since the photoresist is not etched away but rather only dissolved, it remains in the acetone solution in the channels. The only process taking photoresist out of the channel is diffusion, until the equilibrium is reached between the photoresist concentrations in the channel and in the bulk acetone solution. Therefore, frequent changing of the acetone solution can help lower the photoresist concentration inside the channel faster. Ultrasonic agitation can also speed up this equilibrium process, but it may damage freestanding parylene structures as well. Theoretically, the photoresist cannot be completely depleted from the channel, even if the acetone solution is refreshed periodically.

Thirdly, even if the channel has a very low photoresist concentration, which usually appears as a clear channel under optical microscope, the photoresist could still clog small openings when dried. Since acetone is highly volatile while photoresist is

basically non-volatile, photoresist is usually left at the channel exit when the acetone all evaporates. This could cause clogging when the exit is small. Sometime this is so serious that even repetitive acetone dissolving and drying cannot remove the clogs. One way to avoid this is to use large openings whenever possible. Based on past experiences, openings less than 10 μm wide, 3 μm high can be problematic.

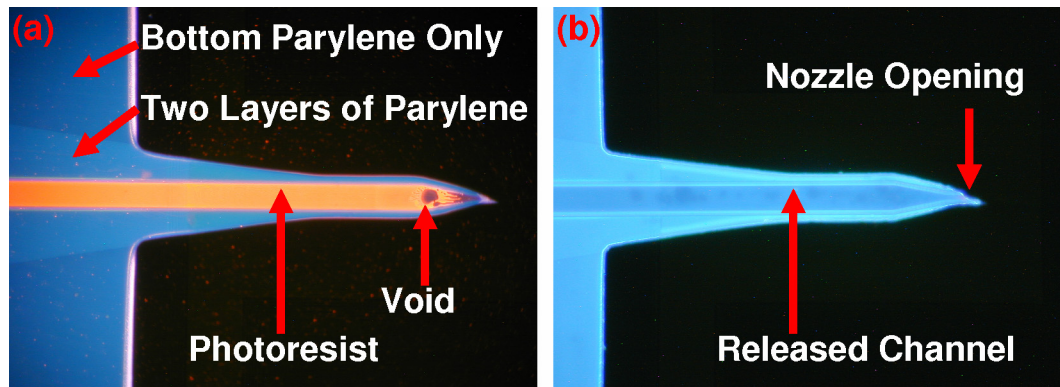


Figure 3-16 Fluorescent diagnostic technique.

Since low-concentration photoresist could still be present in the channel even when the channel looks clear under optical microscope, a fluorescent diagnostic method is developed to confirm the end of the releasing process. Fluorescent detection is chosen because of its high sensitivity. Using a fluorescent microscope, the chip can be imaged to show the contents of the parylene channels and nozzle. Figure 3-16 shows two fluorescent pictures before and after photoresist releasing. Parylene appears to be blue, while photoresist appears brown (Figure 3-16 (a)) to red (Figure 3-17) depending on its concentration. Multiple layers of parylene, hollow parylene channels, and voids can also be easily identified.

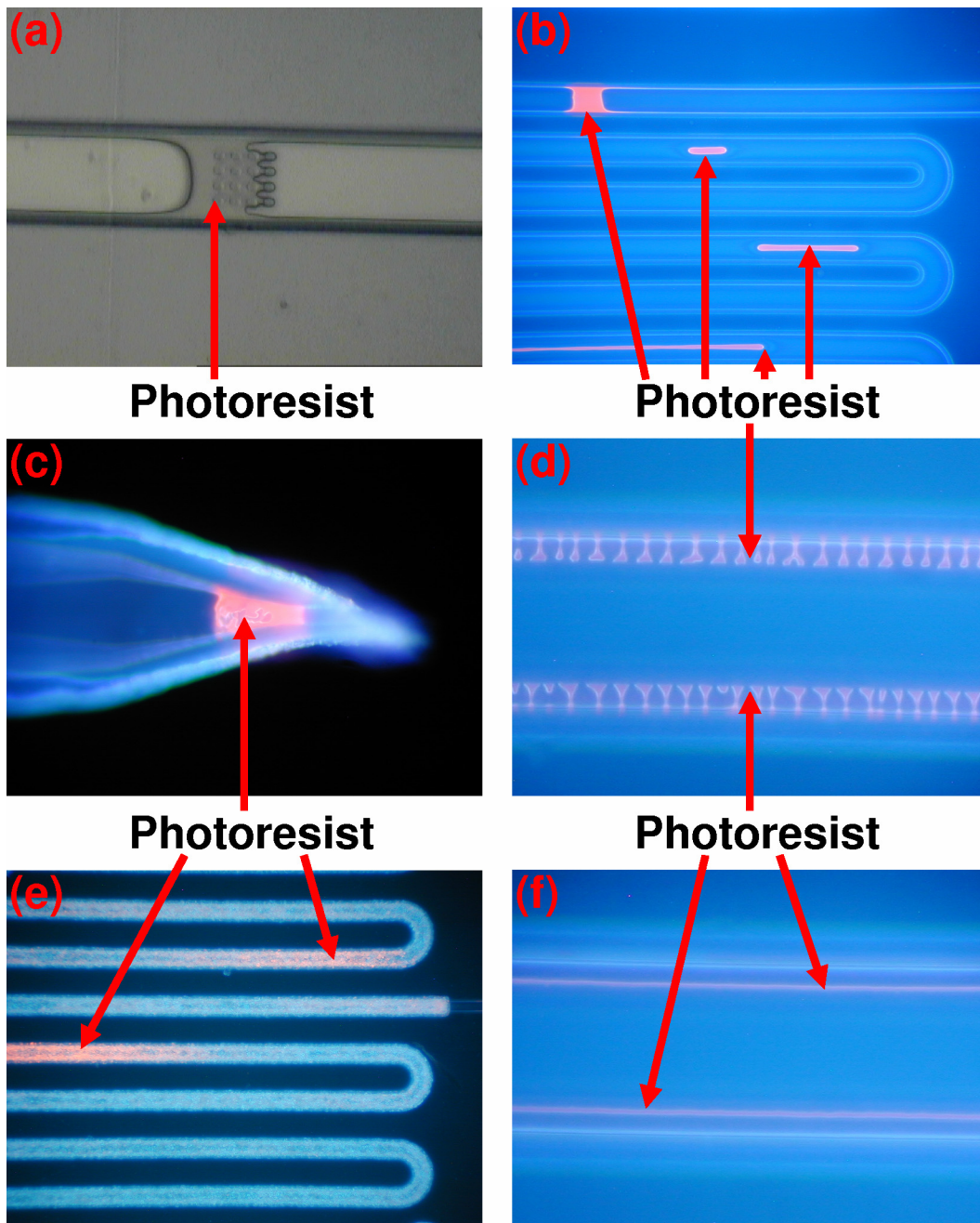


Figure 3-17 The photoresist releasing issue in various forms.

Figure 3-17 (a) shows an optical picture of a typical photoresist clogging, which is caused by an in-channel post array greatly restricting flow. Figure 3-17 (b) to (f) are all fluorescent pictures showing a variety of photoresist releasing problems after drying.

Figure 3-17 (b) is typical where the photoresist either blocks the channel or just stays somewhere in the channel without blocking it. Figure 3-17 (c) shows a clog near nozzle tip. Figure 3-17 (d) and (f) show two forms of photoresist coatings on channel wall after drying. The photoresist in (f) is extremely hard to visualize with an optical microscope, since the photoresist layer is very thin and the concentration is very low (very light color in the picture). Figure 3-17 (e) shows photoresist residue in a bead-photoresist mixture column after incomplete releasing, which is also difficult to visualize with an optical microscope.

3.4.3.3 Packaging

The microchip is packaged with a custom-made jig (Figure 3-18). Figure 3-18 (a) shows the jig body that is 27 mm long, 20 mm wide, and 5 mm thick. The chip is put in the 10.2 mm by 8.8 mm recess with o-rings below the chip to provide sealing. Capillaries are inserted into the jig back hole to feed liquid to the chip. The inserted capillary OD (Outer Diameter) is slightly larger than the jig back hole. The connection withstands tens of psi pressure. A 2 mm thick top cover (Figure 3-18 (b)) is screwed down to compress the chip, holding the chip in place and helping o-ring sealing. The material for the jig is acrylic, since it is commonly available and easy to machine. However, it is found that acrylic does not withstand the solvents used in HPLC experiments. Therefore, for later jigs, PEEK (polyetheretherketone) (McMaster-Carr, Los Angeles, CA) material is always used instead. PEEK is essentially inert to all chemicals and solvents used in HPLC.

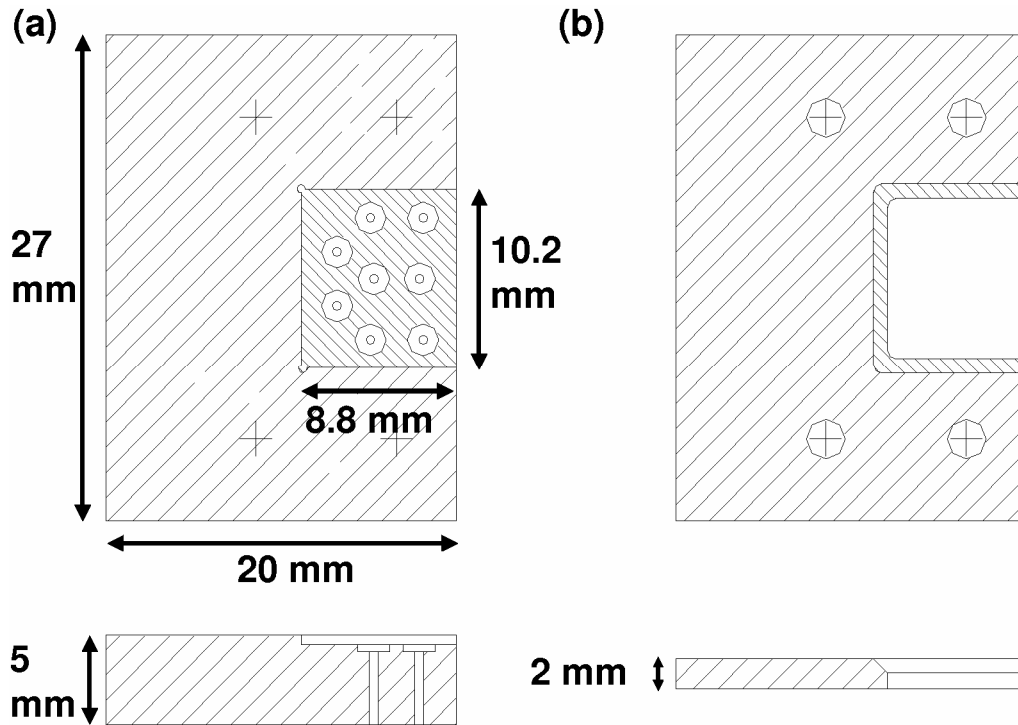


Figure 3-18 Schematics of the packaging jig for the microchip.

3.4.4 Testing Results and Discussion

3.4.4.1 Bead Releasing and Column Packing

While the beads are embedded in photoresist during processing, they are loosely released inside the column after photoresist removal. The beads pack automatically during drying at the nozzle end. They can be further packed into a dense column with a pressurized flow of, for example, DI (deionized) water at 15 psi. Figure 3-19 shows series of photomicrographs of released beads moving in a channel. The channel is 100 μm wide and 25 μm high. Bead diameter is 5 μm . In Figure 3-19 (a), (b), and (c), beads move with liquid; and in (d), air pushes liquid and beads.

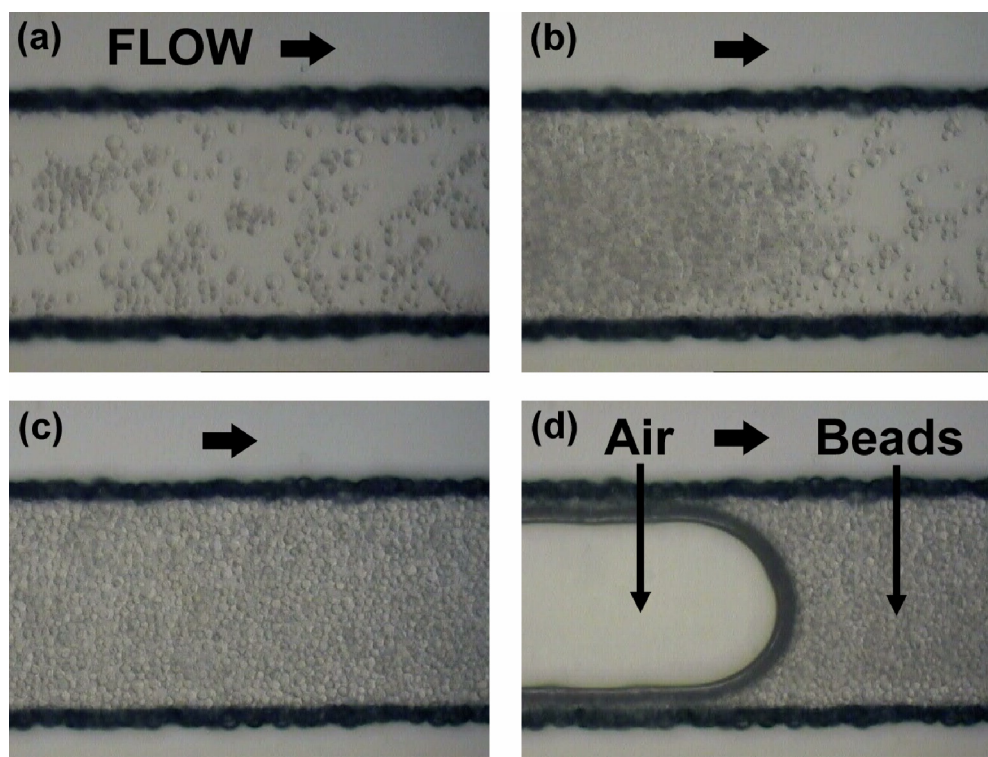


Figure 3-19 Snapshots of released beads moving with liquid in a micro-channel.

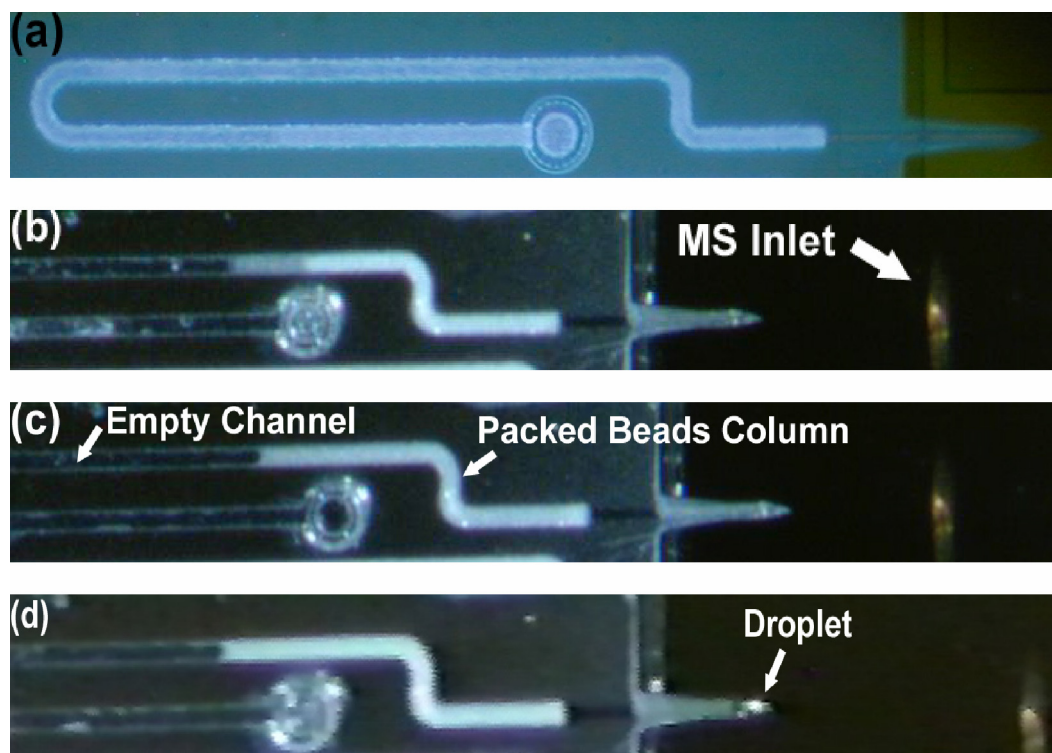


Figure 3-20 Snapshots of packing a column and electro spray to a mass spectrometer.

Figure 3-20 shows the column packing process and electrospray to a mass spectrometer. Figure 3-20 (a) shows a fluorescent overview picture of the device being tested. The full channel length (L_f) is 6800 μm (Figure 3-20 (a)). Since the nozzle end is a much smaller opening than the column inlet, the beads pack to some degree at the nozzle end automatically during drying of the column, as shown in Figure 3-20 (b). After packing (Figure 3-20 (c)), the LC column length (L_c) is 2700 μm , which corresponds to 40% packing ratio (L_c / L_f). This ratio means 1 cm long channel with beads loosely released inside will turn into 4 mm long column heavily packed with beads. The ratio is dependent on original bead-photoresist mixing ratio. The higher the bead content in the mixture, the higher the packing ratio. The current 40% packing ratio is for the original 1:10 bead-to-photoresist volume mixing ratio. To have longer packed columns, large bead “reservoirs” instead of short channels can be used. The packing is done at 15 psi with DI water. The flow rate during packing is, on average, 17 nL/sec. After packing, the flow rate drops to 3 nL/sec because of the increased flow resistance. The breakthrough time for an unretained sample to travel through this column and nozzle is 2.3 seconds. Because of the integration, the post column volume is only 0.05 nL including outlet filter and nozzle. Using the original bead volume ratio of 10% in the mixture and the column packing ratio of 40%, the porosity, ε , of the bead column is estimated to be 0.75, as shown in the following calculation,

$$\varepsilon = 1 - \frac{V_{beads}}{V_{column}} = 1 - \frac{V_{beads}}{V_{channel}} \cdot \frac{V_{channel}}{V_{column}} = 0.75 \quad (3.1)$$

where

$$\frac{V_{beads}}{V_{channel}} \approx 10\% \quad \text{and} \quad \frac{V_{column}}{V_{channel}} = 40\% \quad (3.2)$$

The porosity of a conventional capillary column (Figure 3-21) packed with the same type of beads is also estimated. The bead volume is obtained by the weight difference after and before bead packing divided by the silica density of 2.2 g/cm³. The column volume is calculated by measuring the column ID and length. The estimated porosity is 0.7, which is very close to that of the integrated on-chip column. In fact, most commercial porous-silica-bead LC columns have packing densities between 0.3 and 0.6 g/cm³ [19], corresponding to column porosities from 0.7 to 0.8. Therefore, the on-chip integrated column achieves a porosity consistent with conventional columns.

The testing result of the column physical properties is summarized in Table 3-1.

| | On-Chip Column Properties |
|---------------------------------|--|
| Bead Type | Porous Silica, C18, 5 μm Diameter, 100 Å pores |
| Column Porosity | 0.75 |
| Packed Column Length | 2700 μm |
| Packing Ratio | 40% |
| Column Cross Section | 100 μm wide by 25 μm high |
| Equivalent Column ID | 58 μm |
| Flow Rate during Packing | 17 nL/sec |
| Flow Rate after Packing | 3 nL/sec |
| Post Column Volume | 0.05 nL |
| Breakthrough Time | 2.3 sec |

Table 3-1 Summary of an on-chip column properties.

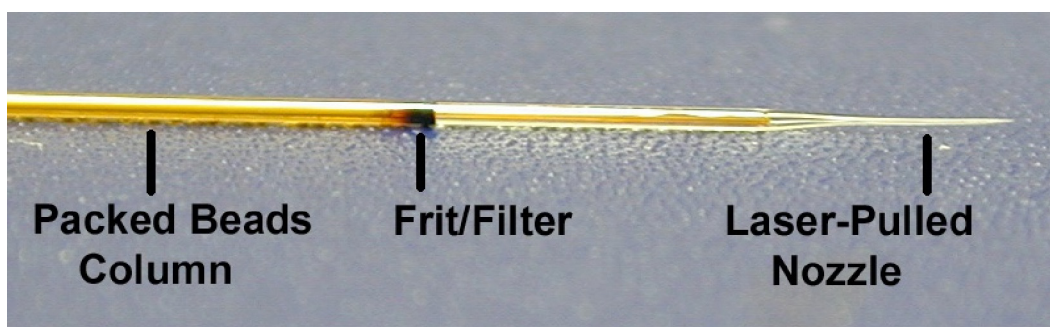


Figure 3-21 Picture of a conventional externally-packed capillary LC column and ESI nozzle.

3.4.4.2 Pressure Rating

Constant-pressure flow is provided to the chip by a pressure bomb. It is comprised of a steel chamber with a glass bottle inside filled with a solvent. A compressed-N₂ tank applies a constant pressure to the solvent inside the chamber, pushing the solvent out through a tube inserted in the solvent. The pressure upper limit of the setup can reach the tank pressure. Another pressure source used in the testing is a commercial Agilent 1100 HPLC pump. However, it can not be regulated under about 50 psi. A back-pressure column needs to be connected between the pump and the on-chip column. The flow rate is regulated, while the real pressure across the on-chip column has to be estimated.

The pressure limit of the chip is found to be about 20 psi. The parylene channels delaminate from the substrate when higher pressures are applied. For microfluidic applications, 20 psi is much higher than what most applications require. For liquid chromatographic separations, however, much higher pressures (hundreds of psi) are often needed. Therefore, on-chip separation is not performed for this chip. Significantly higher pressure rating demands great improvements on not only the parylene technology, but

also the coupling units involved, such as the packaging jig. These issues are well addressed in Section 4.2.

3.4.4.3 Electrospray to a Mass Spectrometer

The electrospray test is performed at 15 psi with 98:2 acetonitrile/water and 0.1% formic acid. The mass spectrometer is an Agilent 1100 system. The original housing for the electrospray interface is removed to allow the on-chip nozzle to access the electrospray inlet (Figure 3-22). The nozzle tip is placed a few millimeters away from the inlet. It should be noted that MS inlet has a rather high temperature between 170 and 210 °C. Therefore, the parylene tip should avoid contacting the inlet. The electrospray voltage of 1.2 kV is applied off-chip at the upstream using the method described in [11]. When the voltage is removed, the liquid coming out the nozzle can form a droplet (Figure 3-20 (d)). When the ESI voltage is on, the sample liquid sprays into the mass spectrometer. A typical electrospray spectrum and chromatogram figure obtained is shown in Figure 3-23. Figure 3-23 (a) is a chromatogram that shows ion intensity over one hour. Some big peaks are seen, which are mostly impurities in the system, such as photoresist residue in the on-chip column or dissolved acrylic from the jig. An eight-hour continuous electrospray test is done without failure or observable performance degradation of the ESI nozzle.

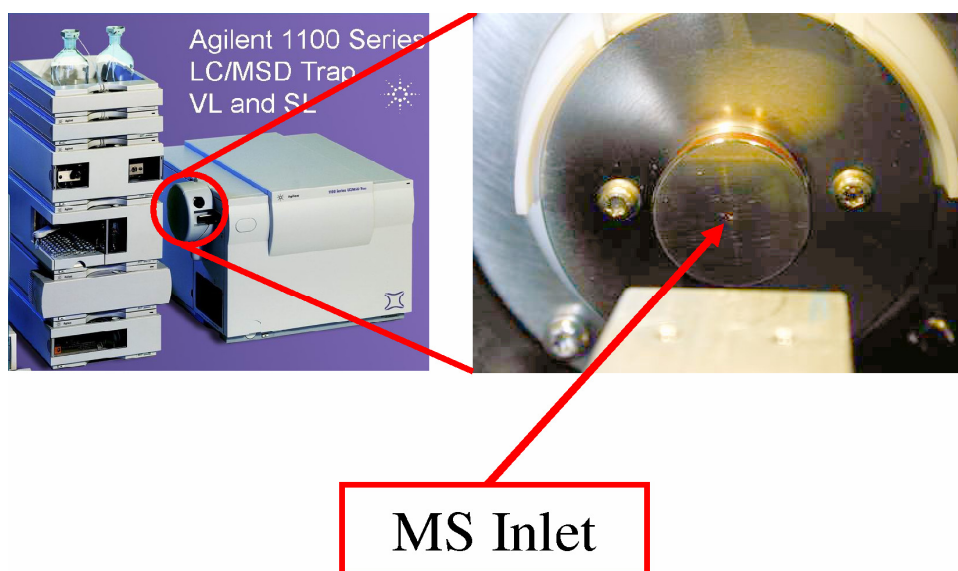


Figure 3-22 Pictures of the mass spectrometer used in the testing.

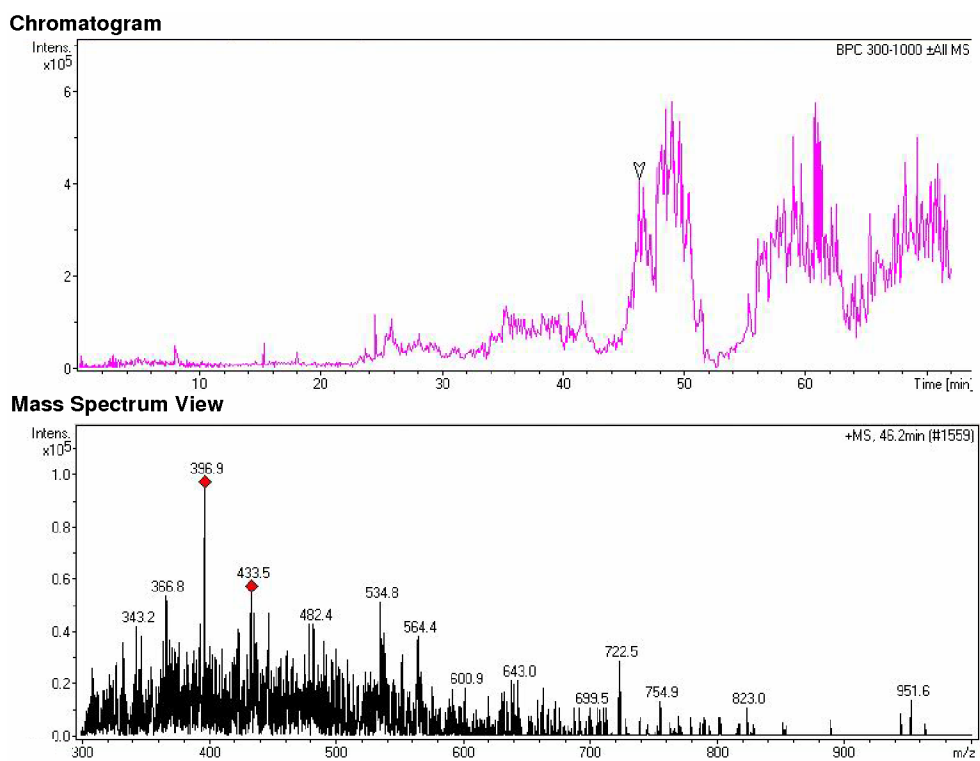


Figure 3-23 A typical electrospray spectrum and chromatogram from the on-chip LC column and ESI nozzle.

3.4.4.4 Method Validation

It is important to validate that the C18 silica beads function as normal after photoresist contamination and acetone cleaning. To do so, a capillary column-nozzle (Figure 3-21) packed with photoresist-contaminated-then-acetone-cleaned C18 beads is prepared. It starts with a 12 cm long, 360 μm OD, and 150 μm ID fused silica tubing. A window is burned in the middle of the tubing to remove its polyimide coating, and then cleaned with water. Using a standard laser pulling machine, the silica tubing is melted in the middle and pulled into two pieces, each with a needle at one end. Then another piece of tubing with 140 μm OD and 25 μm ID is inserted into the original tubing, and is cut leaving only a few millimeters inside the original tubing. The short piece is pushed all the way to the needle end of the large original tubing. Then a glass fiber filter (Whatman, Florham Park, NJ) is inserted to form the frit for column bead packing. The packing process uses the same type of beads and photoresist as those used for the on-chip integrated column. They are mixed thoroughly then suspended in acetone. The suspension is packed into a conventional silica capillary column at 400 psi. The packed column is washed with acetone for three hours, followed by washing with acetonitrile at 400 psi for another three hours before separation testing. The prepared column is used to separate cytochrome c tryptic digest standard, using reversed-phase LC with gradient elution. The separation test uses a sample with 0.1 μM concentration. Injection volume is 1 μL . The MS data (Figure 3-24) shows the column still achieves separation with performance comparable to similar capillary columns packed with fresh C18 beads. With more separation testing, it is found that the background noise level does depend on the

cleanness of the column, as the background drops with more flush-cleaning of the bead column.

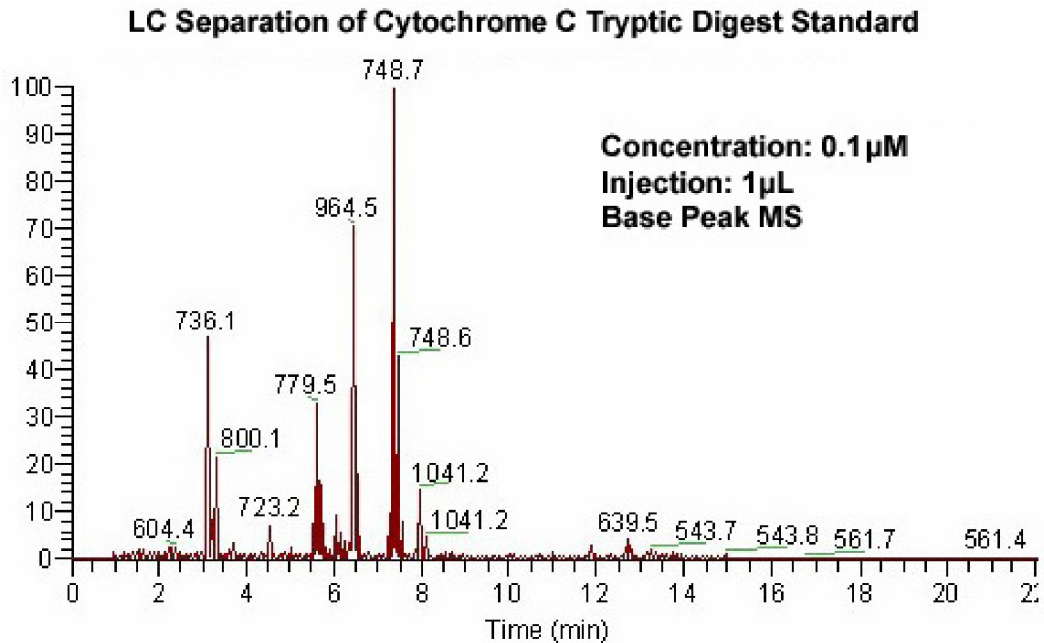


Figure 3-24 MS spectrum for an LC separation of digested cytochrome c using a capillary column packed with photoresist-contaminated-then-cleaned C18 beads.

3.5 Summary

A novel, inexpensive, batch process to integrate beads into micromachined devices is developed. This is a wafer-scale batch process, and can be easily incorporated with other processes and devices. This process is suitable for most micro-beads with a wide range of bead sizes. With this process, introduction and localization of beads into MEMS becomes much less complicated. Considering the many bead applications already available, plus the new opportunities created, this bead integration technology is very promising to enable many interesting bead-based applications for micromachined devices.

The technique is also combined with parylene microfluidics technology to build an LC–ESI chip, with integrated column, filter, and nozzle. No external bead is needed for the column. The column physical properties have been characterized, which shows consistency with conventional capillary columns. The ESI nozzle functions without sign of degradation in an eight-hour continuous electrospray. Although the integrated beads have been contaminated with photoresist during device fabrication, their separation performance is not found to be affected. It is confirmed by standard protein digest separation using a capillary column packed with photoresist-contaminated-then-cleaned LC beads. Limitations of the device include low pressure rating, lack of on-chip injection and detection, and low column capacity, which are addressed in Chapters 4, 5, and 6 respectively.

3.6 Bibliography

- [1] Q. He, C. Pang, Y.-C. Tai, and T. D. Lee, "Ion liquid chromatography on-a-chip with beads-packed parylene column." *Proceedings of the 17th IEEE International Conference on Micro Electro Mechanical Systems (MEMS 2004)*. Maastricht, Netherlands, 2004. p. 212–215.
- [2] G. Ocvirk, E. Verpoorte, A. Manz, M. Grasserbauer, and H. M. Widmer, "High-performance liquid-chromatography partially integrated onto a silicon chip." *Analytical Methods and Instrumentation*, 1995. 2(2): p. 74–82.
- [3] L. Ceriotti, N. F. de Rooij, and E. Verpoorte, "An integrated fritless column for on-chip capillary electrochromatography with conventional stationary phases." *Analytical Chemistry*, 2002. 74(3): p. 639–647.
- [4] K. Killeen, H. Yin, D. Sobek, R. Brennen, and T. v. d. Goor, "Chip-LC/MS: HPLC-MS using polymer microfluidics." *Seventh International Conference on Micro Total Analysis Systems (microTAS 2003)*. Squaw Valley, California, USA, October 5–9, 2003. p. 481–484.
- [5] J. Xie, J. Shih, Y. Miao, T. D. Lee, and Y.-C. Tai, "Complete gradient-LC-ESI system on a chip for protein analysis." *Proceedings of the 18th IEEE International Conference on Micro Electro Mechanical Systems (MEMS 2005)*. Miami Beach, Florida, 2005. p. 778–781.
- [6] A. Manz, Y. Miyahara, J. Miura, Y. Watanabe, H. Miyagi, and K. Sato, "Design of an open-tubular column liquid chromatograph using silicon chip technology." *Sensors and Actuators B-Chemical*, 1990. 1(1–6): p. 249–255.

- [7] J. P. Murrphy, M. C. Breadmore, A. M. Tan, M. McEnery, J. Alderman, C. O'Mathuna, A. P. O'Neill, P. O'Brien, N. Advoldvic, P. R. Haddad, and J. D. Glennon, "Ion chromatography on-chip." *Journal of Chromatography A*, 2001. 924(1-2): p. 233-238.
- [8] B. He, N. Tait, and F. Regnier, "Fabrication of nanocolumns for liquid chromatography." *Analytical Chemistry*, 1998. 70(18): p. 3790-3797.
- [9] C. Ericson, J. Holm, T. Ericson, and S. Hjerten, "Electroosmosis- and pressure-driven chromatography in chips using continuous beds." *Analytical Chemistry*, 2000. 72(1): p. 81-87.
- [10] J. Xie, J. Shih, Q. He, C. Pang, Y.-C. Tai, Y. Miao, and T. D. Lee, "An integrated LC-ESI chip with electrochemical-based gradient generation." *Proceedings of the 17th IEEE International Conference on Micro Electro Mechanical Systems (MEMS 2004)*. Maastricht, Netherlands, 2004. p. 334-337.
- [11] L. Licklider, X. Q. Wang, A. Desai, Y.-C. Tai, and T. D. Lee, "A micromachined chip-based electrospray source for mass spectrometry." *Analytical Chemistry*, 2000. 72(2): p. 367-375.
- [12] M. Elimelech, *Particle deposition and aggregation: measurement, modelling, and simulation*. Colloid and Surface Engineering Series. 1995. Oxford, England; Boston: Butterworth-Heinemann.
- [13] H. Yu and E. S. Kim, "Noninvasive acoustic-wave microfluidic driver." *Proceedings of the 15th IEEE International Conference on Micro Electro Mechanical Systems (MEMS 2002)*. Las Vegas, NV, 2002. p. 125-128.

- [14] T. Deng, G. M. Whitesides, M. Radhakrishnan, G. Zabow, and M. Prentiss, "Manipulation of magnetic microbeads in suspension using micromagnetic systems fabricated with soft lithography." *Applied Physics Letters*, 2001. 78(12): p. 1775–1777.
- [15] P. Griss, H. Andersson, and G. Stemme, "Liquid handling using expandable microspheres." *Proceedings of the 15th IEEE International Conference on Micro Electro Mechanical Systems (MEMS 2002)*. Las Vegas, NV, 2002. p. 117–120.
- [16] P. H. Paul, D. W. Arnold, and D. J. Rakestraw, "Electrokinetic generation of high pressures using porous microstructures." *μ TAS 98*. Banff, Canada, Oct. 13–16, 1998. p. 49–52.
- [17] A. Goodey, J. J. Lavigne, S. M. Savoy, M. D. Rodriguez, T. Curey, A. Tsao, G. Simmons, J. Wright, S. J. Yoo, Y. Sohn, E. V. Anslyn, J. B. Shear, D. P. Neikirk, and J. T. McDevitt, "Development of multianalyte sensor arrays composed of chemically derivatized polymeric microspheres localized in micromachined cavities." *Journal of the American Chemical Society*, 2001. 123(11): p. 2559–2570.
- [18] K. Walsh, J. Norville, and Y.-C. Tai, "Photoresist as a sacrificial layer by dissolution in acetone." *Proceedings of the 14th IEEE International Conference on Micro Electro Mechanical Systems (MEMS 2001)*. Interlaken, Switzerland, 2001. p. 114–117.
- [19] V. R. Meyer, *Practical high-performance liquid chromatography*. 3rd ed. 1998. Chichester; New York: Wiley.

CHAPTER 4

HIGH-PRESSURE PARYLENE MICROFLUIDICS

4.1 Introduction

The pressure requirements for most microfluidic devices are very low. Ten psi of pressure is usually more than enough to drive fluids on-chip. Tens of psi is rare, not to mention hundreds of psi. For bead-packed liquid chromatography columns, however, the operating pressures can easily exceed hundreds of psi, or even a few thousands of psi, due to the extraordinary flow resistance in the column, which holds true even for miniaturized on-chip columns.

The significantly elevated pressure requirements raise challenges in two ways. Firstly, the device itself and its packaging need to be able to withstand high pressure. Secondly, for a complete on-chip HPLC system, a mechanism needs to be developed to generate high pressures on-chip, providing adequate flow rates at the same time. Neither

of the two was available for micromachined parylene devices. Therefore, this chapter first demonstrates an anchoring technique, which dramatically improves the pressure rating of parylene devices from about 30 psi to 1000 psi. Then a high-pressure actuation mechanism based on electrolysis of aqueous solutions is described, which is a great candidate for on-chip HPLC pumping.

4.2 High-Pressure Rating through Anchoring

4.2.1 Background

Parylene adhesion to a substrate is usually improved by using chemical adhesion promoter, such as A-174 (gamma-methacryloxypropyltrimethoxy silane, Specialty Coating Systems, Indianapolis, IN) solution prepared as A-174:DI Water:IPA = 1:100:100 by volume. This simple silane surface treatment does not affect the substrate or parylene coating properties. Parylene-to-parylene adhesion is usually improved by roughening the bottom parylene with oxygen plasma followed by a 5% HF dip prior to the 2nd parylene deposition. Proper application of these procedures will ensure a pressure rating of about 30 psi, above which delamination happens between the top parylene and the bottom substrate/parylene.

Two types of mechanical anchoring techniques for parylene have been used in the past. Prior to parylene deposition, the silicon substrate is treated by either roughening of the surface [1] or etching a special DRIE trench in the substrate [2]. It has been shown using tape tests that both methods improve adhesion. However, the actual pressure ratings for the two anchoring methods have never been measured or compared. In addition, the trench-anchoring method has never been utilized in microfluidic devices before.

4.2.2 Design

Therefore, the two techniques have been adapted here to develop a self-aligned, channel-anchoring technique, where a moat self-aligned to the fluidic channels is exposed to its silicon substrate and treated by either DRIE (Figure 4-1 (a)) or roughening (Figure 4-1 (b)) prior to parylene deposition. The subsequently deposited parylene strongly anchors to either the special trench in the substrate or a roughened surface, which substantially improves adhesion. The anchoring moat surrounds the microfluidic channel, thus no weak point is left. An optional epoxy overcoating layer can also be applied on top to further strengthen and passivate the device.

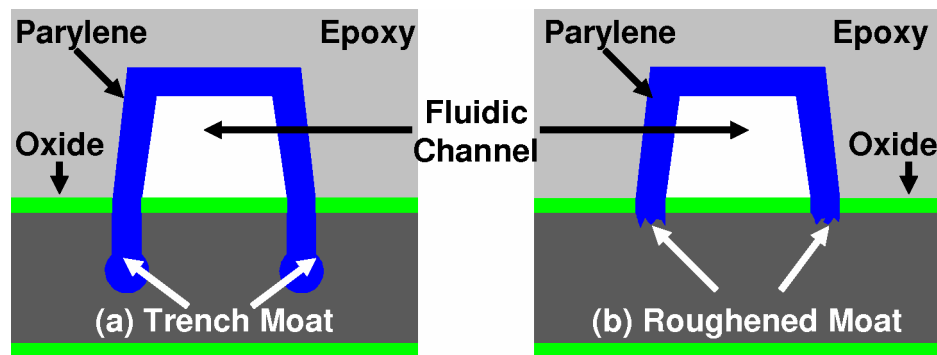


Figure 4-1 Illustration of parylene trench-anchoring and roughening-anchoring.

4.2.3 Fabrication

The anchoring moat is fabricated in a way that makes it self-aligned to the microfluidic channels. This is achieved by etching the oxide and silicon substrate with a mask formed by the channel photoresist and the field photoresist. The only area exposed (to-be-etched) by such a mask is the moat surrounding the channels. Since the moat is patterned with the channel photoresist as part of the mask, the moat and subsequently

deposited parylene is self-aligned to the channel. The other part of the mask, the field photoresist, is stripped after patterning the parylene layer.

The special DRIE trench with a mushroom profile at the bottom is created by adding an additional 36-second SF_6 isotropic etching to the end of the standard BOSCH process, which normally produces vertical trenches. Since the sidewalls of the trench are protected by C_4F_8 during BOSCH etching, only the trench bottom is isotropically etched by the added SF_6 etching, which creates the enlarged area at the trench bottom. Subsequent parylene coating can easily fill in the special trench, due to its conformal coating nature, which locks/anchors parylene to the substrate. Figure 4-2 shows two cross-sectional pictures of a parylene channel anchored 40 μm deep into silicon substrate.

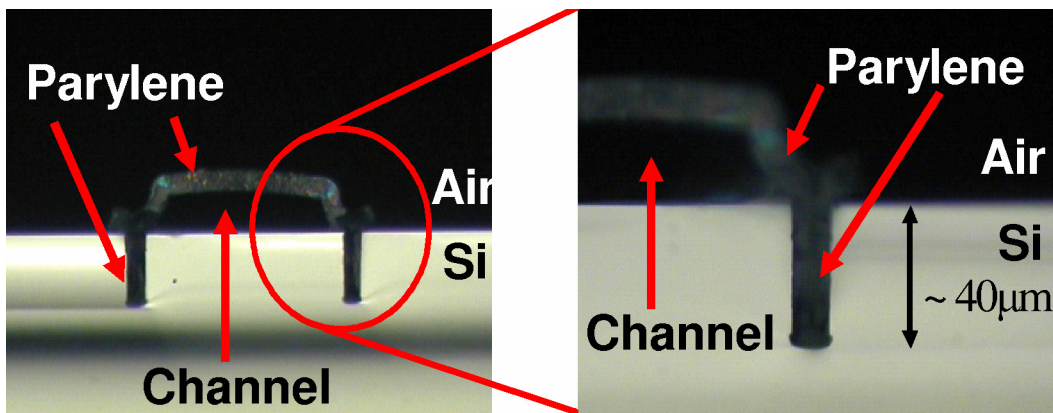


Figure 4-2 Cross-sectional pictures of a trench-anchored parylene channel.

Roughening of the substrate silicon exposed in the moat is achieved with either BrF_3 [1] or XeF_2 [3, 4] gas-phase silicon etching. The roughness of the etched silicon is mainly affected by gas type, gas pressure, and etching time. A top-view picture showing a roughened moat surrounding a photoresist channel before parylene deposition is shown in Figure 4-3.

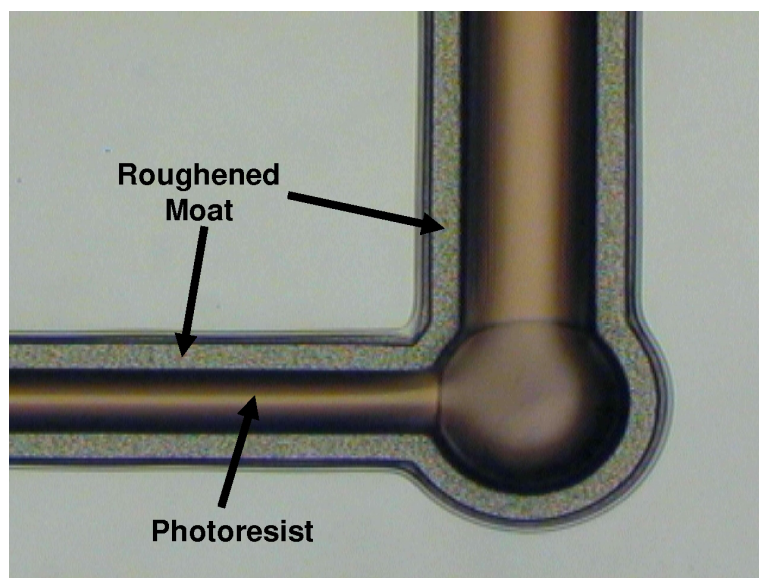


Figure 4-3 Top view picture of a roughened moat surrounding a photoresist channel.

4.2.4 High-Pressure Packaging

The packaging for high-pressure chips needs to be high-pressure proof as well. It should provide convenient access to many fluidic ports on the chip. The ability to view the chip in action is highly desired, especially during chip testing. Considering the packaging will be used for on-chip HPLC, chemical compatibility with all the HPLC chemicals and solvents is mandatory. Finally, for various purposes, such as sensing, actuation, and heating, electronic access to the chip also needs to be conveniently made.

Figure 4-4 shows some of the existing techniques for fluidic coupling between standard tubing and chips. The most primitive one is directly attaching tubing to the chip with the help of epoxy (Figure 4-4 (a)). The couplings have to be performed one at a time, which is time-consuming and labor-intensive. The yield is low and the access to on-chip ports is limited. Also the tubing cannot be removed once glued. Another approach uses microfabricated couplers between the tubing and chip (Figure 4-4 (b)) [5], which enjoys

the advantages of higher yield and high-density access to the on-chip ports. However, the couplings still need to be done one at a time and result in permanent connections. The third one (Figure 4-4 (c)) is a commercial product, Nanoport (Upchurch Scientific, Oak Harbor, WA), which bonds zero-dead-volume receiving ports onto the chip, so tubing can be easily connected and removed. The pressure rating is high. Its main drawback is the large footprint of the receiving port, which greatly limits its access to on-chip ports. In addition, the bonding still has to be done one at a time and is permanent, thus still inconvenient for chip testing. The last approach shown in Figure 4-4 (d) is a custom-made jig described in Section 3.4.3.3, which makes convenient impermanent connections to the chip. No epoxy is needed. It can easily access over ten ports on the chip simultaneously. Its major disadvantage is its low pressure rating of tens of psi, since the tubing is merely inserted into the jig.

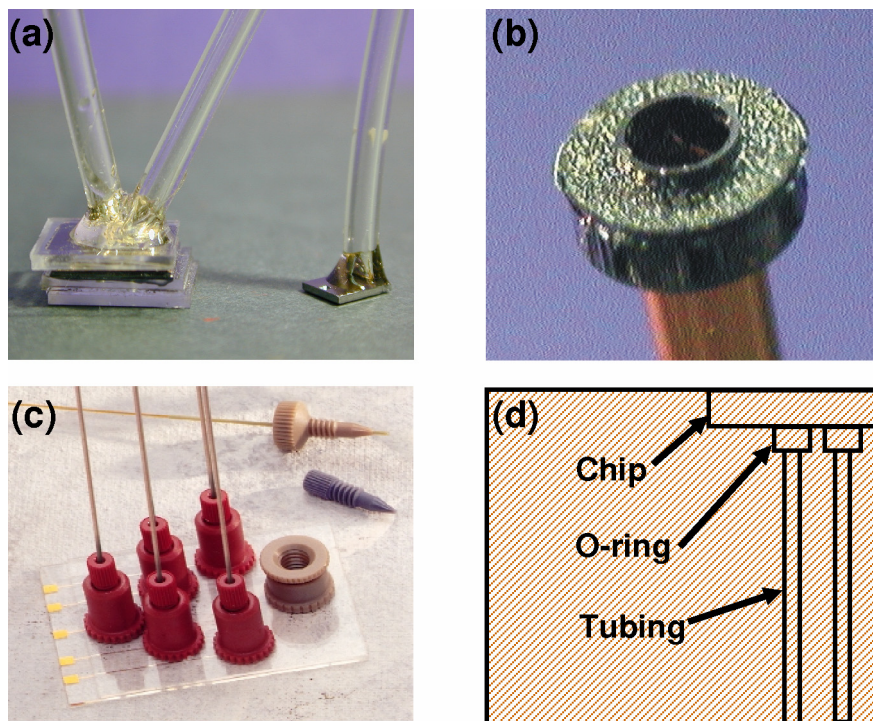


Figure 4-4 Some of the existing coupling techniques.

Here, a new packaging jig is developed to make high-pressure high-density fluidic and electronic access to the chip both conveniently and reliably. Figure 4-5 shows the exploded view of the packaging scheme. An illustration and a picture after assembly are shown in Figure 4-6.

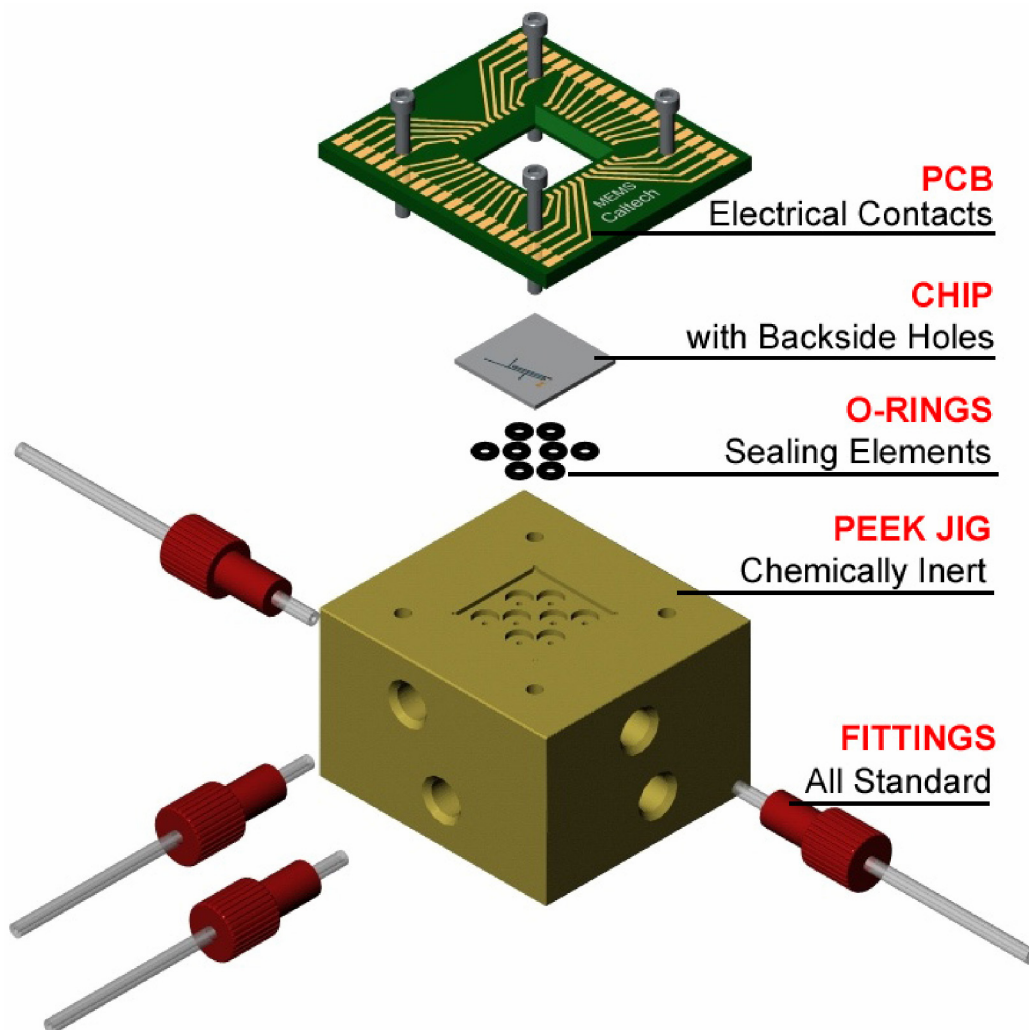


Figure 4-5 Exploded view of the packaging scheme.

The jig body is made of PEEK (polyether-ether-ketone, Figure 4-7) (McMaster-Carr, Los Angeles, CA), which is one of the standard materials used in HPLC instruments. It is inert for most chemicals and solvents. It is only unstable in

dichloromethane, tetrahydrofuran, dimethyl sulfoxide, concentrated nitric acid, and concentrated sulfuric acid. Its upper pressure limit is about 200 bar (2900 psi), although some suppliers claim 350 bar (5075 psi) [6].

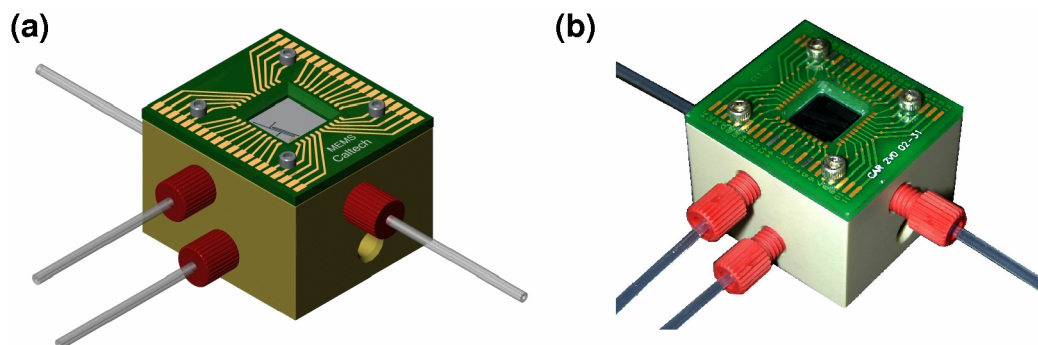


Figure 4-6 Illustration and picture of the packaging after assembly.

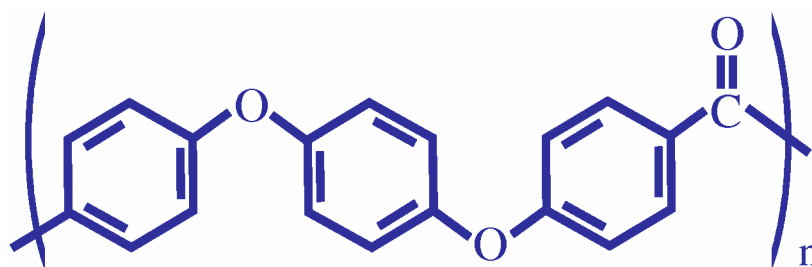


Figure 4-7 Chemical structure of PEEK (polyether-ether-ketone).

Commercial fitting receiving ports are machined in the jig to couple with commercial fittings (Upchurch Scientific, Oak Harbor, WA). Horizontal and vertical holes drilled in the jig lead fluid from the fitting ports to the jig top surface. The top surface has two levels of recess. The square one is used for holding the chip. The circular ones are for o-rings (Apple Rubber Products, Lancaster, NY). There are eight holes in the recess, which connect to the eight receiving ports on the four sides of the jig respectively. Eight holes on the chip can be accessed simultaneously if they share the same coordinates with the jig holes. Keeping the chip orientation, another eight holes on the chip can be

access by rotating the jig by 90° (Figure 4-8 (a) (b)). So in total a 4-by-4 array of 16 holes on the chip can be accessed (Figure 4-8 (c)), at most 8 holes simultaneously. When the o-rings and chip are placed in their recesses, a PCB (Printed Circuit Board) cover is placed on top and is screwed down to compress the chip and o-rings. The compressed o-rings seal the chip and jig. Electrical access to the chip is made by wire-bonds from the chip to the top PCB.

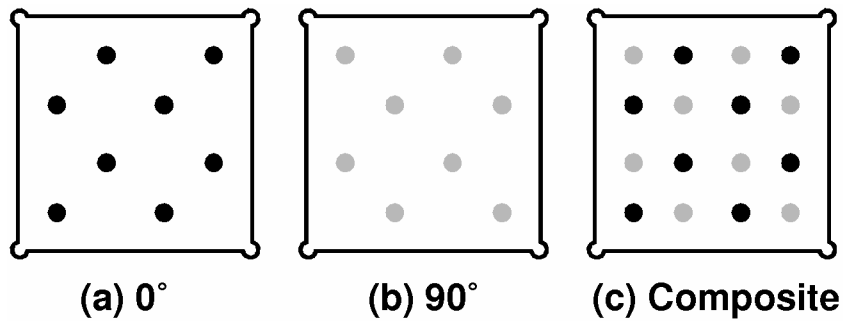


Figure 4-8 Jig holes configuration.

4.2.5 Pressure Rating Testing Results and Discussion

Both trench-anchored and roughening-anchored chips are fabricated with the same design (Figure 4-9). The device has a backside hole to apply pressurized gas to the two dead-end channels, which are $100\ \mu\text{m}$ and $50\ \mu\text{m}$ wide, respectively. The channels both have a height of $25\ \mu\text{m}$ and a length of $1000\ \mu\text{m}$.

During testing, pressurized N_2 gas from a gas cylinder is applied to the device through the packaging jig. The testing channels are covered by a water drop. The nitrogen pressure is increased with 50 psi steps at a rate of 10 minutes per step until bubbles appear in the water, indicating leaks in the channel. The pressure at that point is recorded as the burst pressure of the channel. However, the burst pressure is not a clear-cut number

in nature, which is why the pressure step is set as high as 50 psi in the testing. In addition, it is more useful to find out the practical safe operating pressure for the device, which is chosen to be the maximum pressure under which the device does not leak for one hour.

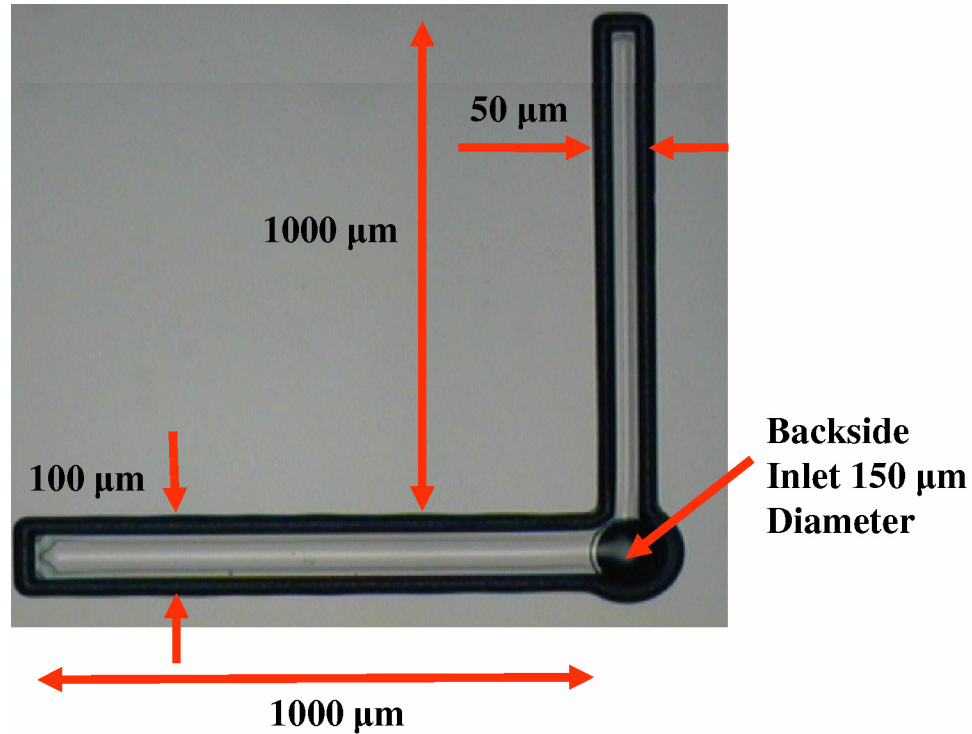


Figure 4-9 Top view picture of the device used in the pressure rating testing.

The results for the safe and burst pressures for roughening-anchored and trench-anchored channels, with and without epoxy overcoating are summarized in Table 4-1. It should be noted that the pressure limits also depend on moat width, trench depth/shape, and parylene thickness. It is clear that trench-anchored channels perform much better than roughening-anchored ones and epoxy overcoating further improves the performance. A maximum pressure limit is achieved with trench-anchored and epoxy-coated channels. At the maximum allowable pressure of the testing setup of 800 psi (leak rate is about 10 nL/min for water and 100 nL/min for air at 800 psi), no leakage is found in one hour.

| | Roughening | Trench | Roughening + Epoxy | Trench + Epoxy |
|-----------------------|-------------------|---------------|-------------------------------|---------------------------|
| Safe Pressure | 250 psi | 600 psi | 700 psi | 800 psi |
| Burst Pressure | ~350 psi | ~700 psi | ~800 psi | >800 psi |

Table 4-1 Summary of the pressure testing results.

It is found that the failure modes for the two anchoring techniques are different. For roughening-anchored channels, leaked air slowly emerges outside of the moat as tiny bubbles that grow over time, while the trench-anchored ones suddenly burst at edges of channels, resulting in big bubbles gushing out. After the channels burst, the structural damages to the channels are also different. The failed roughening-anchored channel has parylene delamination in the moat area (Figure 4-10), while the trench-anchored channel has its channel parylene broken at the channel edges and/or the corners (Figure 4-11). Therefore it can be concluded that roughening-anchored channels can leak out working fluid through tiny pathways in the roughened moat area at high pressures, while the trench-anchored channels do not leak at all until the channel breaks at mechanically weak points.

It worth pointing out here that the chips perform best when cleaned thoroughly before applying epoxy. One way to do it is cleaning in piranha solution at 120 °C for a few minutes, followed by a 5% HF dip and immediate epoxy coating and baking overnight at 80 °C in the oven. With thorough cleaning, pressure ratings as high as 1000 psi have been achieved for the device presented in Chapter 6.

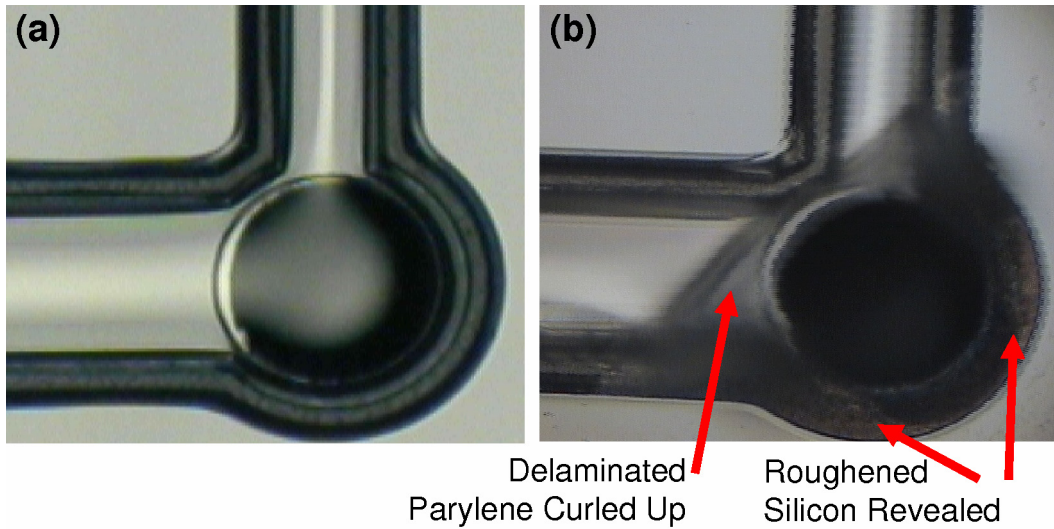


Figure 4-10 Roughening-anchored channel before and after failure at high pressure.

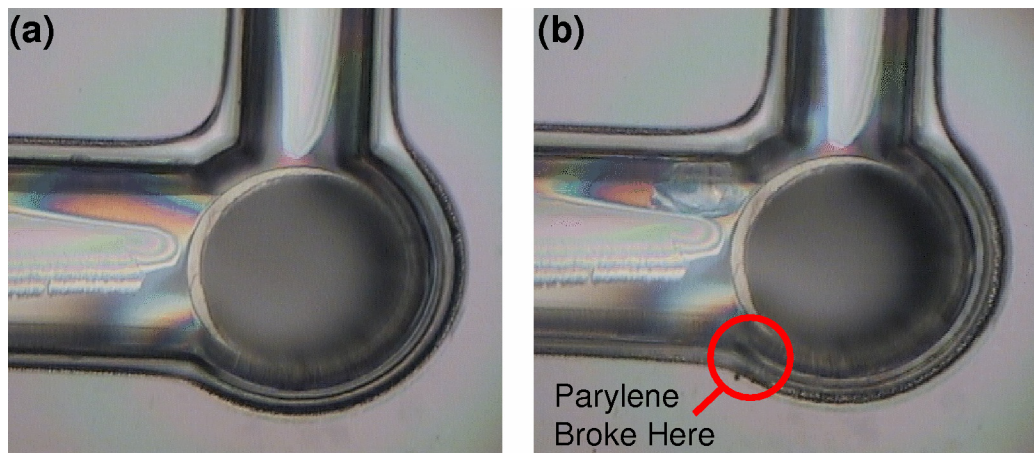


Figure 4-11 Trench-anchored channel before and after failure at high pressure.

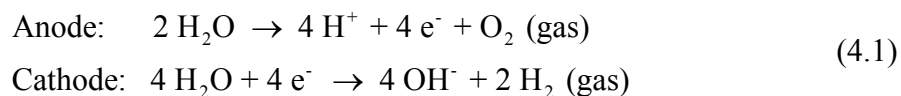
4.3 High-Pressure Generation through Electrolysis

4.3.1 Introduction

The pumping mechanism for HPLC should be able to generate high pressures and high flow rates. Piezoelectric actuators provide large forces but small displacements. Electrically driven comb actuators have large displacements but small force. It turns out that electrolysis-based actuators enjoy large force (high pressure), large deflection (high

flow rate), fast reaction, low power consumption, and low heat dissipation [7, 8], which makes it a great candidate for HPLC pumping. Nevertheless, it is interesting to know that despite the many advantages, electrolysis actuators largely have not been explored before.

It is well known that electricity can separate liquid into gases. In an electrolysis reaction, two electrodes are immersed in an electrolyte solution. The electrodes need to be inert and not easily oxidized. Platinum (Pt), for example, is a good choice. When an adequate voltage is applied between the electrodes, electrolysis happens. Oxidation and reduction occur at the anode and cathode respectively. When DI water is used as the electrolyte, the reactions are,



Therefore, as electric current is injected into the solution, oxygen and hydrogen gases are formed at the two electrodes. The accumulated gases can be used for high-pressure actuation and pumping.

It is interesting to note that the electrolysis reaction can be reversed. The generated oxygen and hydrogen can recombine into water. Although extremely slow under normal conditions, the recombination rate can be greatly enhanced in the presence of platinum as a catalyst. The recombination rate depends on the contact area between platinum and the gases. It also depends on the gas pressure. The higher the pressure, the faster the recombination. The maximum pressure is reached when the gas recombination rate equals the generation rate. Theoretically, devices taking advantage of both forward and reverse electrolysis can be used repeatedly without refilling the electrolyte.

4.3.2 A Parylene Micro Electrolysis Actuator

4.3.2.1 Design and Fabrication

A micro electrolysis actuator with a sealed electrolysis chamber (Figure 4-12) is described in this section. The device is built with parylene microfluidics technology. The chamber is formed by sacrificial photoresist which is later removed in acetone. It has Pt electrodes at the chamber bottom and a flexible parylene membrane as the chamber roof. Electrolysis-generated hydrogen and oxygen deflect the membrane, which makes the actuation. When the electrolysis potential is removed, hydrogen-oxygen recombination happens on top of the Pt catalyst, which deactivates the device.

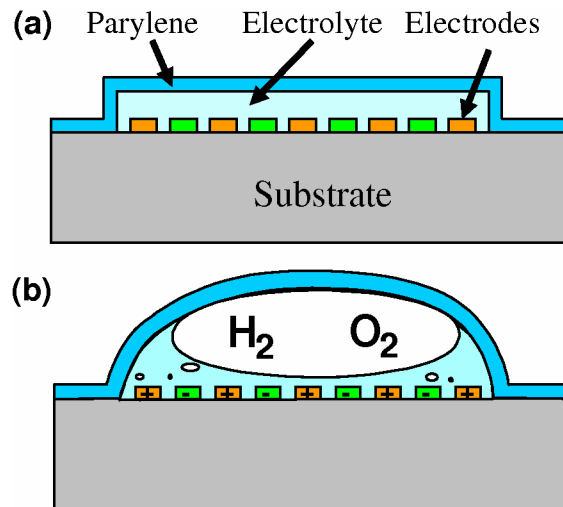


Figure 4-12 Cross-section of a sealed micro electrolysis actuation chamber.

One purpose of the device is to characterize miniaturized electrolysis actuation in a parylene device. The other purpose is to investigate deactivation through recombination. The actuator can be used for active valves, pumps, and many other microfluidic devices. The fact that the electrolyte is sealed in the electrolysis chamber offers several advantages. Firstly, no adverse effect such as change of pH value or other properties is

applied to the processed fluid, which is contained in a second chamber on top of the actuation chamber. Secondly, electrolytes other than water can be used for optimized electrolysis actuations. Thirdly, due to recombination effects, the actuator could be repeatedly activated and deactivated.

A top view illustration of the complete device is shown in Figure 4-13. The electrolysis chamber diameter is 2 mm. The chamber height is 4 μm . The parylene membrane thickness is 2 μm . To ensure uniform gas generation and to enhance the Pt-catalyzed recombination, the electrolysis chamber bottom is almost completely covered with interdigitated Pt electrodes. The chamber is filled by placing the device in the desired solution for some time. To make the chamber self-sealing, stiction effect is exploited. The two large sealing membranes easily stick to the substrate when the device is taken out of the filling solution and allowed to dry in the air. The stiction happens so fast that little liquid is lost from the chamber.

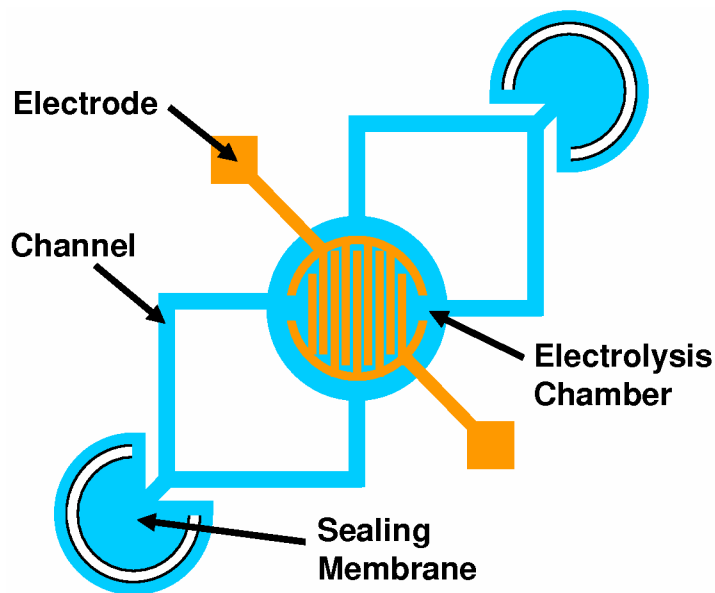


Figure 4-13 Top view of a self-sealing electrolysis actuator.

A picture of the complete device filled with liquid is shown in Figure 4-14 (a). Figure 4-14 (b) shows the sealing membrane after stiction happens. Figure 4-14 (c) demonstrates consistent sealing. And Figure 4-14 (d) shows small bubbles being generated at an electrode tip.

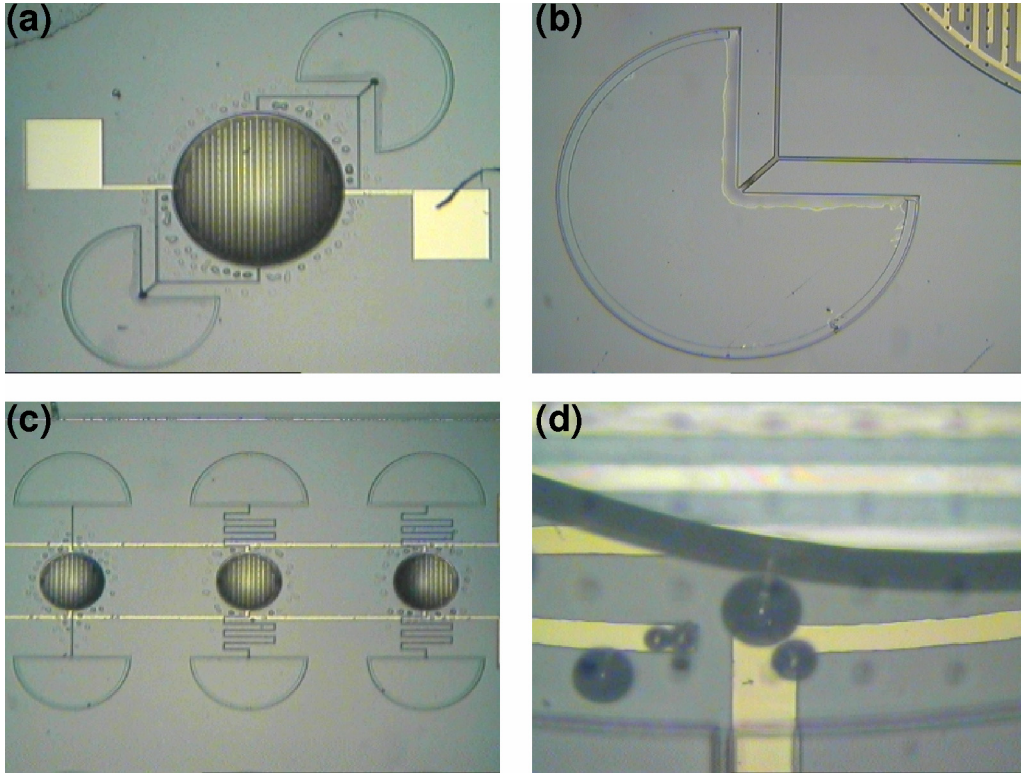


Figure 4-14 Pictures of the sealed micro electrolysis actuator.

4.3.2.2 Electrolysis Bubble Generation and Recombination

First, DI water is used as the testing electrolyte. Video snapshots of a bubble generation-recombination cycle are shown in Figure 4-15. In Figure 4-15 (a), the device is at rest. There is a bubble from the previous cycle at the chamber center. When an adequate voltage is applied to the two electrodes, bubbles appear immediately and then coalesces into one large bubble (Figure 4-15 (b)), deflecting the chamber membrane. In a

controlled actuation, constant current is used instead of constant voltage, which is because the amount of generated gas is directly proportional to the charges injected into the solution. In the very beginning of the electrolysis, voltage and current approximately follows linear relationship. For the particular device tested, the voltage starts at 80 V for a current of 0.24 mA, corresponding to a power consumption of 19 mW. The voltage rises over time for a constant-current operation, since the impedance in the chamber increases. The bubbles continue to accumulate, generating higher and higher pressure, which deflects the membrane more and more until the voltage is removed (Figure 4-15 (c)). The maximum deflection observed for the device is 120 μm , above which the parylene membrane delaminates from the substrate due to high pressures inside the chamber.

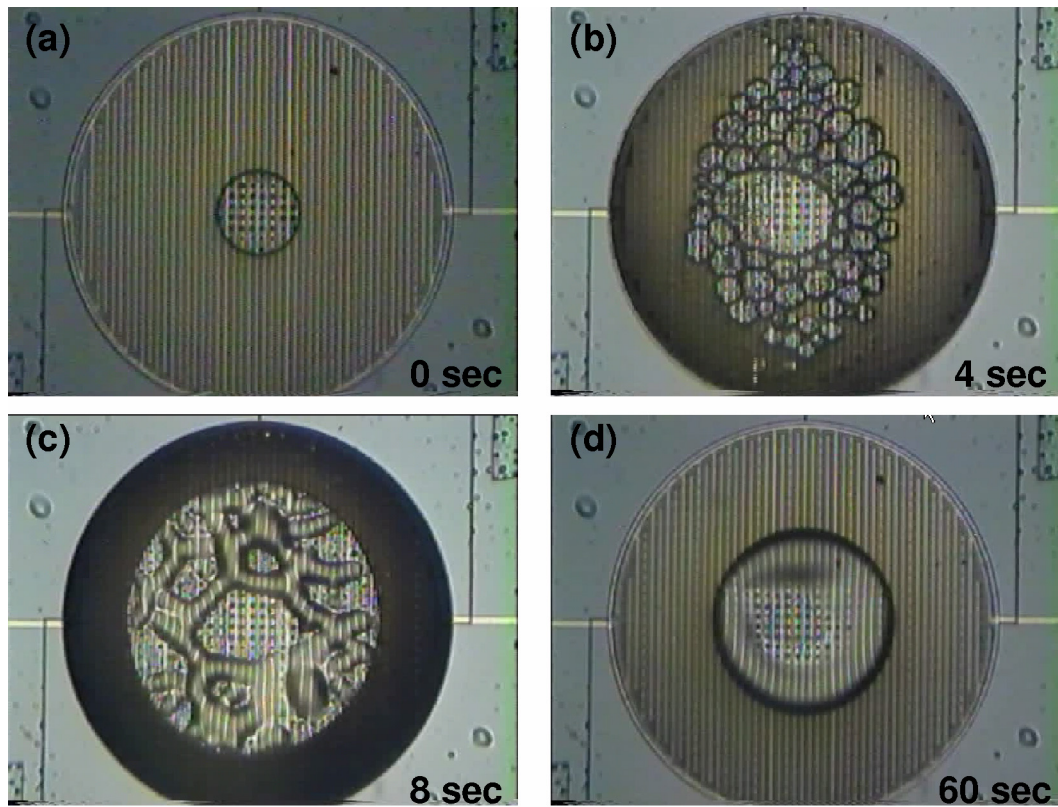


Figure 4-15 Snapshots of activation and deactivation of the actuator filled with DI water.

Since Pt electrodes are used, the recombination of hydrogen and oxygen is catalyzed. The mixed gas bubble shrinks quickly over time when some of the gases are converted back to water. At the same time, the internal pressure reduces, thus the flexible parylene membrane returns to its original position (Figure 4-15 (d)). However, there is always a small bubble left which does not disappear even after several days. It is possibly because that the small bubble is not longer in contact with the Pt electrodes, and therefore the recombination rate is extremely low.

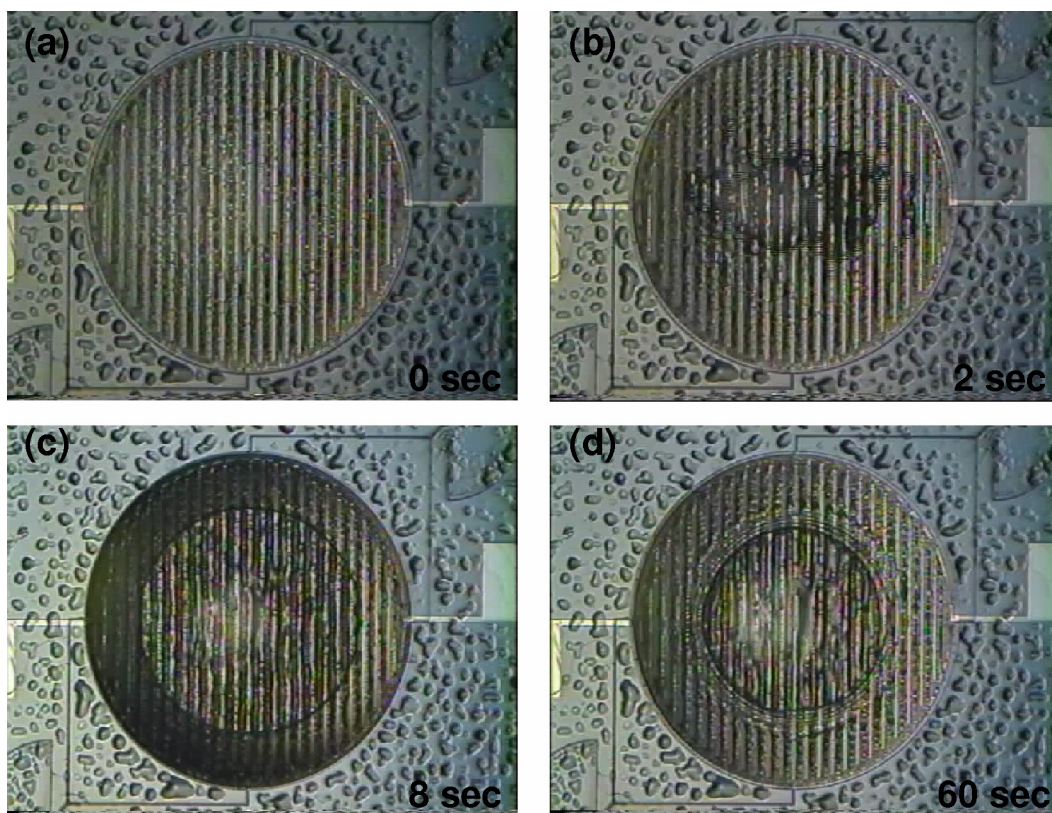


Figure 4-16 Snapshots of activation and deactivation of the actuator filled with 10% of acetonitrile in DI water.

Similar experiments are also performed for two devices, one filled with 10% of acetonitrile in water (Figure 4-16), and the other filled with 10% of methanol in water

(Figure 4-17). Both solvents are widely used in HPLC systems. The obtained results are similar to those in the pure DI water case. One major difference is the fluids seem to be more viscous, causing apparent sluggish bubble growth and recombination.

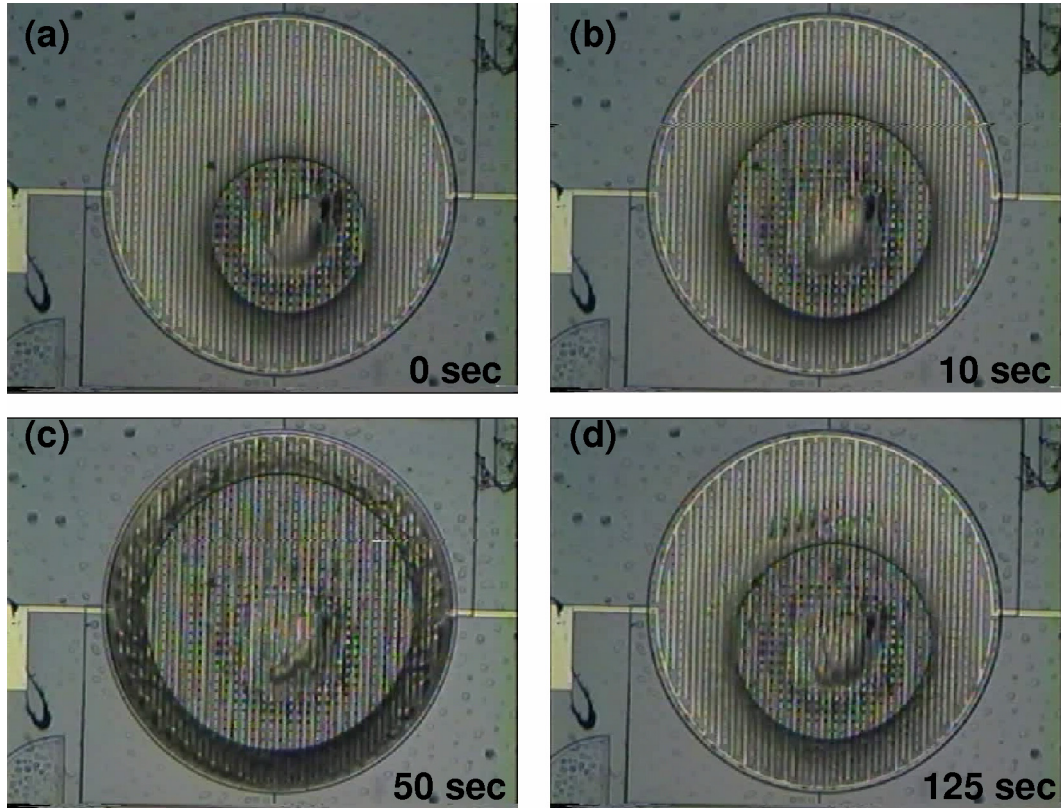


Figure 4-17 Snapshots of activation and deactivation of the actuator filled with 10% of methanol in DI water.

4.3.3 An Electrolysis Device for High-Pressure Generation

4.3.3.1 Design and Fabrication

The previous electrolysis actuator successfully demonstrates activation and deactivation. The achieved pressure, however, is still low. The estimated maximum pressure, based on simple load-deflection theories, is only around 10 psi, which seems correct since non-anchored parylene would be likely to delaminate at that pressure. This

maximum pressure is not limited by electrolysis, but rather by the robustness of the device. Therefore, a roughening-anchored electrolysis device (Figure 4-18) is used to demonstrate much higher pressure generation, which is desired for on-chip HPLC pumping. Contrary to the previous sealed actuator, this device has two fluidic access holes as inlet and outlet. Two devices with slightly different electrode configurations are fabricated and tested. One has 5 μm wide and 5 μm spacing interdigitated electrodes. The other has 3 μm wide and 7 μm spacing electrodes. The channel width is 100 μm and the height is 25 μm . The electrodes cover an area of 80 μm by 1000 μm . The microchip is fabricated in the same way as the one in Figure 4-1 (b), except with the addition of Pt electrodes. The electrodes run across the anchoring moat, which creates weak points lowering the pressure rating of the device. The Pt is 2000 \AA thick with 200 \AA Ti at its bottom for adhesion promotion. The parylene thickness is 10 μm .

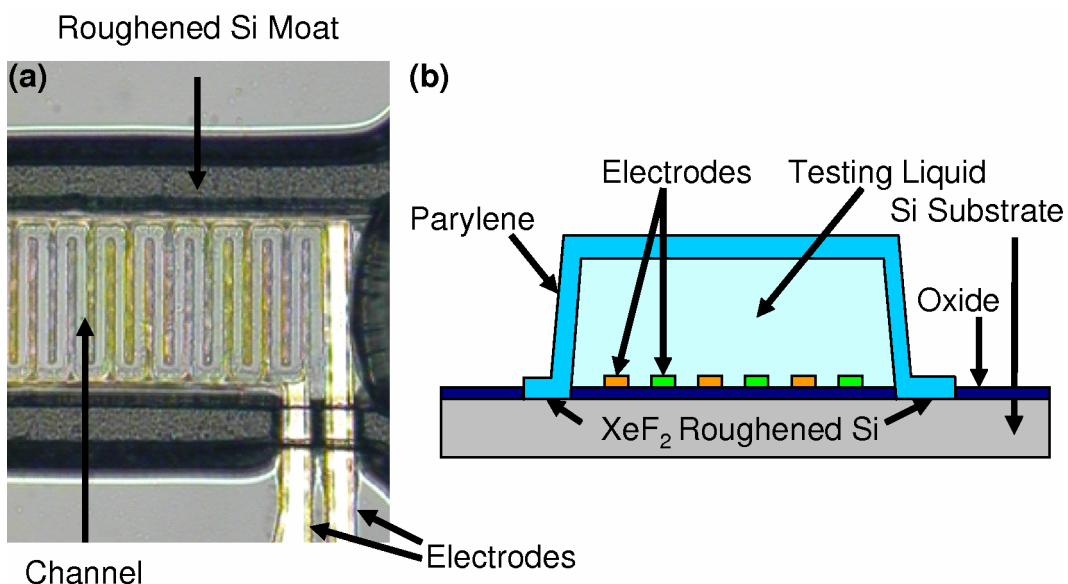


Figure 4-18 Top view picture and cross-sectional illustration of the high-pressure electrolysis device.

4.3.3.2 Testing Method and Results

The electrolyte used in the testing is DI water with 10% ethanol and 1% acetic acid, which is also commonly used in HPLC systems. The electrolyte solution is pumped into the device using a compressed N₂ tank. Then the outlet of the device is sealed. The solution in the device is kept under pressure from the gas tank.

First, a bubble is generated using electrolysis with constant current. The bubble shrinks or expands, depending on whether its internal pressure is lower or higher than the system pressure applied by the compressed nitrogen. By adjusting the nitrogen pressure, a balance pressure can be found for each current level, which maintains the bubble size. At this balance point, gas generation and recombination rates are equal. This pressure can be considered the maximum pressure possible for the device at that fixed current.

At every balance point, the bubble is monitored for over 5 minutes to ensure its size does not change. The error for the obtained balance pressures is about ± 2 psi. The balance pressures are plotted against electrolysis currents in Figure 4-19. The device with 5 μm wide electrodes and 5 μm electrode spacing always generates higher pressures than the one with 3 μm wide electrodes and 7 μm electrode spacing, because the former is more efficient in bubble generation. From the figure, it can be seen that 1.1 μA of current can generate a maximum of 150 psi in the device with 5 μm electrodes. Pressures as high as 300 psi have been achieved when the 5 μm -electrode device was tested at 5 μA .

The voltages at the balance points are also recorded and plotted against the balance pressures (Figure 4-20). The device with 3 μm –7 μm electrodes always needs higher voltage to achieve the same pressure generated by the one with 5 μm –5 μm electrodes. The figure also shows a threshold voltage near 3.2 V, above which the

balance pressure increases rapidly, meaning significantly more bubble generation from the electrolysis reaction.

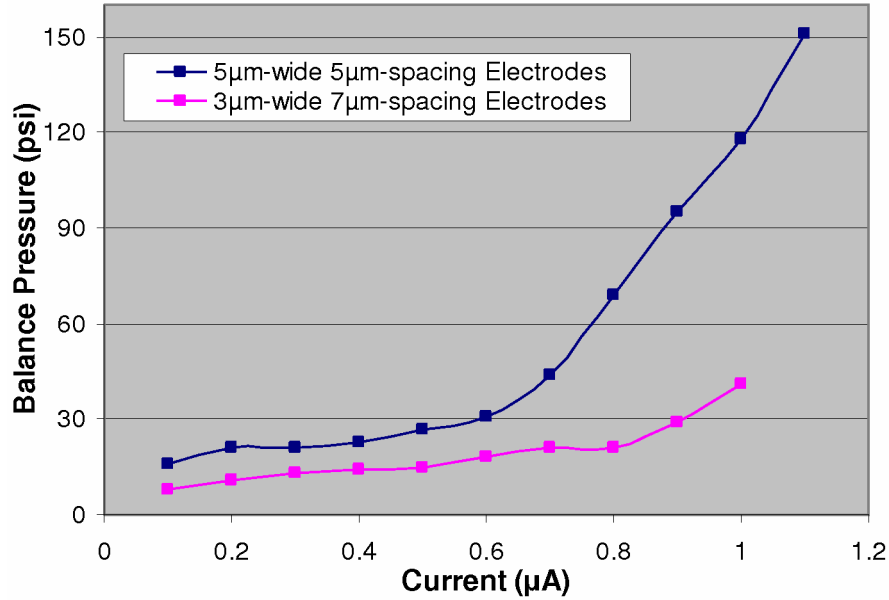


Figure 4-19 Electrolysis generated pressures at fixed currents.

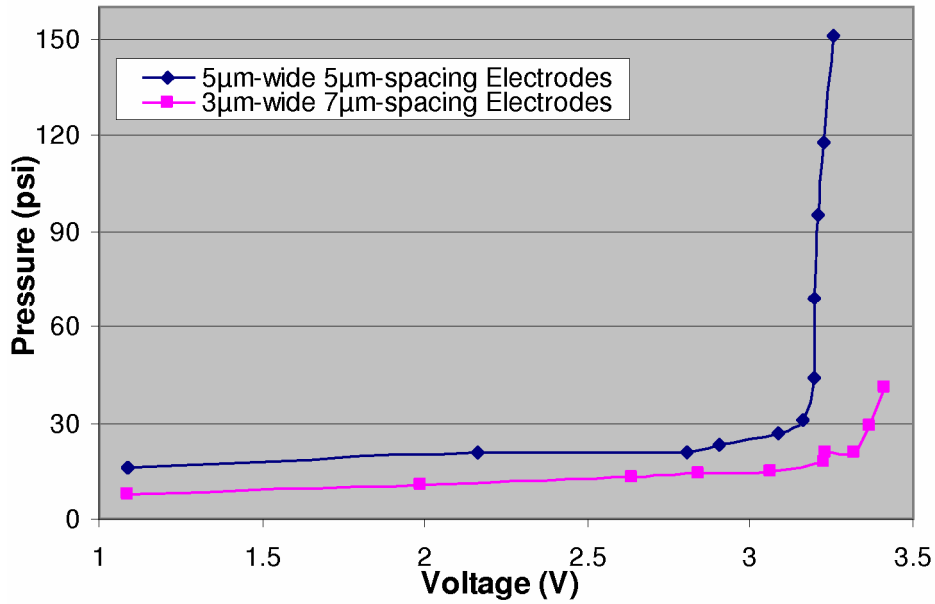


Figure 4-20 Voltage versus balance pressure at fixed currents.

4.4 Summary

This chapter attacks two problems for on-chip high-pressure devices such as HPLC chips. One is high-pressure rating, the other is high-pressure generation. Parylene devices are especially vulnerable to high pressures since parylene does not bond strongly to parylene or to the substrate due to its chemical inertness. The developed mechanical anchoring technique successfully increases the pressure rating of parylene devices from about 30 psi to 1000 psi. For generating high pressures, electrolysis-based actuator turns out to be a great candidate. A micro sealed electrolysis actuator was successfully demonstrated. Hydrogen-oxygen recombination was used to deactivate the device, which then could be used repeatedly without refilling the electrolyte. Finally, to determine the maximum achievable pressures at fixed currents for micro electrolysis actuators, an anchored electrolysis device was tested. The pressure of 300 psi achieved at 5 μ A is already adequate for many HPLC separations.

4.5 Bibliography

- [1] X.-Q. Wang, X. Yang, K. Walsh, and Y.-C. Tai, "Gas-phase silicon etching with bromine trifluoride." *1997 International Conference on Solid-State Sensors and Actuators. Part 2 (of 2)*. Chicago, IL, USA, Jun 16–19, 1997. p. 1505–1508.
- [2] M. Liger, D. C. Rodger, and Y.-C. Tai, "Robust parylene-to-silicon mechanical anchoring." *Proceedings of the 16th IEEE International Conference on Micro Electro Mechanical Systems (MEMS 2003)*. Kyoto, Japan, 2003. p. 602–605.
- [3] F. I. Chang, R. Yeh, G. Lin, P. B. Chu, E. G. Hoffman, E. J. Kruglick, K. S. Pister, and M. H. Hecht, "Gas-phase silicon micromachining with xenon difluoride." *Microelectronic Structures and Microelectromechanical Devices for Optical Processing and Multimedia Applications*. Austin, TX, 1995. p. 117–128.
- [4] H.F. Winters and J. W. Coburn, "Etching of silicon with XeF_2 vapor." *Applied Physics Letters*, 1979. 34(1): p. 70–73.
- [5] E. Meng, S. Wu, and Y.-C. Tai, "Silicon couplers for microfluidic applications." *Fresenius Journal of Analytical Chemistry*, 2001. 371(2): p. 270–275.
- [6] V. Meyer, *Practical high-performance liquid chromatography*. 3rd ed. 1998. Chichester; New York: Wiley.
- [7] C. G. Cameron and M. S. Freund, "Electrolytic actuators: Alternative, high-performance, material-based devices." *Proceedings of the National Academy of Sciences of the United States of America*, 2002. 99(12): p. 7827–7831.
- [8] C. Neagu, H. Jansen, H. Gardeniers, and M. Elwenspoek, "The electrolysis of water: an actuation principle for MEMS with a big opportunity." *Mechatronics*, 2000. 10(4–5): p. 571–581.

CHAPTER 5

ION CHROMATOGRAPHY ON-A-CHIP

5.1 Introduction

5.1.1 Abstract

This chapter presents an integrated ion liquid chromatography system with on-chip bead-packed separation column, bead filters, cross-channel injection structure, and conductivity detector. Sample injection, separation, and detection are all performed on the single chip. The whole chip is integrated on a silicon wafer with a single CMOS-compatible batch fabrication, using parylene microfluidics technology. It has a high integration level, while maintaining a relatively simple fabrication. Utilizing the parylene anchoring technique developed in Chapter 4, the whole chip is tested to be high-pressure compatible up to at least 800 psi. It is found experimentally that the on-chip packed bead column has higher permeability than conventional ones. On-chip 4.5 nL sample injection, pressure-driven LC separation, and conductivity detection of a seven-anion mixture (F^- ,

Cl^- , NO_2^- , Br^- , NO_3^- , PO_4^{3-} , SO_4^{2-}) with concentrations from 12.5 ppm to 25 ppm have been successfully demonstrated.

5.1.2 Ion Chromatography

The term “ion chromatography” applies to any modern method for chromatographic separation of ions [1]. Such separation happens in an ion-exchange column, which is packed with solid ion-exchange beads. Since the introduction of ion chromatography in 1975, the field has grown at a phenomenal rate. A detailed introduction of the evolution of ion chromatography is given in [2].

An ion chromatography separation starts with pumping the eluent (mobile phase) through the system until equilibrium is reached, as evidenced by a stable baseline. During this step, the ion-exchange sites on the beads are replaced by ions from the eluent. For example, a typical reaction in anion-exchange chromatography is,



where the eluent anion, E^- , replaces the original Cl^- on the resin (bead). When the analyte anion, A^- , enters the column, it competes with E^- for the ion-exchange sites,



When the analyte anions are exchanged off the resin they move down the column with the mobile phase. Since different anions have different bonding strengths to the exchange sites, they travel down the column at different speeds, thus can be separated.

Since the solution must be kept electrically neutral during the ion-exchange process, the exchange is stoichiometric. Thus, equation (5.2) can be generalized:



An everyday example for ion-change medium is the filter in the popular Brita pitcher (Figure 5-1). It is comprised of activated carbon and ion-exchange resin joining forces to clean tap water. The carbon absorbs taste and odor compounds. A mixed bed ion-exchange resin "column" acts like a magnet for ions, binding to its surface unwanted cations and anions. In this case, no eluent is used to refresh the column. Therefore, the ion-exchanger will eventually fill up due to its limited capacity.

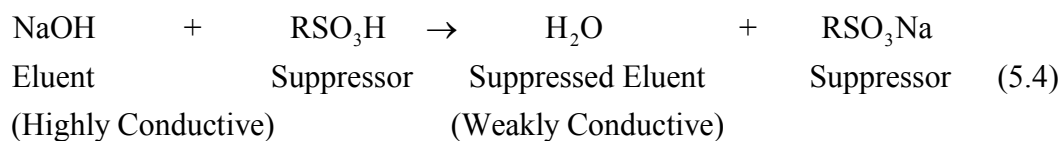


Figure 5-1 Brita ion-exchange filter.

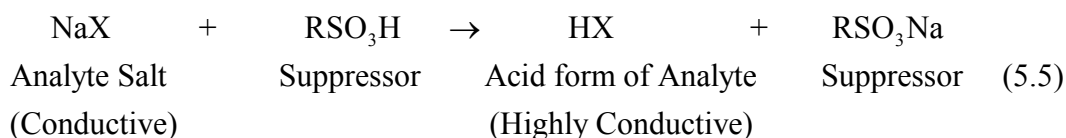
Detection techniques for ion chromatography include conductivity, UV-visible absorbance, amperometric and potentiometric detection, mass spectrometry (MS), and post-separation reaction detection [3, 4]. Among these, conductivity detection is the most popular one because it offers the following advantages. Firstly it is a universal method for ions, which all conduct electricity to some degree. This is especially true for all the anions and cations of strong acids and bases, which do not work well with UV detection due to their weak UV absorbance. Secondly, it can achieve sub-ppm level sensitivity without suppression of the background signal (Table 2-2). Thirdly, it does not require a reference electrode to define a stable baseline. Instead, the total conductivity of the mobile phase represents the baseline.

For on-chip applications, conductivity sensing enjoys even more benefits. It is much easier to integrate on-chip than optical detectors. In addition, it scales favorably with miniaturization. Unlike optical techniques that have greatly reduced signals due to the small optical path on-chip, the conductivity sensing signal can be substantially increased by using smaller electrodes.

The baseline signal generated by the background eluent can be suppressed to enhance detection sensitivity. The most common approach is chemical suppression, which significantly reduces background conductance by converting the mobile phase ions to a neutral form or removing them, while keeping or increasing the conductance of sample ions. The suppression is performed after separation but before detection. A typical suppressor reaction for eluent in anion-exchange chromatography is,



And a typical reaction for analytes is,



A review on the developments of suppressor technology for inorganic ion analysis by ion chromatography with conductivity sensing is found in [5]. Alternatively, the suppression can be done electrically [6].

Ion chromatography has broad applications ranging from water and food safety [7] such as anions in drinking water; environmental monitoring, such as nitrate in soil; and clinical exams, such as sodium and potassium level in body fluids and infusions.

5.1.3 Nitrate Sensing

Although the microchip developed in this chapter is really a general-purpose ion chromatography chip, its original goal is nitrate (NO_3^-) sensing. Nitrate is one of the most common contaminants in groundwater. The detection and quantification of nitrate is considered essential.

Nitrogen is an essential nutrient for plants and animals. It exists in the environment in many forms as part of the nitrogen cycle, with nitrate (NO_3^-) and nitrite (NO_2^-) being the most abundant ones in water systems [8]. These two anions are retained poorly in soil but are highly soluble in water. They remain in water until consumed by plants or other organism. Because of nitrate's stability and solubility, it is often used as an indicator of potential water pollution. An elevated nitrate level may also indicate the presence of other contaminants, microbial pathogens, or pesticides in the water system,

A major source of elevated nitrate level is the use of nitrate fertilizers, which contributes the most to groundwater pollution. High concentrations of nitrate may have significant effects on the environment, as well as on human health.

High nitrate levels in freshwater and marine ecosystems can lead to algal blooms and eutrophication of the ecosystem. Although nitrate is not toxic to humans, once nitrate has entered the body, it can be reduced by stomach bacteria to nitrite and further to N-nitrosamine compounds that are suspected to be carcinogenic. Nitrate does not normally cause health problems if not reduced to nitrite. Since infants have immature digestive systems that allow more reduction of nitrate to nitrite, excess consumption of nitrate can cause methemoglobinemia (blue baby syndrome) for infants. Methemoglobinemia is a blood disorder. Blood contains an iron-based compound called hemoglobin, which carries

oxygen. When nitrite is present, hemoglobin can be converted to methemoglobin, which cannot carry oxygen. Infants suffering from methemoglobinemia can show intermittent signs of blueness around the mouth, hands, and feet.

The current EPA nitrate standard is 10 ppm maximum in drinking water. The standard for nitrite is 1 ppm maximum. These concentrations are well above the detection limits for ion chromatography systems with conductivity sensing.

Besides ppm (parts-per-million) and ppb (parts-per-billion), some other concentration units, such as mg/L and M (molar, mol/L) are also frequently used. Since ppm is a weight percentage and the specific gravity for most dilute aqueous solutions is approximately 1, it is easy to obtain the following conversions:

$$1 \text{ ppm} = 1 \text{ mg/L} \quad (5.6)$$

$$1 \text{ ppb} = 1 \text{ } \mu\text{g/L} \quad (5.7)$$

Using the molecular weight of the solute, concentrations in ppm/ppb can be converted to molar concentrations. For example:

$$\text{For nitrate: } 1 \text{ ppm} = 16 \text{ } \mu\text{M} \quad (5.8)$$

5.2 Microchip Design

5.2.1 Chip Design and Operation

The microchip has four access ports, as shown in Figure 5-2. Two syringe pumps (Harvard Apparatus, Holliston, Ma) are connected, one at port #1 for mobile phase delivery and the other at #3 for sample injection respectively. Four valves (Upchurch Scientific, Oak Harbor, WA) are connected at the four access ports to control the flow

directions. After chip fabrication, LC beads are packed externally into the on-chip column from port #1. On-chip filters trap beads in the column and prevent beads from entering the side channels used for sample injection (Figure 5-3 (a)). The filters are channels with height smaller than the bead diameter. The packed column outlet is right at the inlet of the detector, which also serves as a filter (Figure 5-3 (b)). The column is packed, with monitoring under a microscope, up to the side channel close to #3, which is where the injected sample plug front will be. The integrated chip minimizes dead volume between the injection sample plug and column inlet, and between the column outlet and detector, thus minimizing extra-column peak broadening. Nano-liter-volume sample injection is achieved with a cross-channel injection method [9].

To perform a separation, first the column is flushed with the mobile phase flowing from #1 to #2 pumped by the syringe pump, while valves #3 and #4 are closed (Figure 5-4). After the column reaches equilibrium and is ready for injection (Figure 5-5 (a)), valves #1 and #2 are closed, while #3 and #4 are opened (Figure 5-5 (b)). The sample enters the device from #3 and leaves at #4 (Figure 5-5 (c)). Then by closing #3 and #4, and opening #1 and #2, a sample plug can be defined and injected into the column (Figure 5-5 (d)). Sample components are separated on the column into bands (Figure 5-5 (e)), which widen during elution through the column (Figure 5-5 (f)). When an eluted sample band enters the conductivity detector, a change of signal is generated on top of the mobile phase background conductivity baseline. All of the peak signals are recorded to produce a chromatogram for the separation.

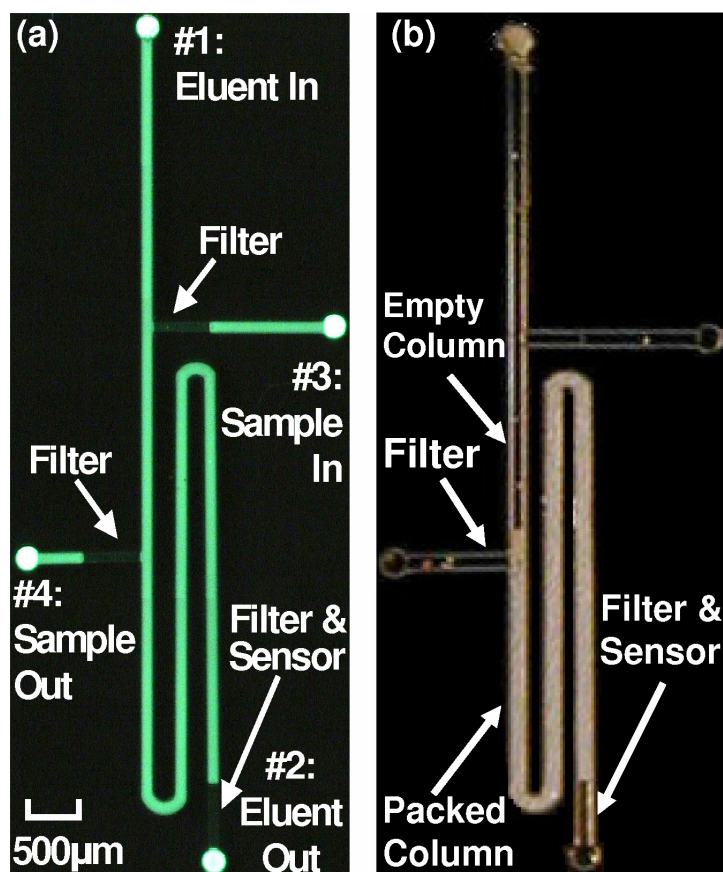


Figure 5-2 (a) Fluorescent overview picture of the integrated ion chromatography chip before column packing. The channels are filled with 0.5% fluorescein. The filters appear darker because they are thinner and thus have lower fluorescent intensities. Electrodes are not visible in the picture. (b) Optical picture of the device after bead packing.

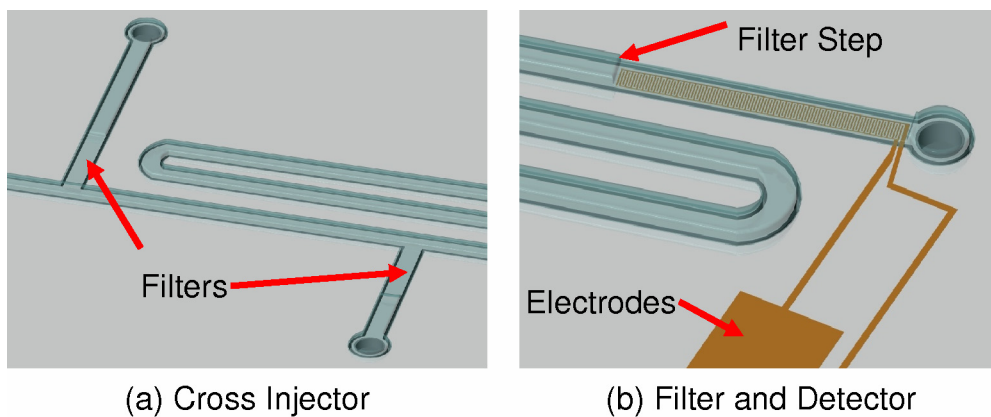


Figure 5-3 3D illustration of the device.

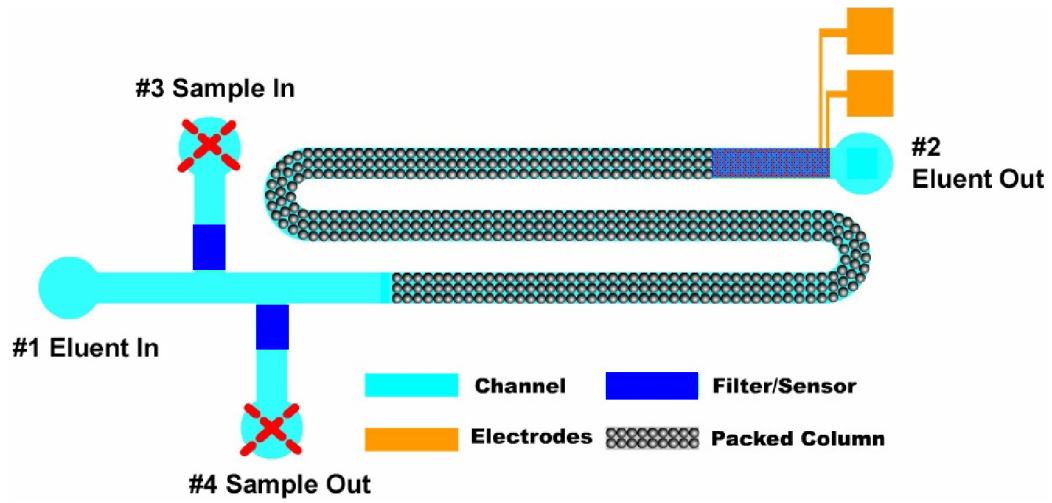


Figure 5-4 Illustration of the ion chromatography chip.

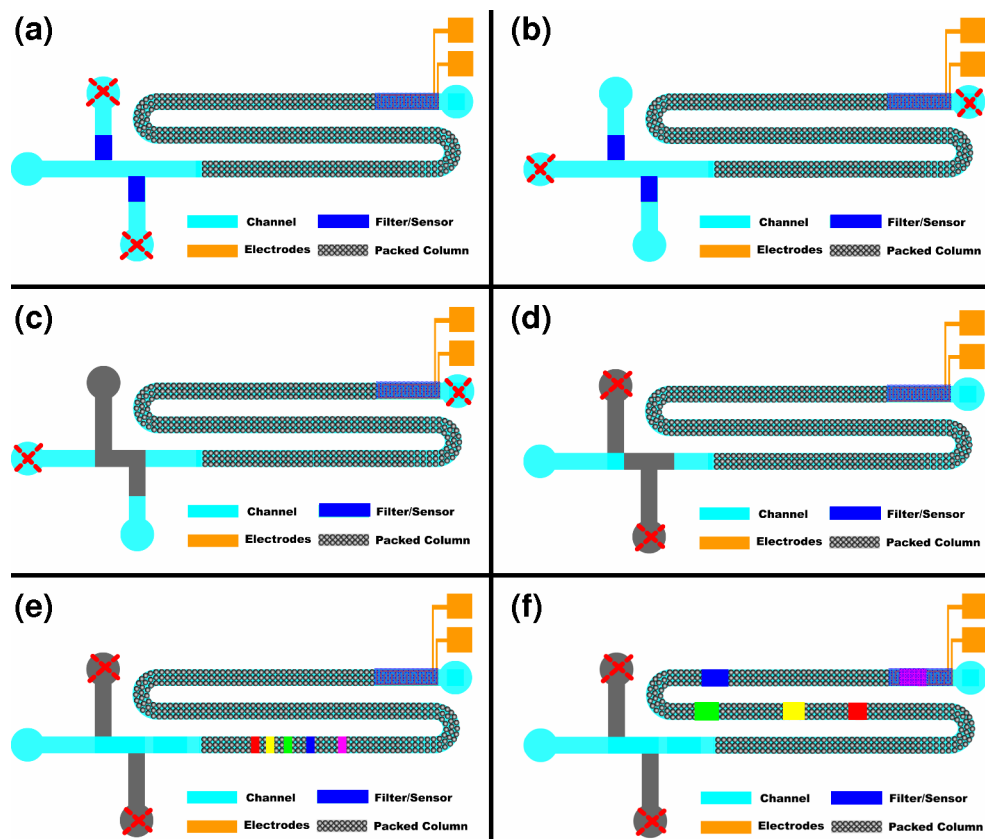


Figure 5-5 Illustrations of on-chip injection, separation, and detection of the ion chromatography chip.

5.2.2 Conductivity Sensing

5.2.2.1 Conductivity Response Theory

Conductivity, κ ($\text{S}\cdot\text{cm}^{-1}$), is the reciprocal of resistivity ρ ($\text{Ohm}\cdot\text{cm}$).

$$\kappa = \frac{1}{\rho} \quad (5.9)$$

Since resistance, R (Ohm), is given by:

$$R = \rho K_{cell} \quad (5.10)$$

Conductance, G , the reciprocal of resistance, can be expressed as:

$$G = \frac{\kappa}{K_{cell}} \quad (5.11)$$

where K_{cell} (cm^{-1}) is the cell constant of the resistance/conductance measuring cell, which is determined by the dimensions of the cell and the electrode configuration. Most K_{cell} values of commercial conductivity sensors are 1 to 10 cm^{-1} . Based on equation (5.11), conductivity can be obtained by directly measuring conductance.

The conductance (in unit of S) of an electrolyte contributed by one of its ions is:

$$G = 1000 \frac{\lambda C}{K_{cell}} \quad (5.12)$$

where C is the concentration of the ion in equivalents per liter (equiv/L), and

$$\text{equiv/L} = \text{Molar} \times \text{Charge-on-Ion} \quad (5.13)$$

λ ($\text{S}\cdot\text{cm}^2/\text{equiv}$) is the equivalent conductance of the ion. λ is a function of the ionic concentration. At high concentrations, ion-ion interactions could decrease the effective conductance of the bulk solution. Fortunately, the solutions commonly encountered in ion chromatography are extremely diluted. Therefore, the conductance in IC can be

calculated with little error using “limiting equivalent conductance,” which is the λ for highly diluted solutions. By adopting the concept of limiting equivalent conductance, conductance in IC is linear with concentration. The limiting equivalent ionic conductances for some common ions in aqueous solution at 25 °C are shown in Table 5-1.

| Ions | λ (S.cm ² /equiv) |
|-------------------------------|--------------------------------------|
| H ⁺ | 350 |
| Na ⁺ | 50 |
| OH ⁻ | 198 |
| F ⁻ | 54 |
| Cl ⁻ | 76 |
| Br ⁻ | 78 |
| NO ₃ ⁻ | 71 |
| PO ₄ ⁻³ | 69 |
| SO ₄ ⁻² | 80 |
| CO ₃ ⁻² | 72 |
| HCO ₃ ⁻ | 45 |

Table 5-1 Limiting equivalent ionic conductances in aqueous solution at 25 °C [1].

The total conductance of a dilute electrolyte is the sum of each individual ion's contributions:

$$G = \frac{1000}{K_{cell}} \sum_i \lambda_i C_i \quad (5.14)$$

Therefore, in an anion-exchange ion chromatography, the background conductance is generated by both the eluent cations and anions. Assuming the eluent is fully ionized, the background conductance, $G_{Background}$, is given by:

$$G_{Background} = 1000 \frac{(\lambda_{E^+} + \lambda_{E^-})C_E}{K_{cell}} \quad (5.15)$$

where λ_{E^+} and λ_{E^-} are the limiting equivalent conductances for the eluent cations and anions, and C_E is the eluent concentration.

During sample elution, the total ion concentration in the column and eluent remains constant throughout the elution process. The eluted sample anions displace an equivalent number of eluent anions from the eluent. The sample cations need not be considered since they are unretained on the anion-exchange column. Thus, the total conductance during elution, $G_{Elution}$, is:

$$\begin{aligned} G_{Elution} &= G_{E^+} + G_{E^-} + G_{S^-} \\ &= \frac{1000}{K_{cell}} [\lambda_{E^+} C_E + \lambda_{E^-} (C_E - C_S) + \lambda_{S^-} C_S] \\ &= G_{Background} + \frac{1000}{K_{cell}} (\lambda_{S^-} - \lambda_{E^-}) C_S \end{aligned} \quad (5.16)$$

where G_{E^+} , G_{E^-} , and G_{S^-} are the conductances of the eluent cations, eluent anions, and sample anions respectively; C_S and λ_{S^-} are the sample concentration and limiting ionic equivalent conductance respectively.

The change of conductance from the background, ΔG , is the sample signal:

$$\Delta G = G_{Elution} - G_{Background} \quad (5.17)$$

It can be derived from equation (5.16) and (5.17):

$$\Delta G = \frac{1000}{K_{cell}} (\lambda_{S^-} - \lambda_{E^-}) C_S \quad (5.18)$$

ΔG is proportional to the concentration of the sample to be detected, which means the minimal detectable concentration is determined by the detection limit of the

conductivity sensor. In addition, ΔG is proportional to the difference in λ between the sample and eluent anions. A proper choice of eluent could enhance the detection sensitivity. Finally, ΔG is inversely proportional to the conductivity sensor cell constant, which therefore should be minimized to maximize the detector sensitivity.

Also from equation (5.18), it can be seen that ΔG could be both positive and negative. When the eluent is more conductive than the sample, ΔG is negative, which shows as valleys on the chromatogram. When the eluent is less conductive, ΔG is positive, appearing as peaks on the chromatogram. Most anion-exchange separations use less-conducting eluents.

It should be noted that the percentage of conductance change over the baseline is usually very small. As shown in the following equation,

$$\frac{\Delta G}{G_{Background}} = \frac{(\lambda_{S^-} - \lambda_{E^-})C_S}{(\lambda_{E^+} + \lambda_{E^-})C_E} \quad (5.19)$$

This percentage decreases linearly with sample concentration. For highly-sensitive detections, the conductance change may approach the noise level, which determines the limit of detection of the sensor. For instance, in a typical scenario, 1 ppm (16 μM) of nitrate (NO_3^-) sample in a 1 mM sodium bicarbonate (NaHCO_3) eluent, the change is only 0.4%. This small change requires the read-out electronics to have ultra-low noise. Moreover, since the conductivity of an ionic solution increases about 2% per degree increase in temperature [1], the temperature in the detector needs to be tightly controlled or compensated. An alternative approach to further lower the detection limit is suppression of the background signal, which can be done either chemically or electrically [6].

5.2.2.2 Conductivity Detector Cell Analysis

A typical conductivity cell has interdigitated sensing electrodes (Figure 5-6). The electrode fingers have a width of W and a spacing of S . All the fingers cover a detector area of A_D , which is equal to $L_E \times L_D$. The total number of fingers is N .

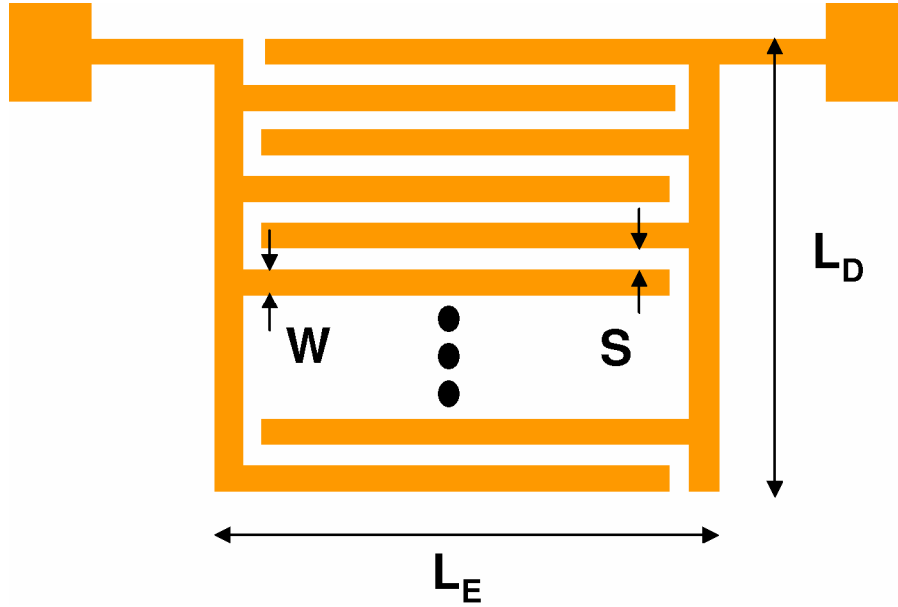


Figure 5-6 Configurations of the interdigitated electrodes in the conductivity detector cell.

As explained in the previous section, in order to maximize signal, the cell constant needs to be as small as possible. Theoretically, the cell constant for the electrode configuration in Figure 5-6 can be expressed as [10]:

$$K_{cell} = \frac{2}{(N-1)L_E} \cdot \frac{K(k)}{K[\sqrt{1-k^2}]} \quad (5.20)$$

where $K(k)$ is an elliptic integral of the first kind with elliptic modulus k :

$$K(k) = \int_{t=0}^1 \frac{1}{\sqrt{(1-t^2)(1-k^2t^2)}} dt \quad (5.21)$$

For a two-finger detector:

$$k = \frac{S}{S+W} \quad (5.22)$$

And for a multiple-finger ($N>2$) detector:

$$k = \cos\left(\frac{\pi}{2} \cdot \frac{W}{S+W}\right) \quad (5.23)$$

The cell constant does not vary much with k value, instead, it decreases significantly with an increasing number of fingers. Practically, it can be assumed that $S = W$ and $N \gg 1$. Then $k = \sqrt{2}/2$, and:

$$\frac{K(k)}{K[\sqrt{1-k^2}]} = 1 \quad (5.24)$$

In this case, equation (5.20) can be simplified with little approximation:

$$K_{cell} = \frac{2}{NL_E} \quad (S = W, N \gg 1) \quad (5.25)$$

which can be rewritten as:

$$K_{cell} = \frac{4S}{A_D} \quad (5.26)$$

From equation (5.26), it can be seen that in order to minimize K_{cell} , the width and spacing of the electrodes should be minimized, which is limited by the patterning technology. Nano-interdigitated electrodes can be made using alternative methods [11–13] and are supposed to deliver significantly better performances. In addition, the detector area should be maximized; this however must be compromised in consideration of minimizing peak broadening and avoiding peak overlapping in the detector.

5.2.2.3 The On-Chip Conductivity Detector

The conductivity detector cell on the microchip has width of 100 μm , height of 4 μm , and length of 1000 μm , which corresponds to a volume of 0.4 nL. The interdigitated electrode fingers are 5 μm wide with 5 μm spacing. The length of each finger is 80 μm . Based on equation (5.26), the cell constant can be calculated to be 2.5 cm^{-1} .

The electrodes are e-beam evaporated platinum (Pt) with a thin titanium (Ti) layer at its bottom to improve adhesion. Another popular electrode pair, Au and Cr, is not suitable for electrochemical applications that require direct electrode-solution contact, since Cr can be easily eroded into dissolvable ions. One way to avoid direct electrode-solution interface is contactless conductivity sensing [14–17], which is often used in capillary electrophoresis, since there is a high voltage applied in the solution. The electrodes are buried under a thin layer of insulation material and capacitively coupled to the solution. It avoids problems such as electrochemical modification or degradation of the electrode surface, and reduces electrolysis bubble generation.

To obtain the conductance of the liquid in the detector cell, 1 V AC voltage at a frequency of 10 kHz is applied to the cell using an HP 3245A universal voltage/current source, and the resulting current is amplified and converted to voltage, which is acquired by a computer through an HP 34970A data acquisition unit. The amplitude of the AC voltage applied is limited by the electrochemical reactions that can happen at high voltages. The frequency has to be in the region where resistance dominates the total impedance in the conductivity cell [18]. 10 kHz frequency is used in most commercial conductivity detectors, for example the model 650 conductivity detector from Alltech

Associates [19]. And this frequency is also verified to be in the right region through an on-chip impedance frequency response experiment described in Section 5.4.3.

5.2.3 Downscaling

Based on HPLC theory, the dimensions and operating conditions of a commercial ion-exchange LC column PRP-X110 (Hamilton Reno, NV) is downscaled to find the corresponding values for the on-chip LC system. The on-chip column uses the same type of beads as those in the commercial column. An isocratic separation of seven common anions using the commercial column is shown in Figure 5-7 [20]. The column ID is 4.1 mm and the length is 150 mm. Bead diameter is 7 μm . The flow rate is 2 mL/min. Sample injection volume is 100 μL . Non-suppressed conductivity detection is used.

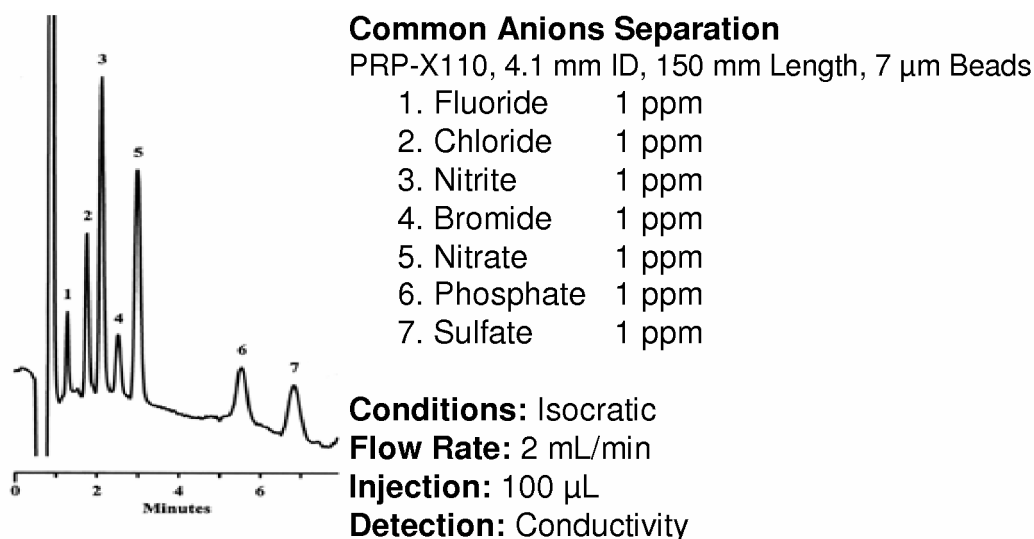


Figure 5-7 Common anions separation using a commercial HPLC system.

The on-chip column has significantly smaller dimensions, only 8 mm long, 100 μm wide and 25 μm high, and shares the same cross-sectional area as a 56 μm ID capillary. This ID is not impractically small, as people have demonstrated improved

separation performance with packed 20 to 50 μm ID capillary columns [21], and there are 75 μm ID packed capillary columns commercially available (Agilent, Palo Alto, CA).

Based on HPLC theory, the maximum allowed injection volume V_i is [22]:

$$V_i = \theta V_R \frac{K}{\sqrt{N}} \quad (5.27)$$

where θ^2 defines the fraction of peak broadening, V_R is the retention volume, K is a parameter characteristic of the quality of injection, and N is the number of plates. From equation (2.21), we know:

$$V_R \propto d_c^2 \quad (5.28)$$

where d_c is the column ID. And from equation (2.19) and (2.20), we can get:

$$N = \frac{L_c}{h d_p} \propto L_c \quad (5.29)$$

where L_c is the column length, h is the reduced plate height, and d_p is the bead diameter. Therefore, it can be derived that:

$$V_i \propto d_c^2 \sqrt{L_c} \quad (5.30)$$

Based on equation (5.29), it can be calculated that the on-chip injection volume should be 4.3 nL. 4.5 nL is used in the actual design. This injection volume is four orders of magnitude smaller than that of the commercial system.

The maximum allowed detector cell volume, V_{D-Max} , is given by:

$$V_{D-Max} = \frac{V_i}{2} \quad (5.31)$$

Thus, the on-chip detector volume should be less than 2.25 nL. The volume of the actual cell (100 μm wide, 1000 μm long, and 4 μm high) is 0.4 nL, which minimizes peak broadening and avoids peak overlapping in the detector. The detector cell volume of the commercial system is not given. Generally, most such conductivity cells have volumes on the order of 1 μL , such as the one from Alltech Associates [19], which has a cell volume of 0.5 μL .

As described in Chapter 2, the optimal linear flow velocity, u , is mostly on the order of 1 mm/s, regardless of the column dimension. This can be verified by calculating the u value for the commercial column, based on the following equation:

$$u = \frac{F}{\varepsilon A_c} \quad (5.32)$$

where F is the volumetric flow rate, ε is the column porosity, and A_c is the column cross-sectional area. Assuming ε is 0.8, u can be found to be 3 mm/s for the commercial column. For on-chip separation, if 1 mm/s flow velocity is used, then the corresponding volumetric flow rate is 0.12 $\mu\text{L}/\text{min}$, again assuming ε is 0.8. For simplicity, 0.2 $\mu\text{L}/\text{min}$ flow rate (1.7 mm/s flow velocity) is used in the real separation experiments. This flow rate is four orders of magnitude smaller than that of the commercial system.

The operating pressure can be calculated based on the following equation:

$$\Delta P = \frac{\Phi \eta L_c F}{\varepsilon d_p^2 A_c} \quad (5.33)$$

where Φ is dimensionless flow resistance of the column, and η is the solution viscosity. Φ is assumed to be 500, which is an empirical value for a column packed with porous spherical beads. Since all solutions used in ion chromatography are very diluted aqueous

solutions, η is about the same as water's viscosity, which is $1 \text{ mPa}\cdot\text{s} = 1.455 \times 10^{-7} \text{ psi}\cdot\text{s}$. Therefore, the operating pressures for the commercial and on-chip columns can be calculated to be 703 psi and 20 psi respectively. The calculated pressure for the on-chip column is close to, but slightly higher than what is measured. As described in Section 5.4.2, it is due to the reduced flow resistance of miniaturized on-chip columns.

Table 5-2 summarizes the downscaling results from the Hamilton LC system to the on-chip LC system.

| | Hamilton | Chip LC | Scaling Factor |
|------------------------------|--------------------------|------------------------------|-----------------|
| Column Beads | 7 μm PRP-X110 | | N/A |
| Column ID | 4.1 mm | 56 μm (equiv.) | 73 |
| Column Length | 150 mm | 8 mm | 19 |
| Linear Flow Velocity | 3 mm/s | 1.7 mm/s | 1.8 |
| Flow Rate | 2 mL/min | 0.2 $\mu\text{L}/\text{min}$ | 1×10^4 |
| Pressure (calculated) | 703 psi | 20 psi | 35 |
| Injection Volume | 100 μL | 4.5 nL | 2×10^4 |
| Detector Cell Volume | 1 μL (est.) | 0.4 nL | 2500 |

Table 5-2 Downscaling from the Hamilton LC system to the on-chip LC system.

5.3 Microchip Fabrication

5.3.1 Fabrication Process Flow

The process used to fabricate the ion chromatography chip is illustrated in Figure 5-8. It starts with growing a 1.5 μm SiO_2 layer on both sides of a 4-inch silicon wafer by thermal oxidation. Then using a delay-mask technique described below, two-level backside holes are created with DRIE. First, the backside oxide is patterned and etched

with buffered HF, which defines the 150 μm diameter small holes. Then an 8 μm photoresist AZ4620 (Clariant, Somerville, NJ) layer is patterned on the backside to define the 510 μm diameter big holes, which are concentric with the small holes. DRIE is done to etch the small holes 200 μm deep into the silicon wafer backside using the small-hole oxide mask. After etching the backside oxide using the big-hole photoresist as a mask, DRIE is performed again to etch the backside until only a 50 μm thick diaphragm is left. The big holes are “delayed” compared to the small holes, which creates the two-level structure used for fluidic access ports. The two-level structure can be used as a tubing stopper when coupling tubing is directly inserted into the chip.

Following frontside oxide patterning, 300 \AA titanium/2000 \AA platinum/1000 \AA gold are e-beam evaporated and patterned through wet etching processes. Au is used only for wire bonding purpose, since it is very difficult to directly bond to Pt. Au is patterned with Au etchant (Transene, Danvers, MA), and is left only at the bonding pads. Pt is the sensing electrode and is patterned with Aqua Regia ($\text{HNO}_3:\text{HCl}:\text{H}_2\text{O}=1:6:3$ by volume) at 80 $^\circ\text{C}$. The etching solution has to be heated to a relatively high temperature in order to start etching the Pt. Ti is used as an adhesion layer between the Pt and the substrate, and it is patterned with Ti etchant ($\text{HF}:\text{H}_2\text{O}_2:\text{H}_2\text{O}=1:1:20$ by volume).

25 μm thick photoresist AZ4620 is spun on the front side of the substrate and patterned with two masks to form a two-level photoresist structure using a double-exposure method. One full exposure (1st mask) and one partial exposure (2nd mask) are performed prior to developing the photoresist. Areas around the fluidic channels are fully exposed, which reveals a 15 μm wide oxide ring underneath. Bead filters and field areas are partially exposed to leave only 4 μm high photoresist after developing. The

unexposed photoresist is for the 25 μm high liquid chromatography column and inlet/outlet chambers. After photoresist patterning, the revealed oxide ring around fluidic channels is etched away with buffered HF. Then 40 μm deep trenches with a mushroom profile at the bottom are created in the moat area using a modified DRIE Bosch process [23], which adds a 36-second isotropic SF_6 plasma etching at the end of the standard DRIE Bosch process. Alternatively, the moat area can be roughened in XeF_2 . This is using the self-aligned trench/roughening-anchoring technique described in Chapter 4, to increase the pressure rating of the parylene device.

10 μm thick parylene C (Specialty Coating Systems, Indianapolis, IN) is then conformally deposited on the wafer frontside, filling up the trenches and covering the photoresist structures. Parylene is patterned and etched with oxygen plasma from outside the channels and anchoring moats. Field photoresist outside the channels and moat is then stripped. Backside holes are opened with DRIE. Finally the channels are released by dissolving the photoresist in the channels. To further strengthen and passivate the device, an optional epoxy overcoating layer can be applied to the device.

Then chromatographic beads can be packed into the column from the chip backside hole, as shown in Figure 5-9 (a). The beads are trapped by the on-chip filter. The detailed packing process is described in the testing part, Section 5.4.1. Figure 5-9 (b) shows a picture of a device after bead packing. Some individual beads can be clearly seen at where the column and filter meet. The column and filters are anchored to the substrate. Figure 5-9 (10) shows a fluorescent picture of a section of column packed with beads.

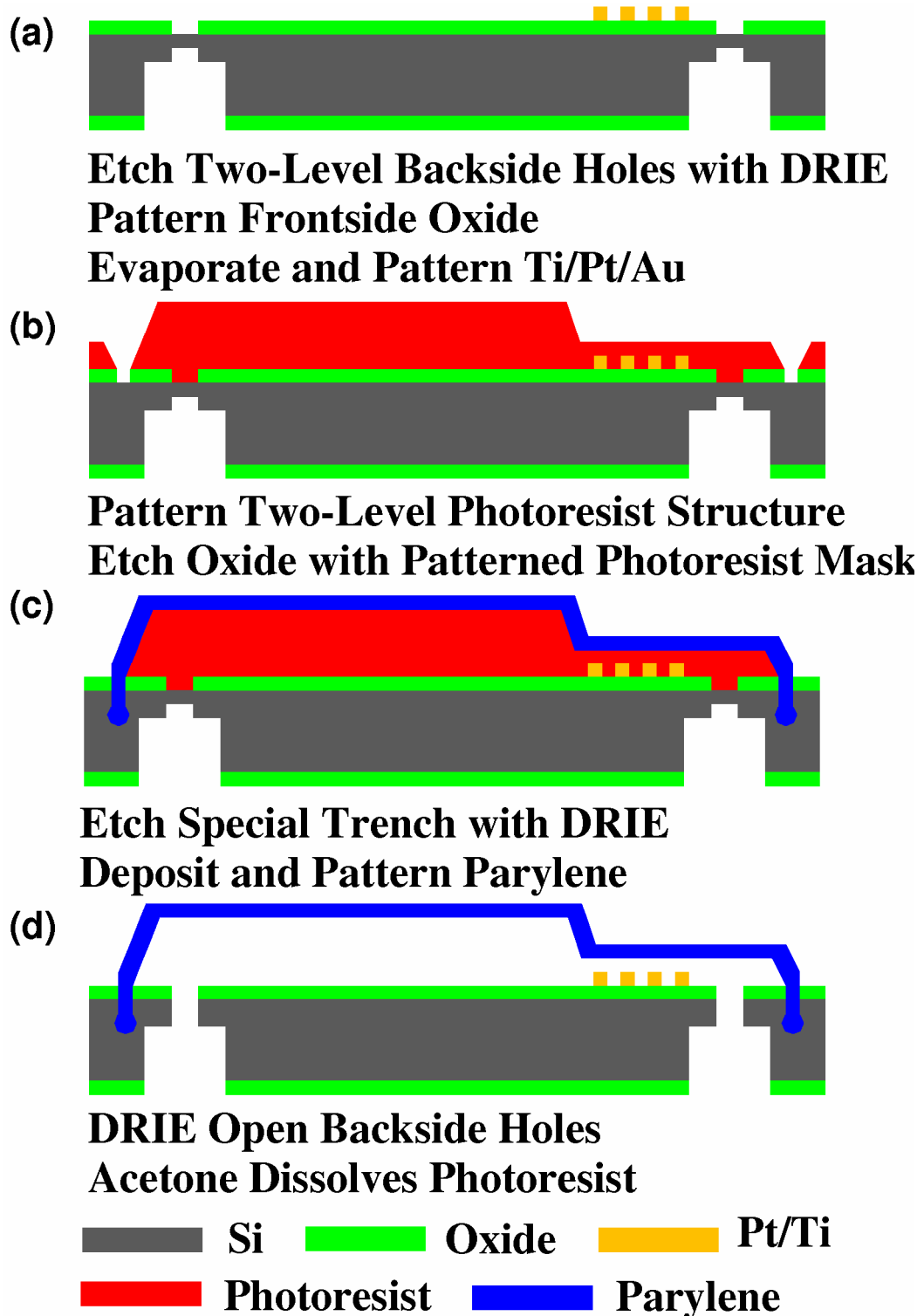


Figure 5-8 Fabrication process flow.

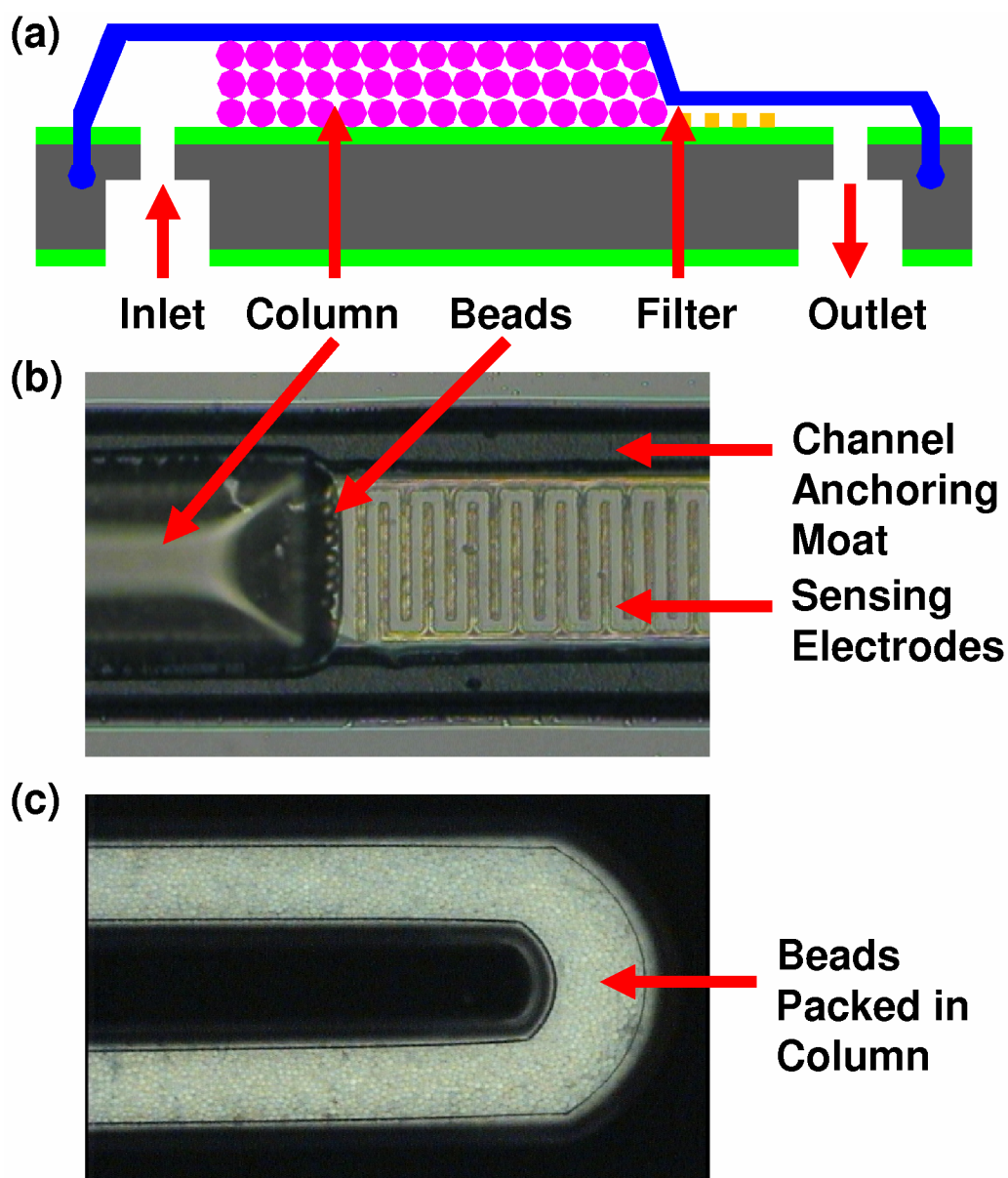


Figure 5-9 Illustration and pictures of the fabricated device after bead packing.

5.3.2 Chip Packaging

Fluidic and electronic access to the chip is achieved with a custom-made packaging jig, as described in Section 4.2.4. The jig body is made of PEEK (McMaster-Carr, Los Angeles, CA), which is inert for all the chemicals and solvents used in the

testing of this ion chromatography chip. The jig is capable of accessing a 4-by-4 array of 16 holes on the chip, at most 8 holes simultaneously. The ion chromatography device only uses four of the holes. O-rings provide sealing between the jig and chip. A PCB (Printed Circuit Board) cover is placed on top and is screwed down to compress the chip and o-rings. Electrical access to the chip is made by wire-bonds from the chip to the top PCB. A packaged chip after wiring bonding is shown in Figure 5-10.

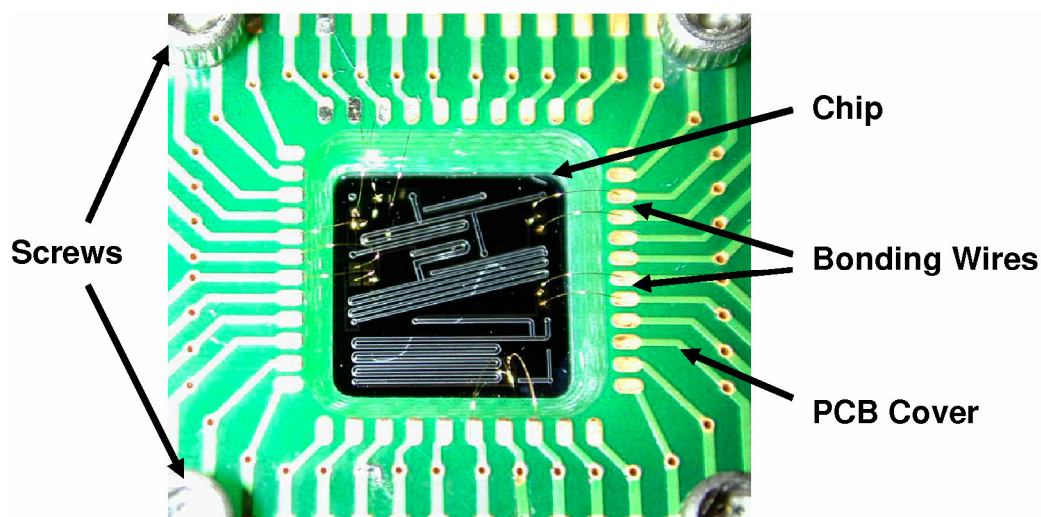


Figure 5-10 Packaged chip after wire bonding.

5.4 Testing Results and Discussion

5.4.1 Separation Column Packing

The separation column is the heart of an LC system. In order to get good and repeatable separation, column packing has to be void-free, dense, and uniform, which usually has to be packed at relatively high pressures. Packing of beads into the on-chip column is achieved with the conventional slurry technique. The packing slurry is prepared by mixing beads with deionized water, followed by agitating the mixture with a

vortexer (Scientific Industries, Bohemia, NY) to homogenize the solution and prevent beads from precipitating. The mixture solution is sucked into a syringe and injected into a section of tubing, which is used as a bead solution reservoir. The tubing is switched on-line, and an off-chip pressure source is used to pack the beads into the on-chip column at 200 psi. Pressurized nitrogen gas is used as the pressure source, which is filtered with 0.5 μm filters before entering the chip packaging jig. The gas pressure is controlled through metering valves and monitored with a pressure transducer (PX120-2KGV, Omega, Stamford, CT) in conjunction with an Omega DP25-S strain gage panel meter. The setup has an upper limit of 800 psi with a precision of 1 psi.

The stationary phase material used to pack the on-chip columns is PRP-X110 anion exchange resin from Hamilton (Reno, NV). The resins are the same as those used in Hamilton's anion exchange column PRP-X110, which has been popular in anion-exchange chromatography systems. The resins are 7 μm diameter spherical porous PS-DVB (poly(styrene-divinylbenzene)) beads with trimethyl-ammonium functional groups ($\text{N}(\text{CH}_3)^{+3}$) (Figure 5-11). The bead polymer base material has a specific gravity of 1. The average pore-size is 100 \AA . And the exchange capacity is 0.11 mequiv/g.

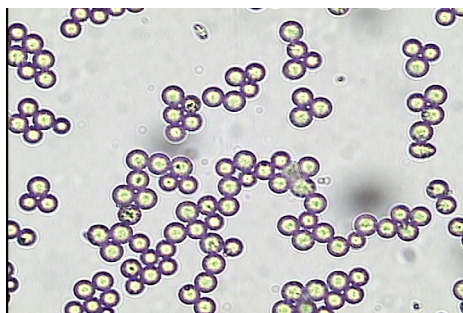


Figure 5-11 Anion exchange beads used in the column packing.

Resin capacity is an extremely important parameter in ion chromatography. Ion chromatography usually employs low-capacity ion exchangers, ranging from 0.01 to 0.2 mequiv/g. For anion-exchange, and especially for non-suppressed IC to be successful, it is necessary to have resins with a low exchange capacity. Low capacity will result in faster elution and/or elution with weaker eluents. Capacity is usually given in “milli-equivalents (of exchangeable ions)/gram (of resin).”

5.4.2 Pressure–Flow Rate Relation

By measuring the pressure–flow rate relation of the on-chip packed column, the column permeability can be acquired, which is usually a good indicator of the column packing quality. Moreover, based on the pressure–flow rate relation, the operating pressure of the on-chip column can be estimated for variations in column length, bead diameter, solvent viscosity, and flow rate. In the testing, DI water is pushed through the column with pressurized nitrogen gas, and the volumetric flow rate is obtained by measuring the liquid front moving velocity in a capillary connected at the column outlet. Since the column is packed at 200 psi, the measurement pressure is only up to 200 psi. Theoretically [22], the column volumetric flow rate, F , is proportional to the pressure applied, ΔP . The linear relation is expressed as:

$$F = \frac{\varepsilon d_p^2 A_c}{\Phi \eta L_c} \Delta P \quad (5.34)$$

where ε is the column porosity, Φ is the dimensionless flow resistance, d_p is the bead diameter, A_c is the column cross-sectional area, η is the fluid viscosity, and L_c is the column length.

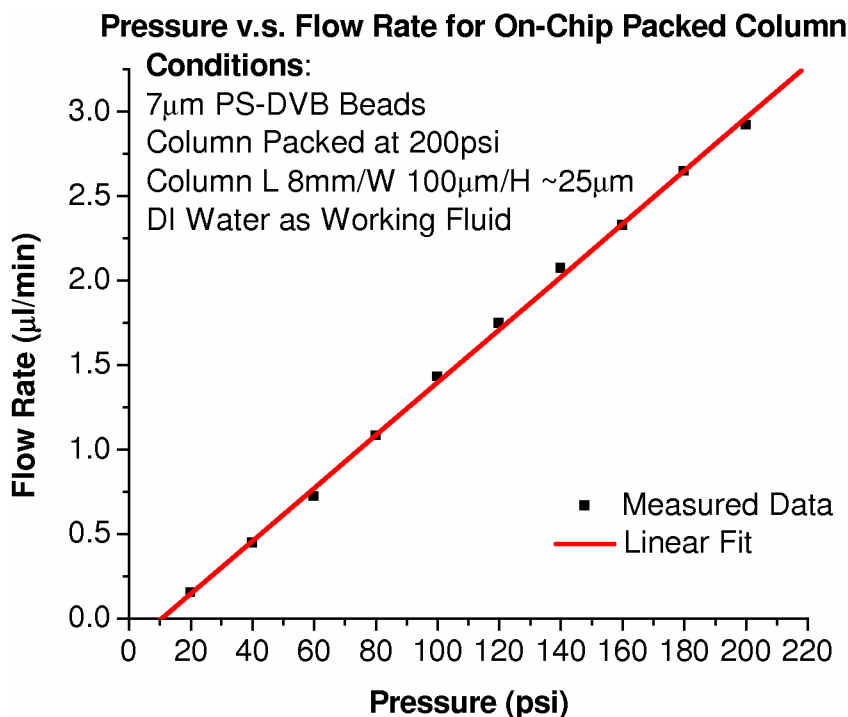


Figure 5-12 Pressure vs. flow rate curve for an on-chip packed column.

The measured pressure–flow rate data and fitted linear curve is shown in Figure 5-12. The straight line does not extend back to the origin because of a non-linear pressure–flow rate relation at very low pressures. From the fitted line, it is found that $\Phi / \varepsilon = 444$. Assuming the porosity of the packed column is 0.7 to 0.85, which is normal for porous-bead column, then Φ is 311 to 377, which is close to but smaller than its empirical value of 500 for conventional LC columns. This result is confirmed again in Section 6.3.2. The high permeability of the on-chip column is due to the fact that the column dimension is approaching the order of magnitude of particle size. In this case, the column becomes effectively “less dense” than conventional ones because walls disturb the regular structures of the packed bed. Similar results have been reported before [21], where Φ is found to decrease with decreasing capillary column IDs from 50 μ m to 20 μ m. Although

the permeability is higher, the micro-columns actually have better separation performance according to the same paper, which also means the pressure requirement can be lower for micro-columns.

5.4.3 Impedance Frequency Response

Since the electrodes are in direct contact with the solution, double layer capacitance (C_{DL}) and detector cell capacitance (C_{Cell}) also contribute to the total impedance. The equivalent electrical circuit (Figure 5-13) and impedance frequency response analysis for the interdigitated planar electrodes are presented in [18]. In Figure 5-13, R_{Cell} is the resistance of the solution to be measured in the detector and R_{lead} is the resistance of the electrical leads.

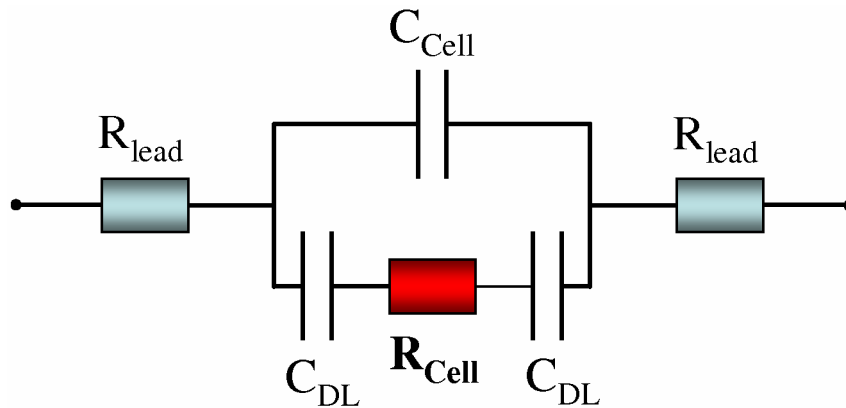


Figure 5-13 Conductivity detector cell equivalent circuit.

When the frequency is low, C_{DL} dominates the total impedance, until a cut-off frequency of f_{low} is reached.

$$f_{low} = \frac{1}{\pi R_{Cell} C_{DL}} \quad (5.35)$$

Above this frequency, R_{Cell} dominates the total impedance, and the impedance becomes almost frequency independent. When the frequency reaches f_{high} , C_{Cell} starts to dominate the total impedance.

$$f_{high} = \frac{1}{2\pi R_{Cell} C_{Cell}} \quad (5.36)$$

Above f_{high} , the impedance once again drops with increasing frequency. The theoretical impedance frequency response is shown in Figure 5-14. The conductivity measuring frequency has to be in the resistance dominant region to minimize capacitive effects, which is the frequency range between f_{low} and f_{high} .

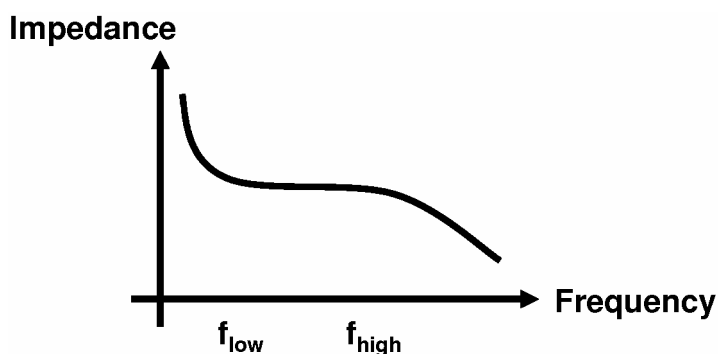


Figure 5-14 Theoretical impedance frequency response.

The impedance frequency response for the ion chromatography mobile phase solution (1.7 mM sodium bicarbonate/1.8 mM sodium carbonate, Alltech, Deerfield, IL) with on-chip interdigitated platinum electrodes is measured with an HP 4192A LF impedance analyzer and the result is shown in Figure 5-15. The trend largely follows what is predicted in Figure 5-14 except for the middle region, which is shown to have decreasing impedance with increasing frequency, although much less sharply than the low and high frequency regions. This is due to the fact that the resistance does not

completely dominate over the capacitances from the double layers and the cell. From this experiment, it is verified that the chosen measuring frequency of 10 kHz is in the resistance “dominating” region.

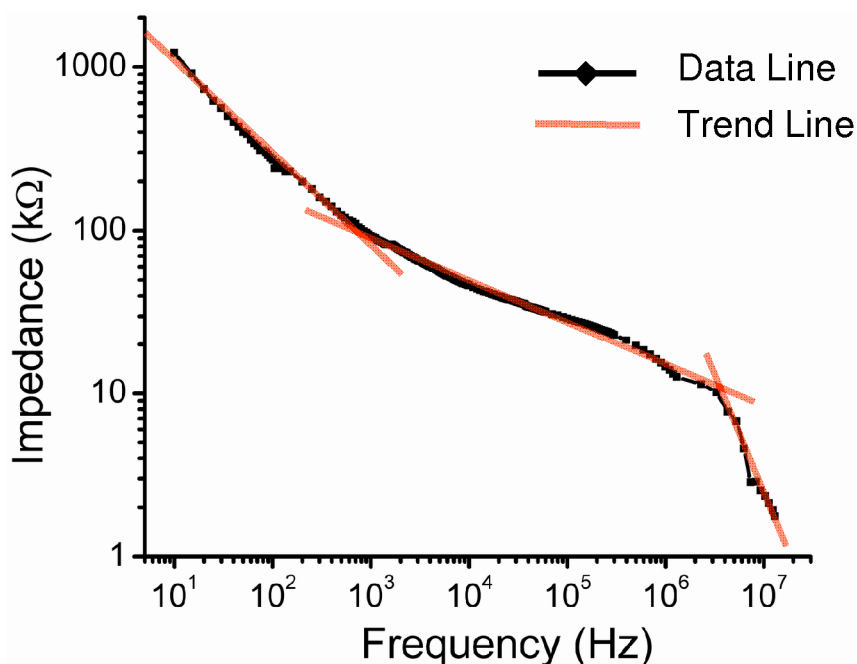


Figure 5-15 Impedance frequency spectrum of the mobile phase solution in contact with the on-chip interdigitated platinum electrodes.

5.4.4 Ion Chromatography Separation

Isocratic anion-exchange ion chromatography is used to separate seven common anions on-chip. The bead-packed column is 8 mm long, 100 μm wide, and 25 μm high, and shares the same cross-sectional area as a 56 μm ID capillary. The beads are anion exchange 7 μm diameter PS-DVB resins. 1.7 mM sodium bicarbonate/1.8 mM sodium carbonate solution is used as mobile phase. The flow rate is 0.2 $\mu\text{L}/\text{min}$, provided by a syringe pump. The injection volume is 4.5 nL achieved on-chip. Certified ion chromatography seven-anion mixture in water with known anion concentrations (Alltech,

Deerfield, IL) is diluted to obtain a sample solution containing 12.5 ppm fluoride (F^-), 25 ppm chloride (Cl^-), 25 ppm nitrite (NO_2^-), 25 ppm bromide (Br^-), 25 ppm nitrate (NO_3^-), 25 ppm phosphate (PO_4^{3-}), and 25 ppm sulphate (SO_4^{2-}).

The seven anions have been successfully separated and the chromatogram is obtained with the on-chip conductivity detector (Figure 5-16). The ion identifications are determined by the sequence of peaks, since the ions have fixed affinities to the column stationary phase. All seven anions are resolved in about 90 seconds, demonstrating a fast separation and detection on-chip. The precise time when the injected sample plug enters the column is difficult to determine, due to the external pumps, valves, and o-rings used in the packaging. The peaks are sharp due to the small column dimensions and minimized dead volume of the integrated system.

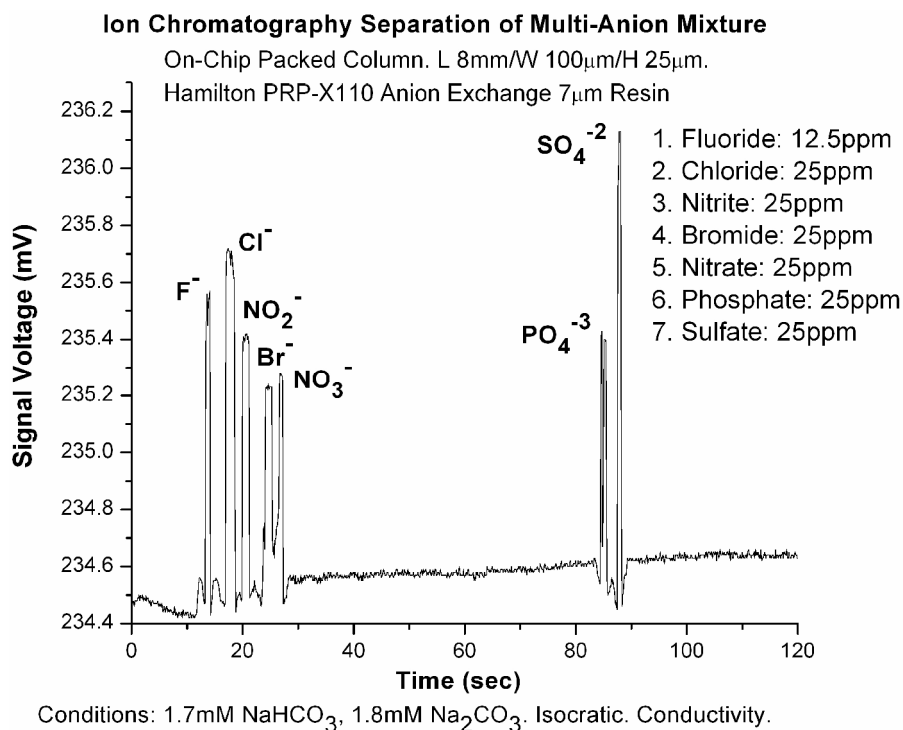


Figure 5-16 Chromatogram of an on-chip ion chromatographic separation of seven anions.

Since non-suppressed conductivity sensing is used, the background signal is relatively high and the sample ion signals are only about 0.3% to 0.7% of the background, which is the main factor determining the limit of detection of the current device. Assuming the minimum tolerable signal-to-noise ratio is three, the limit of detection for the common anions is estimated to be around 1 ppm using the current chip and conductivity read-out electronics.

5.5 Summary

A microchip with an integrated LC system has many promising applications that are impossible or impractical before, such as remote-site environmental monitoring, networked sensing, and consumer health care. The ion chromatography chip presented in this chapter has on-chip bead column, filters, sample injection structure, and conductivity detector. The microchip is made with a single CMOS-compatible batch fabrication, which is low-cost, high-volume production, and allows the measuring electronics and signal conditioning circuitry to be integrated on the same chip.

The current system has a detection limit of 1 ppm for the common anions. A lower detection limit is expected with electronic baseline suppression [6] and/or better read-out electronics. Better injection, in terms of accuracy, repeatability, and precise injection time control, can be achieved by integrating more conductivity sensors on the chip to monitor the injection process better. While common anions are used in the separation experiment, other conducting samples such as organic acids and some peptides can also be analyzed. By packing the column with cation exchange beads, the chip can be used to analyze cations as well.

Unlike the bead integration method developed in Chapter 3, a new method to introduce beads into the column is used, which is the slurry-packing technique. This method can reduce the complexity and increase the yield of device fabrication. The anchoring technique developed in Chapter 4 is used in this chip to achieve a high-pressure-rated device. However, this chip is not intended to be a high-pressure, high-capacity LC chip. Also it does not have the capability of direct coupling with mass spectrometry for really powerful compound identification and analysis. These will be the focuses of the device presented in Chapter 6.

5.6 Bibliography

- [1] J. S. Fritz and D. T. Gjerde, *Ion chromatography*. 3rd, 2000. Weinheim, Germany; New York: Wiley-VCH.
- [2] C. A. Lucy, "Evolution of ion-exchange: From Moses to the Manhattan Project to modern times." *Journal of Chromatography A*, 2003. 1000(1–2): p. 711–724.
- [3] W. W. Buchberger, "Detection techniques in ion analysis: what are our choices?" *Journal of Chromatography A*, 2000. 884(1–2): p. 3–22.
- [4] W. W. Buchberger, "Detection techniques in ion chromatography of inorganic ions." *Trac-Trends in Analytical Chemistry*, 2001. 20(6–7): p. 296–303.
- [5] P. R. Haddad, P. E. Jackson, and M. J. Shaw, "Developments in suppressor technology for inorganic ion analysis by ion chromatography using conductivity detection." *Journal of Chromatography A*, 2003. 1000(1–2): p. 725–742.
- [6] F. Laugere, M. J. Vellekoop, J. Bastemeijer, P. M. Sarro, G. Van der Steen, and A. Bossche, "Electronic baseline-suppression for liquid conductivity detection in a capillary electrophoresis microchip." *First IEEE International Conference on Sensors (IEEE Sensors 2002)*. Orlando, FL, United States, Jun 12–14, 2002. p. 450–453.
- [7] S. D. Richardson, "Water analysis." *Analytical Chemistry*, 2001. 73(12): p. 2719–2734.
- [8] L. M. L. Nollet, *Handbook of water analysis*. 2000. New York: Marcel Dekker.
- [9] A. P. O'Neill, P. O'Brien, J. Alderman, D. Hoffman, M. McEnery, J. Murrphy, and J. D. Glennon, "On-chip definition of picolitre sample injection plugs for

- miniaturised liquid chromatography." *Journal of Chromatography A*, 2001. 924(1-2): p. 259–263.
- [10] W. Olthuis, W. Streekstra, and P. Bergveld, "Theoretical and Experimental-Determination of Cell Constants of Planar-interdigitated electrolyte conductivity sensors." *Sensors and Actuators B-Chemical*, 1995. 24(1–3): p. 252–256.
- [11] P. Van Gerwen, W. Laureyn, A. Campitelli, P. Jacobs, P. Detemple, K. Baert, W. Sansen, and R. Mertens, "Cost effective realization of nanoscaled interdigitated electrodes." *Journal of Micromechanics and Microengineering*, 2000. 10(3): p. 1–5.
- [12] P. Van Gerwen, W. Laureyn, W. Laureys, G. Huyberechts, M. O. De Beeck, K. Baert, J. Suls, W. Sansen, P. Jacobs, L. Hermans, and R. Mertens, "Nanoscaled interdigitated electrode arrays for biochemical sensors." *Sensors and Actuators B-Chemical*, 1998. 49(1–2): p. 73–80.
- [13] W. Laureyn, D. Nelis, P. Van Gerwen, K. Baert, L. Hermans, R. Magnee, J. J. Pireaux, and G. Maes, "Nanoscaled interdigitated titanium electrodes for impedimetric biosensing." *Sensors and Actuators B-Chemical*, 2000. 68(1–3): p. 360–370.
- [14] W. Olthuis, A. J. Sprenkels, J. G. Bomer, and P. Bergveld, "Planar interdigitated electrolyte-conductivity sensors on an insulating substrate covered with Ta₂O₅." *Sensors and Actuators B-Chemical*, 1997. 43(1–3): p. 211–216.
- [15] E. Baltussen, R. M. Guijt, G. van der Steen, F. Laugere, S. Baltussen, and G. W. K. van Dedem, "Considerations on contactless conductivity detection in capillary electrophoresis." *Electrophoresis*, 2002. 23(17): p. 2888–2893.

- [16] M. Pumera, J. Wang, F. Opekar, I. Jelinek, J. Feldman, H. Lowe, and S. Hardt, "Contactless conductivity detector for microchip capillary electrophoresis." *Analytical Chemistry*, 2002. 74(9): p. 1968–1971.
- [17] F. Laugere, R. M. Guijt, J. Bastemeijer, G. van der Steen, A. Berthold, E. Baltussen, P. Sarro, G. W. K. van Dedem, M. Vellekoop, and A. Bossche, "On-chip contactless four-electrode conductivity detection for capillary electrophoresis devices." *Analytical Chemistry*, 2003. 75(2): p. 306–312.
- [18] S. Bohm, B. Timmer, W. Olthuis, and P. Bergveld, "A closed-loop controlled electrochemically actuated micro-dosing system." *Journal of Micromechanics and Microengineering*, 2000. 10(4): p. 498–504.
- [19] Alltech Associates, *Alltech model 650 conductivity detector, instrument support sheet*, www.AlltechWEB.com
- [20] Hamilton, "Common anions separation by conductivity detection," <http://www.hamiltoncomp.com/product/hplc/prpx110.html>
- [21] R. T. Kennedy and J. W. Jorgenson, "Preparation and evaluation of packed capillary liquid-chromatography columns with inner diameters from 20 to 50 μm ." *Analytical Chemistry*, 1989. 61(10): p. 1128–1135.
- [22] V. R. Meyer, *Practical high-performance liquid chromatography*. 3rd ed. 1998, Chichester; New York: Wiley.
- [23] M. Liger, D. C. Rodger, and Y.-C. Tai, "Robust parylene-to-silicon mechanical anchoring." *Proceedings of the Sixteenth IEEE International Conference on Micro Electro Mechanical Systems (MEMS 2003)*. Kyoto, Japan, 2003. p. 602–605.

CHAPTER 6

A NANO HPLC/MS CHIP

6.1 Introduction

This chapter presents an integrated microchip with high-pressure liquid chromatography column, bead filter, and electro-spray ionization (ESI) nozzle. Compared to what has been done in the previous chapter, this microchip intends to demonstrate higher operating and maximum pressures, higher performance LC with longer column and smaller beads, and the integration of ESI nozzle with this HPLC chip platform for direct coupling with on-line mass spectrometry (MS) detection. An important application of this chip is HPLC-MS, which is the workhorse for today's proteomics and pharmaceutical industry. There is much interest in significantly cutting sample requirements, reducing cost and size, and dramatically boosting the throughput of existing HPLC-MS systems. A total realization of all these dreams will be revolutionary, which could help scientists reveal the secrets of life faster, combat aging better, and

discover drugs sooner. It is a difficult problem, however. This microchip will serve as an important step towards achieving those goals.

6.2 Design and Fabrication

6.2.1 Microchip Design

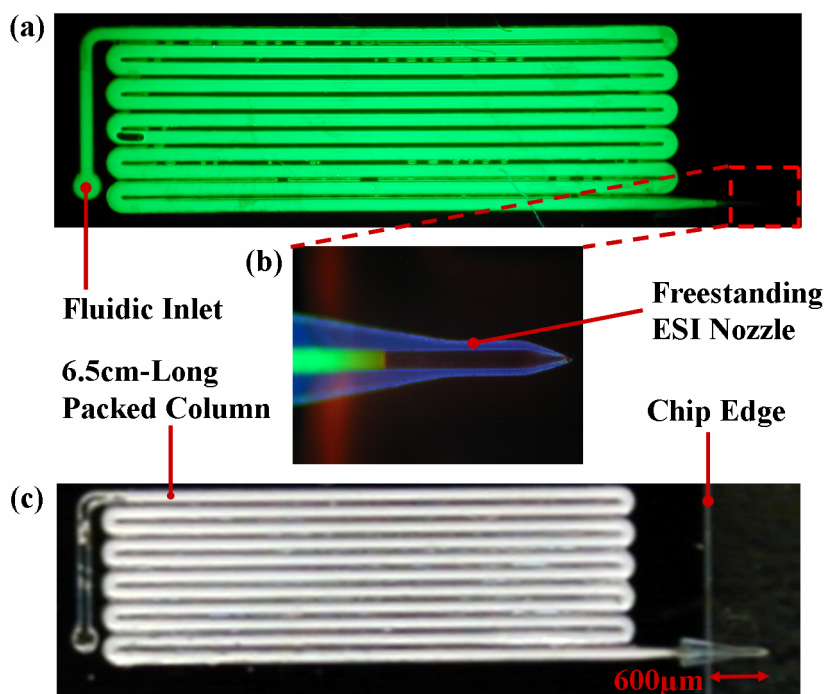


Figure 6-1 Overview of the HPLC-ESI/MS microchip before and after bead packing.

The microchip (Figure 6-1) has one access port. The fluid enters the chip from the chip backside, flows through the column and filter, and exits from the nozzle. The separation column is 6.5 cm long, 100 µm wide, and 25 µm high with rounded cross-sections. And it is packed with 5 µm C18 silica beads using a conventional slurry packing technique described in Section 5.4.1. The filter is a 3 µm-high channel leading to the ESI nozzle. The freestanding nozzle is 600 µm long with a 15 µm wide, 3 µm high opening.

The filter traps beads in the column and prevents beads from entering the ESI nozzle. The packed column outlet is the inlet of the nozzle, which minimizes extra-column peak broadening.

Figure 6-1 (a) is a fluorescent overview picture of the device before bead packing. The fluidic channel is filled with fluorescein. A close-up picture of the freestanding electrospray nozzle is shown in Figure 6-1 (b). The fluorescent solution is seen traveling half-way through the nozzle. An optical picture of the device after bead packing is shown in Figure 6-1 (c). It can be seen clearly in the picture that the freestanding nozzle extends 600 μm off the edge of the chip.

6.2.2 Fabrication Process

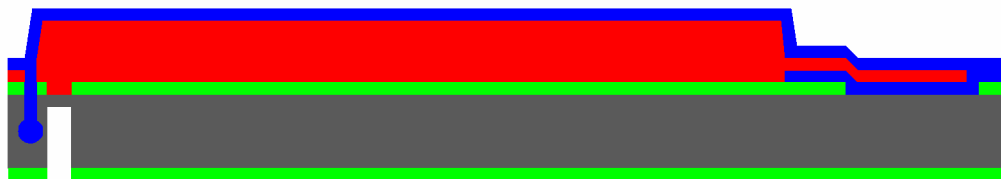
The chip is microfabricated on a silicon wafer with a single batch-fabrication process compatible with IC technology. The fabrication process is shown in Figure 6-2. The process starts with growing a 1.5 μm thick SiO_2 layer on both sides of a 4-inch silicon wafer by thermal oxidation. Then the backside oxide is patterned with an AZ4620 (Clariant, Somerville, NJ) photoresist mask and etched with buffered HF, which defines the 150 μm diameter backside fluidic access hole. With the backside patterned photoresist and oxide as mask, DRIE is performed to create the backside fluidic access hole, leaving only a 50 μm thick diaphragm. The frontside oxide is patterned to open areas for the fluidic access hole and for nozzle release. Then a 3 μm thick parylene C (Specialty Coating Systems, Indianapolis, IN) is conformally deposited on the frontside only. The wafer backside is covered during the parylene deposition. This first parylene layer is patterned to form the bottom of the electro-spray nozzle. 25 μm thick photoresist

AZ4620 is spun on the front side of the substrate and patterned with two masks to form a two-level photoresist structure using a double-exposure method. One full exposure (1st mask) and one partial exposure (2nd mask) are performed consecutively prior to developing the photoresist. Areas around the fluidic channels are fully exposed, which reveals a 15 μm wide oxide ring underneath. Bead filters and wafer field areas are partially exposed to leave only 3 μm high photoresist after developing. The unexposed photoresist is for 25 μm high liquid chromatography columns and inlet/outlet chambers. After photoresist patterning, the revealed oxide ring around the fluidic channels is etched away with buffered HF. Then an approximately 100 μm deep moat around the fluidic channels is etched into the silicon wafer with a modified DRIE Bosch process [1], which adds a 36-second isotropic SF_6 plasma etching at the end of the anisotropic standard Bosch process. It creates trenches with a mushroom profile at the bottom, which provides excellent mechanical anchoring strength for the subsequently-deposited parylene layer. A 10 μm thick parylene C layer is then conformally deposited on the wafer frontside, filling up the trenches and covering the photoresist structures. Parylene is patterned and etched away with oxygen plasma outside the channels and anchoring moat. The field photoresist outside the channels and moat is then stripped. The backside hole is opened with DRIE. The frontside substrate silicon underneath the nozzle and along a trench perpendicular to the nozzle is etched with XeF_2 gas-phase silicon etching, in order to make the nozzle freestanding. The etching depth is approximately 150 μm . Then, the channels are released by dissolving photoresist in the channels. Chromatographic beads are packed into the channels by a conventional slurry packing technique described in Section 5.4.1. The

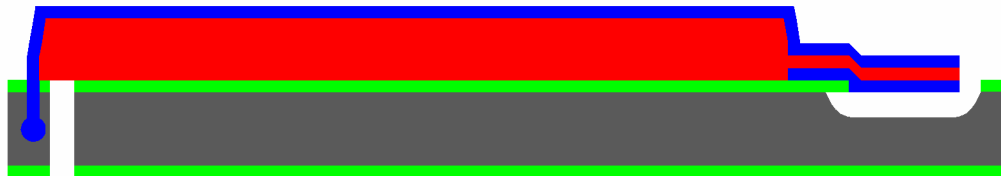
packing pressure is 750 psi. Finally the nozzle is freed by detaching a piece of the chip along the across-chip trench.



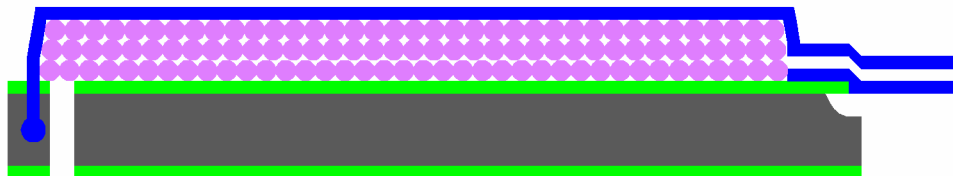
**Pattern Backside Oxide then DRIE;
Pattern Frontside Oxide;
Deposit and Pattern 1st Parylene Layer.**



**Pattern Bi-Level Photoresist;
Pattern Oxide using Patterned Photoresist;
DRIE Anchors; Deposit 2nd Parylene Layer.**



**Pattern 2nd Parylene Layer;
Open Backside Hole with DRIE;
XeF2 Releases Nozzle and Makes Trench (not shown).**



**Acetone Dissolves Photoresist;
Pack the Column with Beads;
Break Chip Along Trench to free nozzle.**

Si
 Oxide
 Parylene
 Photoresist
 Beads

Figure 6-2 Fabrication process flow for the chip.

Figure 6-3 shows the anchored parylene channels in two cross-sectional device pictures. The top fluorescent picture shows multiple channels anchored to the silicon substrate, one of which is shown in the close-up optical picture at the bottom. The depth of the anchor is approximately 100 μm .

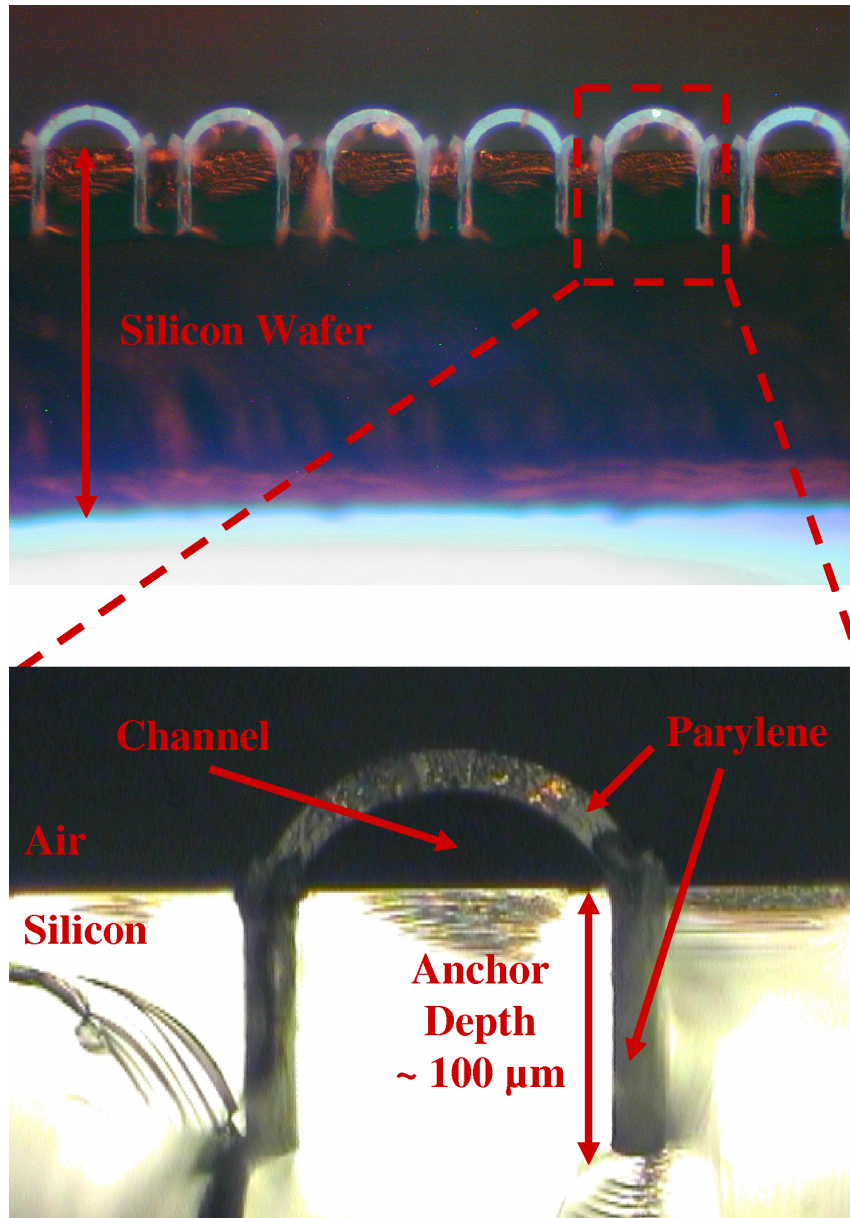


Figure 6-3 Cross-sectional pictures of the fabricated device. The parylene microfluidic channels are anchored to the silicon substrate, greatly improving its pressure rating.

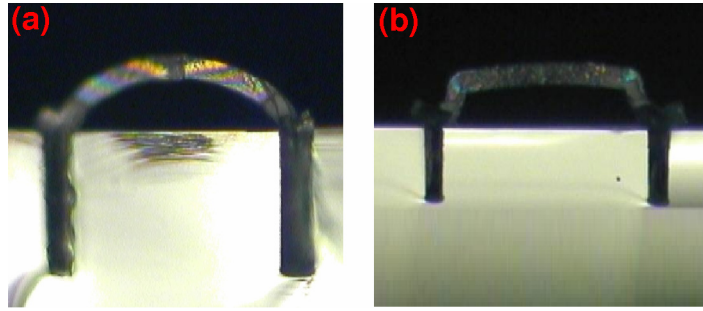


Figure 6-4 Comparison of two anchored-channel cross-sections.

The anchor and the channel profile of this chip are compared to those in the previous chapter (Figure 6-4). The previous one (Figure 6-4 (b)) has shallower anchors, and the cross-section is roughly rectangular. The current one (Figure 6-4 (a)) has much deeper anchors, and has a semi-circular cross-section. The rounded cross-section is due to the channel-forming sacrificial photoresist reflow during the trench DRIE etching. This shows the capability of this process to tailor the column cross-sectional shape, which is considered a factor for column optimization.

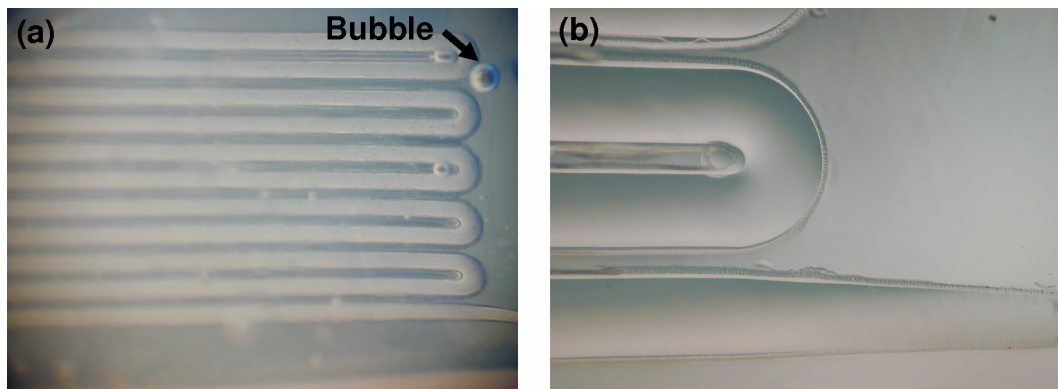


Figure 6-5 Epoxy overcoating for device strengthening and passivation.

To further strengthen and passivate the device, an optional epoxy overcoating layer can be applied to the device. Figure 6-5 (a) shows a packed device with top epoxy coating. Since the two-part epoxy preparation involves mixing the resin with the hardener,

bubbles may occur as shown in the picture, which should be avoided when possible. Figure 6-5 (b) shows the inner side of the epoxy coating after it is peeled off from the chip. It is smooth and conforms to the shape of the channels on the chip.

6.2.3 Processing Challenges

6.2.3.1 Bubbling

During the etching step for the second parylene layer, bubbles can form inside the photoresist channels (Figure 6-6 (a)). When the etching continues, the bubbles can grow drastically, deform the top parylene into a balloon, finally explode and break the parylene cover (Figure 6-6 (b)). This dramatic phenomenon was unheard of before. It is mainly a thermal process, which happens when the channels have a deep moat filled with thick parylene anchors.

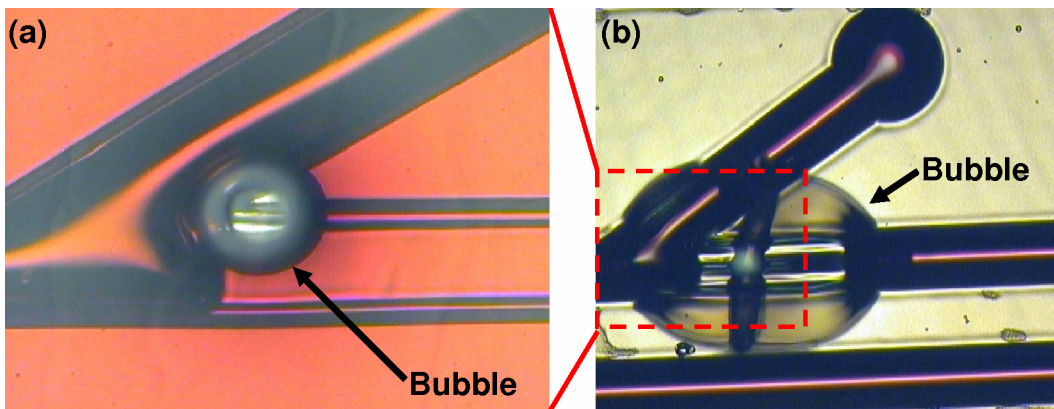


Figure 6-6 Bubbling in the photoresist channels during parylene etching.

Since parylene is an excellent thermal insulator (parylene C's thermal conductivity, $0.84 \text{ mW}/(\text{cm}\cdot\text{K})$, is only four times that of air, $0.21 \text{ mW}/(\text{cm}\cdot\text{K})$), heat generated during the plasma etching of parylene cannot be removed from the photoresist

channel fast enough. In fact, most bubbles appear at places that have the worst thermal conduction, like the corner in Figure 6-6. The plasma heating can bake out the photoresist solvents that were not eliminated during photoresist baking. The solvents vaporize into gas, which is trapped by the top parylene due to its ultra low gas permeability. Finally, continued heating increases the size of the bubble, which pops the parylene channel.

This bubbling issue is very serious, since it destroys the device irretrievably at almost the last step of the whole fabrication. Reducing heating by decreasing plasma etching power and time helps in some cases. But it is far from solving the problem.

Since the gas bubble comes from the photoresist solvent, one solution is to more effectively bake out the solvent. An experiment is carried out to investigate this option in more detail. All the chip samples are fabricated on a silicon wafer with a 1.4 μm thermal oxide layer. The photoresist is patterned to have two thicknesses, 25 μm and 3 μm , using the same set of masks for the real device. The patterned photoresist is postbaked for 15 minutes at 100 $^{\circ}\text{C}$, followed by standard descum process. Then the samples are divided into three groups and treated differently. Group 1 is kept the same, no parylene coating is performed. Group 2 is coated with 15 μm thick parylene. And group 3 is baked for five hours at 100 $^{\circ}\text{C}$ prior to a 15 μm thick parylene coating. All baking processes are performed in a convection oven. For testing, the sample chips are directly placed on hotplate for uniform heating across the chips at various temperatures.

The purpose of group 1 is to verify that the bubbles are indeed solvent gas trapped under the parylene. As shown in Figure 6-7, photoresist channels appear intact after 10 minutes of baking at 180 $^{\circ}\text{C}$, meaning parylene sealing is responsible for the solvent gas trapping.

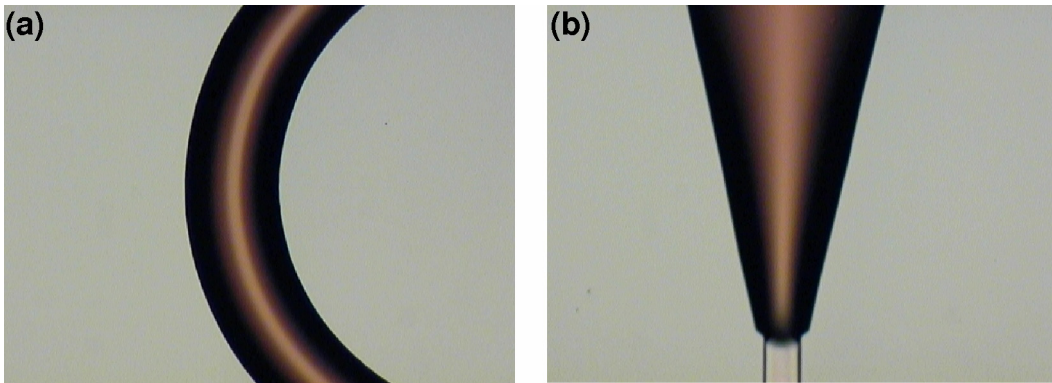


Figure 6-7 Samples without parylene coating are intact after baking 10 minutes at 180 °C.

Samples from group 2 show no sign of bubbling after 5 minutes at 150 °C and another 5 minutes at 160 °C. However, when placed on hotplate at 170 °C, which is over the vaporization threshold for the solvent, the samples almost immediately generate bubbles everywhere. In Figure 6-8 (a), bubbles are generated along the channel and cause the parylene to delaminate, since the parylene is not anchored. The situation is even worse in Figure 6-8 (b), where most of the channel photoresist is pushed out of the channels by the bubbles, and large areas of parylene delaminate from the substrate.

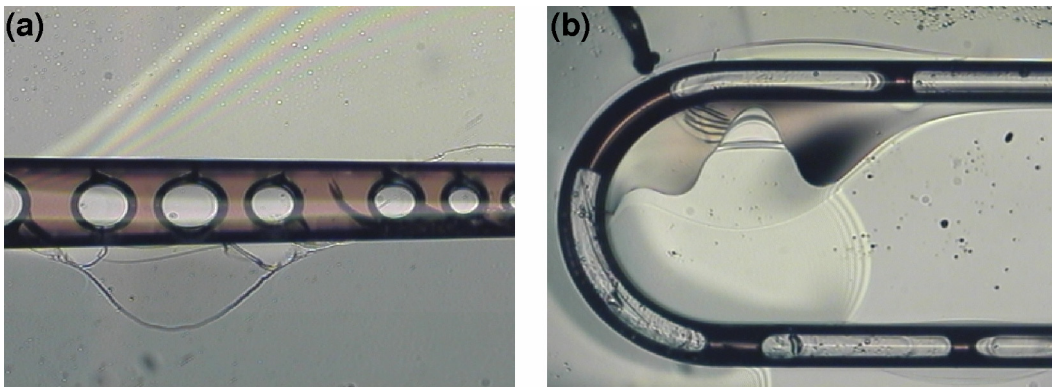


Figure 6-8 Samples with parylene coating generate bubbles in the channels immediately after being heated at 170 °C.

Group 3 delivers the most successful result. For most of the sample chips, there is no bubbling at all even after 10 minutes of baking at 180 °C (Figure 6-9 (a) (b)). While for some chips, there are a few little bubbles appearing at the channel ends and cross-sections. They grow very slowly over time and do no damage to the channels after 10 minutes of continuous baking (Figure 6-9 (c) (d)).

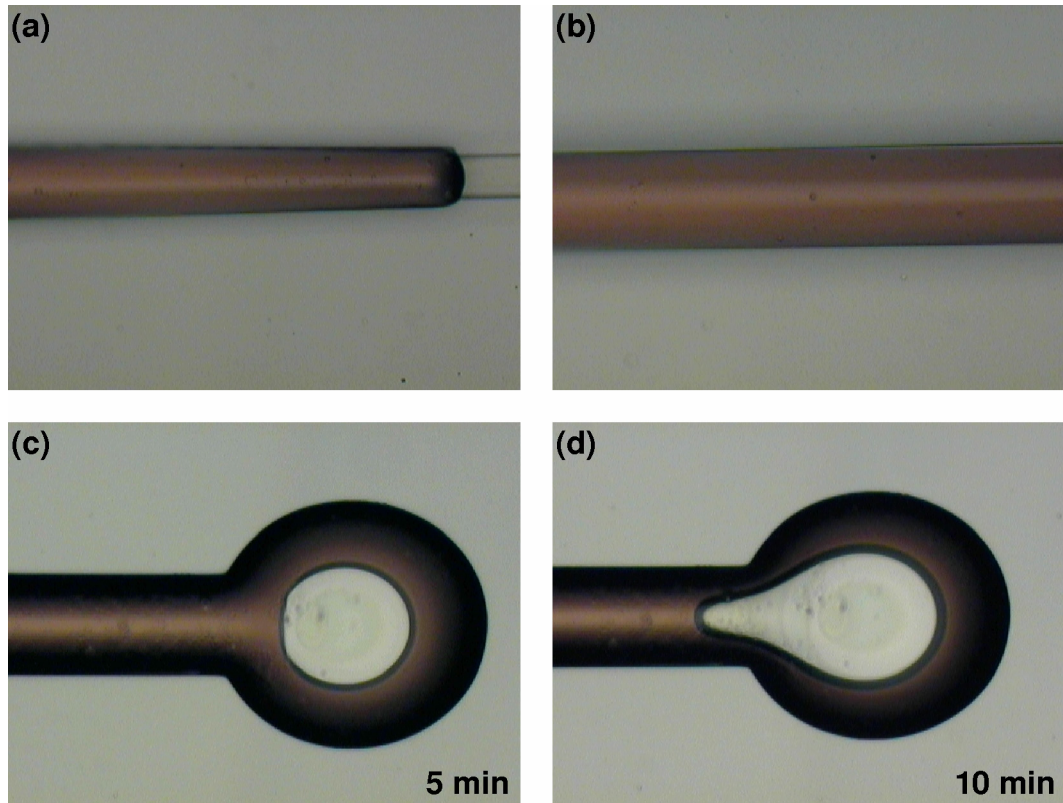


Figure 6-9 Samples with 5 hours of extra baking before parylene coating, baked for 10 minutes at 180 °C.

It can be concluded from the above experiments that thorough removal of photoresist solvent, through extra-long postbake before parylene coating, solves the bubbling problem effectively. In addition, this extra baking has little effect on the length of the channel releasing process, because postbake has little impact on the channel

photoresist dissolution rate [2]. Therefore, if necessary, much longer baking times can be used.

6.2.3.2 Black Silicon

In order to reduce the dead volume in the backside hole, the hole is usually designed to be as small as the DRIE process allows. This, however, can result in black silicon [3] with too narrow a trench and/or a dirty wafer/machine. Dense silicon needles generated during DRIE etching form “grass” at the trench bottom, which appears to be black. Figure 6-10 (a) shows silicon needles at the bottom of a trench. The dotted line illustrates the profile of the trench. A close-up picture of the trench-bottom silicon needles is shown in Figure 6-10 (b). When black silicon appears, it is almost impossible to remove and it becomes very difficult to etch the trench through the wafer. To avoid it, larger holes should be used and the wafer needs to be cleaned more thoroughly.

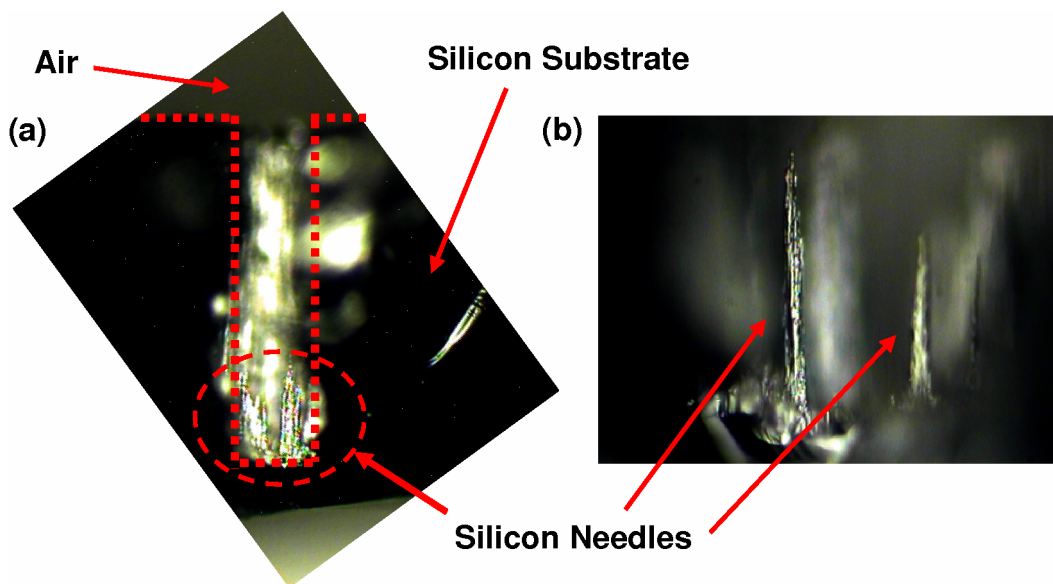


Figure 6-10 Silicon needles at the bottom of trench.

6.2.4 Packaging

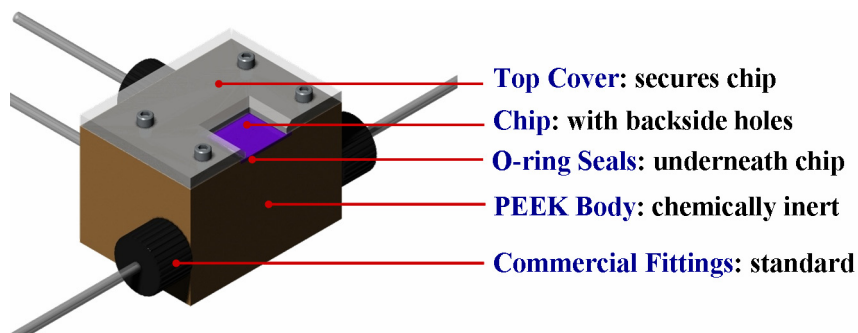


Figure 6-11 Packaging for the chip.

High-pressure fluidic access to the chip is achieved with a custom-made packaging jig. The jig body is 3.01 cm long, 2.2 cm wide, and 2 cm thick. Figure 6-11 shows the packaging scheme. The jig body is made of PEEK (polyetheretherketone) (McMaster-Carr, Los Angeles, CA), which is chemically inert for most chemicals and solvents. Commercial fitting receiving ports are machined in the jig to couple with commercial fittings (Upchurch Scientific, Oak Harbor, WA). Horizontal and vertical holes drilled in the jig lead fluid from the fitting ports to the jig top surface. The top surface has two levels of recess. The first level is square and is used for holding the chip. The second level has circular recesses for o-rings (Apple Rubber Products, Lancaster, NY). The o-rings have a durometer hardness of 70 and are made of ethylene propylene, which is compatible with all the chemicals and solvents, such as acetone and acetonitrile, used in the chip testings. When the o-rings and chip are placed in their recesses, a PEEK cover is placed on top and is screwed down to compress the chip and o-rings. The o-rings are compressed by about 25% to 30% in thickness, which seals the chip and jig. Four fluidic channels on the chip can be accessed simultaneously with this jig, although only

one of them is used for the testing of the device described in this chapter. This jig is used for both the bead packing and separation test, with thorough cleaning in between.

6.3 Testing Results and Discussion

6.3.1 Column Pressure Rating

The parylene microfluidic channels are mechanically anchored deep into the silicon substrate (Figure 6-3), which greatly improves the channels' pressure compatibility. From earlier studies [4] presented in Chapter 4, we know that the trench-anchored parylene structures can withstand an upper pressure of about 700 psi without failure. The failure mode is not delamination of parylene from the substrate, but rather breakage of the parylene layer. Thus, with an epoxy overcoating layer, the chip is strengthened and passivated. The chips perform best when properly prepared, which includes cleaning in a piranha solution at 120 °C for 5 minutes, followed by an HF dip and immediate epoxy coating and baking overnight at 80 °C in the oven. The pressure upper limit achieved with this device is 1000 psi.

6.3.2 Pressure–Flow Rate Relation

As explained in Section 5.4.2, pressure vs. flow rate measurement is a useful tool for determining the column packing quality and calibrating the column operation. In this testing, deionized water is pumped through the column using pressurized nitrogen gas from a compressed gas cylinder. The liquid front moving velocity is measured in a capillary connected at the outlet, which is then used to calculate the volumetric flow rate using the capillary I.D. Since the column is packed at 750 psi, the measurement pressure

is only up to 700 psi. Based on equations (2.2) and (2.13), the column volumetric flow rate is proportional to the pressure applied, and the linear relation is expressed as:

$$F = \frac{\varepsilon}{\Phi} \frac{d_p^2 A_c}{\eta L_c} \Delta P \quad (6.1)$$

where F is the volumetric flow rate, ΔP is the pressure drop across the column, ε is the porosity of the packed column, Φ is the dimensionless flow resistance, d_p is the bead diameter, A_c is the column cross-sectional area, η is the viscosity of the fluid, and L_c is the column length.

The measured pressure–flow rate data and fitted linear curve are shown in Figure 6-5. The straight line does not extend back exactly to the origin because of a non-linear pressure–flow rate relation at very low pressures. From the fitted line, it is found that $\Phi/\varepsilon=449$ for this 6.5 cm long, 100 μm wide, and 25 μm high column packed at 750 psi with 5 μm diameter porous silica beads. This agrees well with the result from last chapter, in which Φ/ε is found to be 444 for the on-chip 8 mm long, 100 μm wide, 25 μm high column packed at 200 psi with 7 μm diameter porous PS-DVB beads. It can be seen that although the column lengths and bead types differ, the permeability is almost unchanged when the column cross-sections are the same and packing pressure is roughly proportional to column length. Now assuming the porosity of the packed column is 0.7 to 0.85, which is normal for porous-bead column, then Φ is 314 to 382, which is close to but smaller than its empirical value of 500 for conventional-scale LC columns. The high permeability of the on-chip column is due to the small on-chip column to bead size ratio, which makes the column effectively “less dense” than conventional ones. Similar results

have been reported before [5], which also points out that the micro-columns actually should have at least the same, if not better, separation performances.

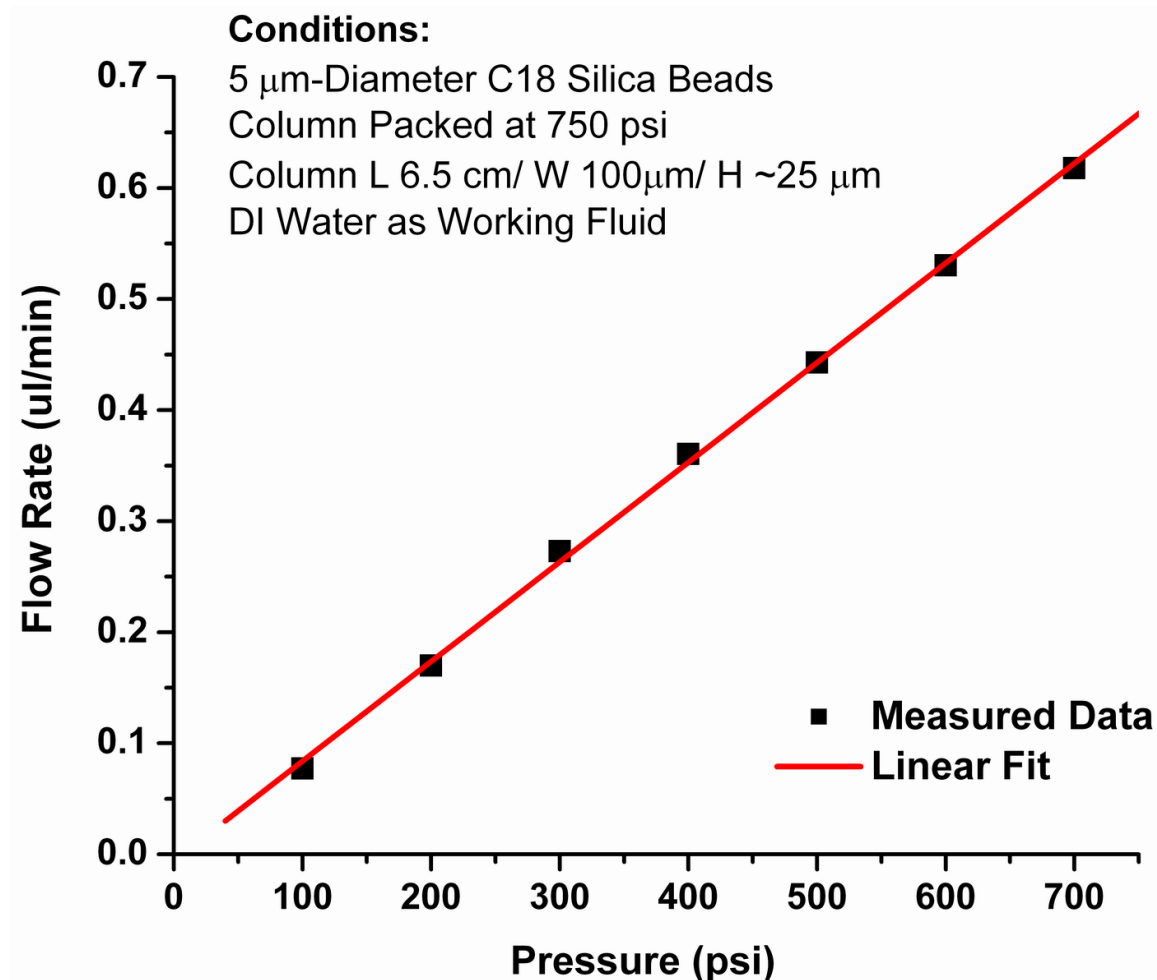


Figure 6-12 Pressure vs. flow rate testing result for the on-chip packed column.

6.3.3 LC Separation with On-Line MS Detection

On-chip reversed-phase gradient liquid chromatographic separation coupled with on-line mass spectrometry detection is successfully demonstrated with tryptic digested cytochrome c sample. The on-chip separation column is packed with 5 μm C18 porous silica beads. The column is 6.5 cm long, 100 μm wide, 25 μm high, and shares the same

cross-sectional area as a 56 μm ID capillary. The electrospray potential is added to the flow path upstream of the chip [6, 7]. A commercial LC gradient pump and autosampler are used to provide the gradient flow and sample injection. Mobile phase A is water with 0.1% formic acid. Mobile phase B is acetonitrile with 0.1% formic acid. The flow rate is 0.4 $\mu\text{L}/\text{min}$. Thus, the pressure across the on-chip packed column is estimated to be around 450 psi, based on the measured pressure–flow rate curve. 1 μL (1 pmol) sample is injected with autosampler. Figure 6-6 shows the MS chromatogram result of a successful separation. Compared to the chromatogram of a similar separation obtained with commercial system, this separation result is not optimal, mainly due to the dead volume associated with the packaging jig. There is still much room for improvement in the jig in terms of dead volume reduction. Significantly smaller dead volume is expected to produce much better separations.

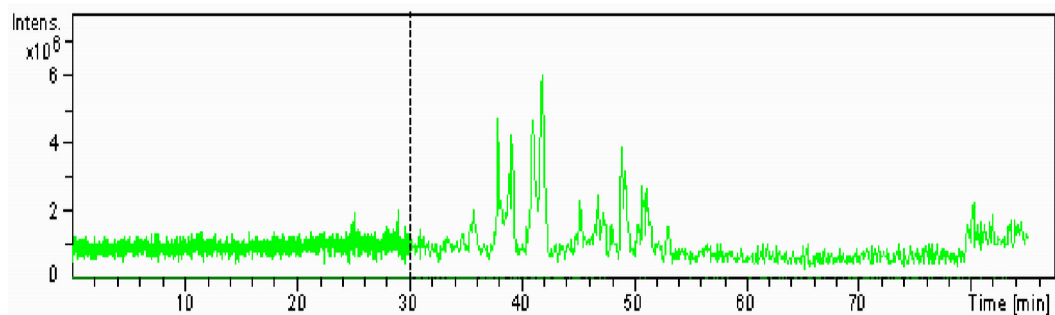


Figure 6-13 Separation result of tryptic digested cytochrome c sample using on-chip reversed-phase gradient separation coupled with online mass spectrometry detection.

6.4 Summary

This chapter presents a batch-fabricated high-pressure liquid chromatography microchip for HPLC-MS applications. The chip is conventionally-packed and used for

pressure-driven separation. This integrated chip provides high-pressure separation in a miniaturized column and direct coupling for mass spectrometry detection. Higher permeability of on-chip packed column is again confirmed through pressure–flow rate measurements. On-chip separation and on-line MS detection of digested cytochrome c protein is successfully demonstrated at an operating pressure of 450 psi. This chip further extends the line of parylene microfluidic and liquid chromatography devices that have been developed, which brings us even closer to a totally integrated HPLC system on-a-chip.

6.5 Bibliography

- [1] M. Liger, D. C. Rodger, and Y.-C. Tai, "Robust parylene-to-silicon mechanical anchoring." *Proceedings of the 16th IEEE International Conference on Micro Electro Mechanical Systems (MEMS 2003)*. Kyoto, Japan, 2003. p. 602–605.
- [2] K. Walsh, J. Norville, and Y.-C. Tai, "Photoresist as a sacrificial layer by dissolution in acetone." *Proceedings of the 14th IEEE International Conference on Micro Electro Mechanical Systems (MEMS 2001)*. Interlaken, Switzerland, 2001. p. 114–117.
- [3] H. Jansen, M. Deboer, R. Legtenberg, and M. Elwenspoek, "The black silicon method - a universal method for determining the parameter setting of a fluorine-based reactive ion etcher in deep silicon trench etching with profile control." *Journal of Micromechanics and Microengineering*, 1995. 5(2): p. 115–120.
- [4] Q. He, C. Pang, Y.-C. Tai, and T. D. Lee, "Ion liquid chromatography on-a-chip with beads-packed parylene column." *Proceedings of the 17th IEEE International Conference on Micro Electro Mechanical Systems (MEMS 2004)*. Maastricht, Netherlands, 2004. p. 212–215.
- [5] R. T. Kennedy and J. W. Jorgenson, "Preparation and evaluation of packed capillary liquid-chromatography columns with inner diameters from 20 to 50 μm ." *Analytical Chemistry*, 1989. 61(10): p. 1128–1135.
- [6] M. T. Davis and T. D. Lee, "Rapid protein identification using a microscale electrospray LC/MS system on an ion trap mass spectrometer." *Journal of the American Society for Mass Spectrometry*, 1998. 9(3): p. 194–201.

- [7] L. Licklider, X. Q. Wang, A. Desai, Y.-C. Tai, and T. D. Lee, "A micromachined chip-based electrospray source for mass spectrometry." *Analytical Chemistry*, 2000. 72(2): p. 367–375.

CHAPTER 7

CONCLUSION

The enormous success of the integrated circuit industry demonstrates the power of miniaturization and integration. The field of μ TAS has the potential of accomplishing a similar revolution in the fluidic world. One of the challenges in μ TAS today is integrated liquid chromatography on-a-chip. Miniaturized LC chips offer significant advantages over conventional LC systems. The chips are smaller and cheaper, provide better sensitivity without loss of separation efficiency, and require less sample and solvent. Due to their small sizes, on-chip LC systems are inherently nano LC.

Totally-integrated LC on-a-chip needs a truly versatile and powerful technology. Parylene microfluidics technology appears to be a great candidate. In this thesis, the parylene technology is greatly enhanced, and the line of parylene microfluidic devices is significantly extended. Some of the issues facing LC chips, such as bead integration and high-pressure generation, are well addressed. Moreover, three different LC chips are demonstrated.

The bead integration technology, for the first time, provides a way to introduce beads into the on-chip column in a batch-fabrication fashion. Besides a few novel aspects, it is basically a modified photolithography process, which makes it convenient to integrate with other processes and devices.

The first LC-ESI/MS chip presented here uses this bead integration technology to make its on-chip bead column. The column is found to have consistent porosity with conventional capillary columns. It is verified that the beads contaminated with photoresist during fabrication are unaffected in terms of their separation performance.

The pressure requirements for LC chips are well above those for most microfluidic devices. Two types of self-aligned parylene anchoring techniques are developed, which increase the pressure rating of the parylene devices to 1000 psi. Trench-anchoring with epoxy-overcoating delivers the best performance.

Since bead-packed columns have significantly increased flow resistance, it takes high pressures to pump liquid through the columns. Electrolysis-based micro-actuators are demonstrated to generate high pressure and large deflection, with low power consumption. The deactivation of the actuator through gas recombination in the presence of a platinum catalyst is also explored. A sealed electrolysis actuator has the potential of running many actuation and deactivation cycles without refilling the electrolyte.

The second LC chip presented is an ion chromatography chip that has applications in water safety, environmental monitoring, and clinical exams. Sample injection, separation, and detection are all performed on a single chip. Seven common anions are separated, based on an anion-exchange mechanism, and detected with unsuppressed conductivity sensing. In addition, it is found that the on-chip column has higher

permeability than conventional ones, which actually lowers the operating pressure requirements for on-chip LC. This effect is due to the small size of the column compared to the bead dimension. The regular bead packing structures are disturbed by the column walls, which makes the column less dense.

The last nano HPLC-MS chip is mainly targeted for the fields of proteomics and drug discovery. The presented chip is capable of running high-pressure, high-capacity separations on-chip, and capable of coupling for on-line MS detection through its integrated ESI nozzle. A digested protein sample is successfully separated and detected. The high permeability of on-chip columns is confirmed again. Despite the fact that this column has very different column length, bead size, and packing pressure from those of the ion chromatography chip, the obtained dimensionless column flow resistance values are very close.

Complete LC chips may one day become portable and/or disposable. They can be used for field tests, networked sensing, real-time environmental monitoring, and so on, which would be impossible with today's bulky LC instruments in the labs. LC on-a-chip can also be integrated with other on-chip chemical and biological sensors, eliminating the need for highly-specific sensing. Moreover, LC chips have the potential of achieving high-throughput LC separations, which can make the drug discover process much faster. While we are still a long way from achieving these goals, the work described in this thesis serves as an important step in that direction.